Mechanical Inputs to Cardiac Fibroblasts and Myocytes Affect Structure, Function, and Signaling Response

BY

Michael A. Mkrtschjan
B.S., University of Illinois at Urbana-Champaign, 2011

THESIS

Submitted as partial fulfillment of the requirements for the degree of
Doctor of Philosophy in Bioengineering
in the Graduate College of the
University of Illinois at Chicago, 2018

Chicago, IL

Defense Committee:

Brenda Russell, Chair and Advisor
Thomas Royston, Bioengineering
Jae-Won Shin, Bioengineering
Chong Wee Liew, Physiology & Biophysics
R. John Solaro, Physiology & Biophysics

DEDICATION

“Whatever you do, work heartily, as for the Lord and not for men, knowing that from the Lord you will receive the inheritance as your reward” – Colossians 3:23-24

I have been given a beautiful, encouraging wife, Heidi, to whom I am forever indebted for marrying me in the midst of this program.

ACKNOWLEDGEMENTS

My advisor, Brenda Russell, who taught me to seek the truth first in my work and has taught me all she can about being a scientist.

The remaining members of my committee: Thomas Royston, Jae-Won Shin, Chong Wee Liew, and John Solaro.

Past and present members of the Russell Lab who have come alongside me as I completed my degree.

The Department of Physiology & Biophysics, who took me in for all these years—particularly, John Solaro and Jan Kitajewski, who served as department heads during my tenure. Additionally, I am grateful to Dr. Solaro for providing funding on his training grant.

The University of Illinois at Chicago Center for Clinical and Translational Science, from which I received funding through the PECTS award.

The Desai Lab at the University of California, San Francisco—namely, Long Le, who provided much of the materials and added to the research needed to complete this dissertation.

The Department of Bioengineering faculty and staff, who allowed me to study and learn the discipline at the University of Illinois at Chicago.

Contribution of Authors

Chapter II: Contributions by Dr. Brenda Russell, Snehal Gaikwad (Figures 7 and 14), Sagar Dommaraju (Figure 7), Kevin Kappenman (Figures 8 and 15), Long Le (Figure 14 and microrod production), and Dr. Christopher Solís (Figures 9, 17, and 18) on experimentation, analysis, or interpretation.

Chapter III: Contributions by Dr. Brenda Russell, Admasu Wondmagegn (Figure 19), Janki Majithia (Figure 23), Jieli Li (Figures 24 and 25), and Dr. Christopher Solís (Figures 26 and 27) on experimentation, analysis, or interpretation.

TABLE OF CONTENTS

TABLE OF CONTENTS (CONTINUED)

LIST OF TABLES

TABLE **PAGE**

LIST OF FIGURES

LIST OF FIGURES (CONTINUED)

LIST OF ABBREVIATIONS

AFM	Atomic Force Microscopy
βAR	Beta Adrenergic Receptor
BSA	Bovine Serum Albumin
cAMP	Cyclic Adenosine Monophosphate
CapZ	Actin Capping Protein
CM	Cardiomyocyte
DAPI	4′,6-diamidino-2-phenylindole
DMEM	Dulbecco's Modified Eagle Medium
ECM	Extracellular Cellular Matrix
FAK	Focal Adhesion Kinase
FLIM	Fluorescence Lifetime Imaging Microscopy
FRAP	Fluorescence Recovery After Photobleaching
FRET	Förster Resonance Energy Transfer
GPCR	G-Protein Coupled Receptor
HA	Hyaluronic Acid
ISO	Isoproterenol
kPa	Kilopascal
MOI	Multiplicity of Infection
cMyBC	Myosin Binding Protein C
NRVF	Neonatal Rat Ventricular Fibroblast
PAA	Polyacrylamide
PBS	Phosphate Buffered Saline

LIST OF ABBREVIATIONS (CONTINUED)

PDMS	Polydimethylsiloxane
PEG	Poly(ethylene glycol)
PEGDMA	Poly(ethylene glycol) dimethacrylate
PI3K	Phosphoinositide 3-kinase
PIP2	Phosphatidylinositol 4,5-bisphosphate
PIP3	Phosphatidylinositol 3,4,5-triphosphate
PKA	Protein Kinase A
PKCε	Protein Kinase C epsilon
PPC	Particles Per Cell
RACK	Receptor for Activated C Kinase
ROI	Region of Interest
RyR	Ryanodine Receptor
SD	Standard Deviation
SEM	Standard Error of the Mean
SANPAH	sulfosuccinimidyl 6-(4'-azido-2'-nitrophenylamino)hexanoate
TCP	Tissue Culture Plastic
TnI	Troponin I
TPT	Time to Peak Tension
WASP	Wiskott-Aldrich Syndrome Protein

SUMMARY

The function of the heart is to beat regularly and pump blood to the body. This dynamic environment has implications for the cues experienced by cells within cardiac tissue. Moreover, within normal aging or in response to disease, the heart undergoes significant stiffening, altering the tissue as a whole and thus at the level of the individual cells. In order to better understand physiology at the tissue level, cell and tissue engineers utilize fabrication techniques to more accurately tune the surfaces and environments in which they culture cells. Thus, relevant physiological or pathological responses can be mimicked *in vitro*. Indeed, it has been shown that cardiomyocytes exhibit varying contractile properties whether grown on stiffness akin to healthy or fibrotic myocardium.

In this dissertation, I test the hypothesis that mechanical properties of the cell's underlying substrata elicit differential structural, functional, and signaling responses to drug treatment. I control the physical cues to study the physiological responses of the two predominant cell types of the heart, first in cardiac fibroblasts, and second in cardiomyocytes. Using polyacrylamide hydrogels of defined stiffness and micropost topography manufactured through soft lithography techniques, I examine migration and adhesion properties, as well as response to altered phosphatidylinositol 4,5-bisphosphate signaling in fibroblasts. I then use hydrogels to study the physiology of cardiomyocytes under various stiffness of substrata with an additional work load as applied through by β-adrenergic stimulation. Briefly, interactions of both cell types with potentially therapeutic hyaluronic acid microrods are studied. Microrods were originally developed for direct inject into the myocardium to attenuate fibrosis following myocardial

infarction. I utilize a variety of imaging and biochemical assays to determine how the mechanical environment affects response to neurohumoral stimulation. The data presented demonstrate a variety of examples in which the mechanical environment not only regulates the physiology of cells, but also the response to drug treatment.

I. INTRODUCTION

Tissues within the body are subject to a variety of biophysical and chemical cues, many of which play varying roles in maintaining physiological homeostasis or triggering pathologies. In particular, most tissues function optimally at a specific stiffness (Figure 1). Although a material property, the term “stiffness” has been used colloquially within the scientific community, and will be used throughout this thesis, to refer to the Young’s Modulus of the material. Change of the tissue stiffness, generally through fibrosis, leads to dysfunction. Mechanical stimuli are often less examined by researchers than biochemical cues such as neurohumoral compounds or growth factors. However, the mechanical cues of pressure, stress, and strain lead to outside-in transmission of signals in cells through the focal adhesion complex, resulting in physiological adaptation and potential maladaptation. Furthermore, inside-out changes are developed by actomyosin interactions as directed by internal changes in cytoskeletal tension, resulting in altered contractile, migratory, or structural changes. As signals reach their destination, they effect changes in post-translational modifications, protein expression, or gene expression, each of which can have profound impact on physiology of the individual cell. Elucidating these signals is critical in the development of therapeutics and understanding the physiology of various tissues.

One goal of cell and tissue engineers is to define and control mechanical cues to better understand cell behavior. In order to do this, we use a variety of materials and techniques to control both the stiffness and topography of the microenvironment. Once cells are within a defined microenvironment, we can then test their physiological responses and associated molecular signaling through biochemical assays. Additional

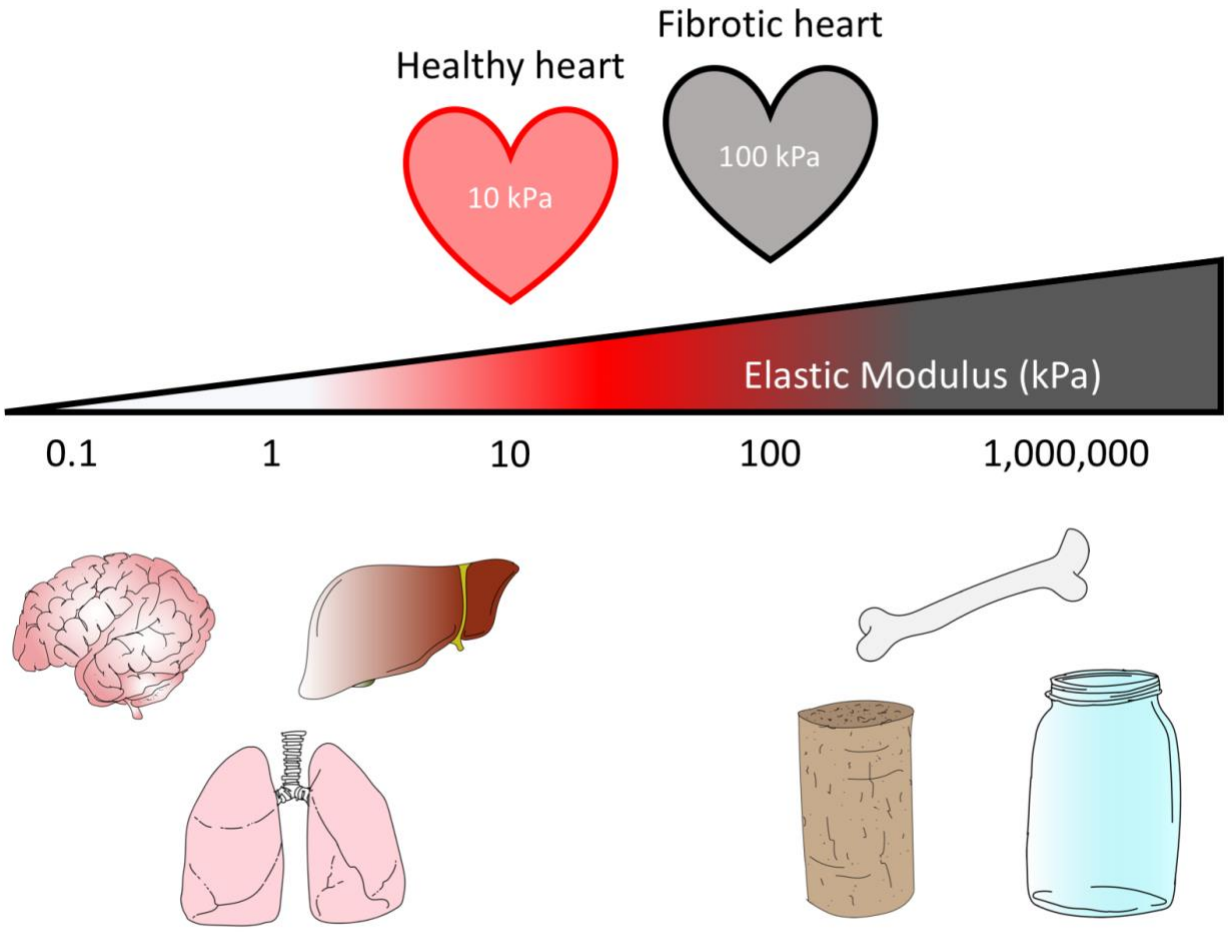

Figure 1. Biological tissues come in a wide range of stiffnesses

challenge through drug treatment is used to test differential cell responses in various mechanical conditions and whether or not targeting particular signaling pathways can be used to overcome inherent acute or chronic mechanical signaling. Ultimately, these kinds of studies are used to gain understanding that can be applied to future therapeutics in cell and tissue engineering. A goal of any tissue engineering implantable is for it to integrate with the surrounding environment and cells without eliciting a negative response in the recipient. Thus, a major benefit for a better understanding of mechanical signaling is for the improvement of scaffolds for tissue constructs in regenerative medicine.

According to the 2018 American Heart Association report on heart disease and stroke statistics, cardiovascular disease remains the number one cause of death in the United States, accounting for one of every three deaths (Benjamin et al., 2018). Despite extensive efforts by researchers to find effective treatments and cures, there remains a great need for continued research in the field. The heart is a highly dynamic system, undergoing contraction about once every second for the entire duration of one's life. This makes the contractile cells within the heart, cardiomyocytes (CMs), subject to constant changes in mechanical stresses and strains, leading to increased or decreased contraction of individual cells or cytoskeletal remodeling. Moreover, resident cardiac fibroblasts serve to provide structural support to the tissue through the deposition of extracellular matrix proteins (ECM), which through normal aging or especially through ischemic injury, can become pathological. Although myocytes also deposit ECM, the vast majority comes from fibroblasts. The pathological condition of cardiac fibrosis, or stiffening of the heart, causes aberrations in cardiac contractility and

remodeling of the CMs. In response to mechanical stress through acute injury, interspersed fibroblasts undergo transformation to a state that produces increased amounts of ECM, stiffening of the heart, and results in a need for myocytes to increase contractile strength, resulting in cardiac hypertrophy (Figure 2). Cardiac fibroblasts and myocytes are largely responsible for maintaining homeostasis of this tissue, but altered mechanical properties leads to abnormal cell behavior and disease.

A. Tools to study mechanical signaling in muscle and non-muscle cells

Our lab and others have used a variety of tools to study various mechanical inputs to cells for mechanotransduction. One of the most effective means of controlling the environment is through using substrata of tunable stiffness. This approach can be done using hydrogels such as polyacrylamide (PAA) and poly(ethylene glycol) (PEG) or non-hydrogel silicone based materials such as polydimethylsiloxane (PDMS). Both materials are elastic and can be functionalized to allow for cell attachment. Varying the ratio of base to crosslinker in these materials yields surfaces of variable stiffness, which can be tested using atomic force microscopy (AFM) to obtain Young's moduli. A drawback of these materials is that they require additional functionalization to adsorb or covalently bind ECM proteins for cellular attachment. For CMs, a cell-type dependent on alignment and shape for optimal function, ECM patterning through stamping procedures has been used in cell culture (Bray et al., 2008). The importance of shape and geometry is seen in traction force microscopy studies that demonstrate an optimal ratio of myocyte length to width to generate maximum amount of contractile force (Kuo et al., 2012; Ribeiro et al., 2015). As well, this approach has been used in non-muscle cells,

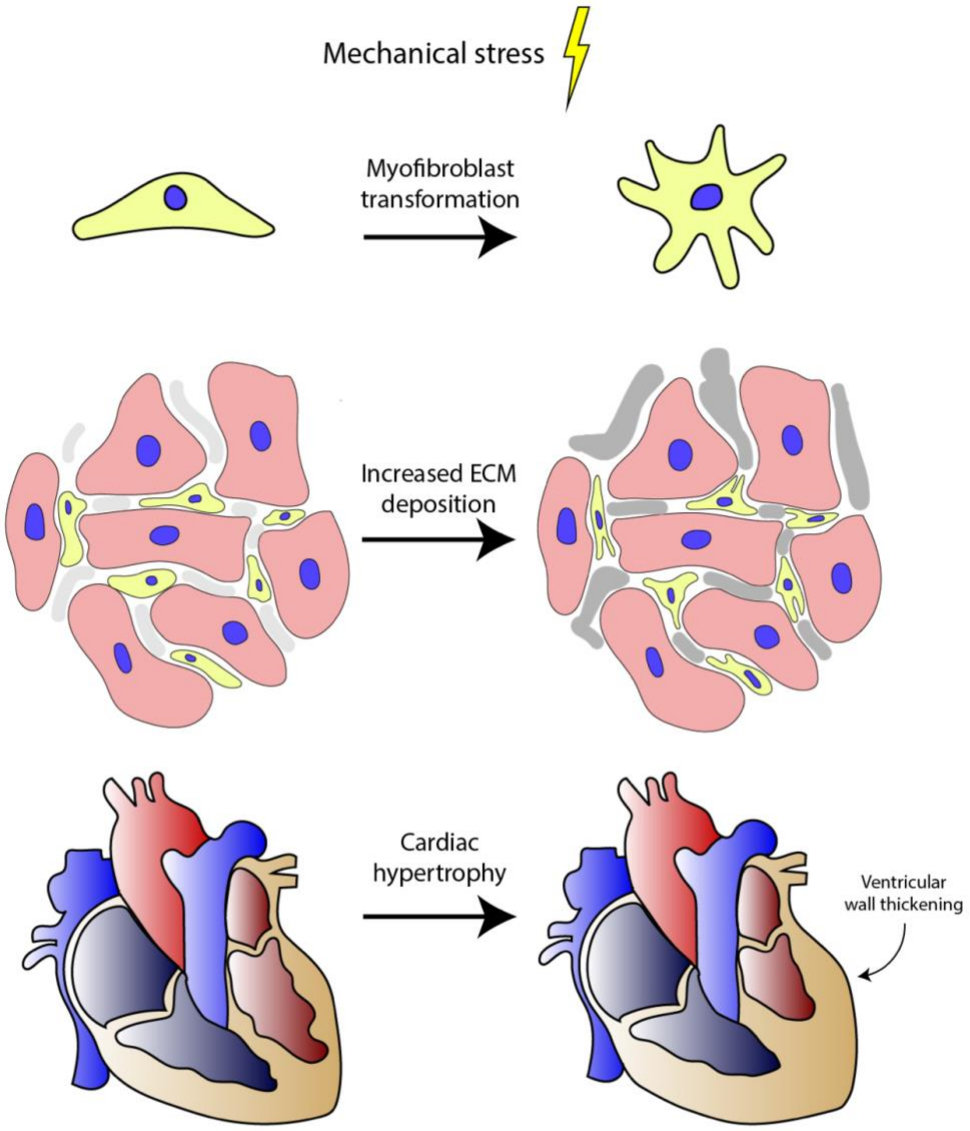

Figure 2. Cardiac fibrosis leads to hypertrophy of the heart. Following mechanical stress, cardiac fibroblasts undergo transformation to a myofibroblast state. The resultant increase in ECM deposition can lead to hypertrophy of the heart.

including fibroblasts, to study contractile forces (Oakes et al., 2014). An approach that has received recent attention is the use of photoactivatable surfaces that change in stiffness upon exposure to UV light. In particular, the ability of stem cells to retain "mechanical memory" in a YAP/TAZ-dependent manner was studied (Yang et al., 2014). This approach is effective, as it allows for the study of the same culture in response to acute and chronic changes in substrate stiffness.

In addition to tuning the stiffness of the surface, various topographical surfaces have been used by a number of labs. Our lab has experimented extensively with micropost topography (15-25 μm diameter) in order to provide additional anchorage for cells and a pseudo three-dimensional environment, and affecting migration, proliferation, and gene expression (Boateng et al., 2004; Biehl et al., 2009; Doroudian et al., 2012). Often times, these kinds of environments are created through a combination of photolithography and soft lithography. Posts can also be used on a smaller scale (1-5 μm diameter), on top of which cells rest and deflections of posts can be measured to calculate traction forces in muscle and non-muscle cell types (Sniadecki and Chen, 2007). Microgrooved surfaces using a similar approach have been used to not only align cells but provide depth and volume akin to how they might be geometrically configured within the heart (Motlagh et al., 2003).

A number of methods have been developed to measure both static and cyclic stretch of cells in culture. Our lab has often used the Flexcell system to study bouts of acute or chronic stretching (Li et al., 2013; Lin et al., 2013), but it is limited in that it does not allow for live imaging of cells. Myofibril and biochemical prep has been used for decades as a technique to study contractile changes in loaded situations, but it does not

allow for analysis of the single cell behavior. Newer methods have been developed to try and overcome the shortcomings of these approaches. Attempts have been made using magnetically actuated micropost surfaces to provide forces along the underlying surface of a cell (Sniadecki et al., 2008; Bidan et al., 2017), but these do not necessarily mimic the type of end-to-end, longitudinal strain that would primarily be felt by a CM *in vivo*. More recently, advances were made using a system that combines PDMS microgrooves with an optically ready uniaxial stretching device to capture sarcomerogenesis of a uniaxially stretched cell (Yang et al., 2016), a phenomenon that had previously been captured by our lab without the benefit of live imaging (Yu and Russell, 2005). A relatively newer approach to study cardiac mechanics is through the use engineered heart tissues. This approach often involves seeding primary myocytes or induced pluripotent stem cell-derived myocytes onto protein-based or decellularized tissues between two pillars (Schwan et al., 2016). This approach is advantageous, as cells derived from patient with specific mutations can be studied in a tissue-like preparation. A similar method has been used recently while adjusting the afterload experienced by the spontaneously contracting construct in order to better mature the tissue, highlighting the importance of the mechanical conditions used in cell & tissue culture (Leonard et al., 2018).

B. **Cardiac fibroblasts—homeostasis, migration, signaling, and pathology**

By sheer cell number, cardiac fibroblasts are the most abundant cells within the heart—naturally, they serve a major role in maintaining tissue homeostasis, structure, and intercellular communication (Zhou and Pu, 2016). Fibroblasts are a highly migratory

cell type, coinciding with their role in structural remodeling and healing at injury sites. Within the normal aging process and markedly within chronic pathologies such as hypertension and diabetes, fibroblasts are responsible for excess deposition of ECM proteins, resulting in global tissue stiffening and impaired cardiac function. The heart adapts through strengthening of the ventricle by increasing assembly of myofibrils, but this compensatory mechanism can ultimately become maladaptive and manifests as hypertrophic cardiomyopathy.

In response to ischemic injury or myocardial infarction, endogenous fibroblasts will undergo activation into the myofibroblast phenotype (Figure 2). This change is characterized by increased deposition of ECM proteins (e.g. collagen I, III, and IV; fibronectin; periostin), expression of highly contractile α-smooth muscle actin, and maturation of focal adhesions (Stempien-Otero et al., 2016). Acute injury results in increased TGF-β signaling, transition to myofibroblast state, and directed migration to the site of injury (Acharya et al., 2008). Although perhaps initially adaptive and necessary, fibroblast localization and ECM protein deposition results in substantial local stiffening of the tissue (Fu et al., 2018). For the heart, this stiffening can lead to pronounced impaired function and heart failure. Additionally, the development of electrically inert blockages or slowed electrical conduction due to fibrosis is a major cause of arrhythmias and can serve only to compound the problem of cardiac fibrosis (Nguyen et al., 2017).

Although highly responsive to acute injury and changes in demand, the heart has a limited capacity to remodel existing matrix in order to improve function. As a result, elucidating the physiology of cardiac fibroblasts in terms of migration, ECM deposition,

and the molecular signaling therein is imperative in developing therapies geared toward halting and perhaps reversing the maladaptive response. To do so, it is necessary to use both mechanical and pharmacological means to alter the fibroblast response.

C. Cardiomyocytes sense the mechanical environment

Cardiac tissue stiffness can vary dependent on age and disease. Methods to measure stiffness are imperfect and lead to further confusion, though AFM is often employed. Embryonic and neonatal heart stiffness is around 10 kPa as measured by AFM (Discher, 2005; Bhana, 2010), but can increase to over 70 kPa in adult rats (Yoshikawa, 1999). Post-infarct stiffness and collagen content increase with time so that by 6 weeks, it may rise to as high as 400 kPa (Fomovsky, 2010). Muscle stiffness is also dynamic, increasing when contracted (Berry, 2006; Bhana, 2010; Majkut, 2012). Isolated embryonic CMs cultured on extremely stiff surfaces do not have well-formed myofibrils, and CMs do not survive long-term when cultured on extremely soft surfaces. Furthermore, at physiological stiffness (10-30 kPa), myofibrils are robust and cells contract optimally (Discher, 2005; Engler, 2008; Jacot, 2008).

As a result of variations in blood volume, as well as long-term adaptation to static load, the CM has evolved to respond to changes in tensions through internal sensors. There are a variety of individual sensors within the CM, ranging from components of the focal adhesion complex such as vinculin and talin to proteins further downstream within the sarcomere, including titin and Z-disc components (Hoshijima et al., 2006; Pandey et al., 2018). Rapid response is reliant primarily on length-dependent activation, widely considered the primary effector in the Frank-Starling Law of the heart, via increased

myofilament Ca^{2+} sensitivity, while an additional slow response also occurs over the course of minutes (Solaro, 2007; de Tombe et al., 2010). Long-term alteration of myocyte contractility is often a product of changes to the cytoskeleton and structural remodeling of the myocyte. Moreover, due to the CM's limited capacity to undergo cell division, myofibril addition is the primary way the heart can become stronger.

In response to hypertrophic stimuli, individual CMs undergo sarcomere addition to strengthen myofibrils, which has been shown to be directly regulated at the filament by behavior of CapZ (Li et al., 2013; Lin et al., 2013) (Figure 3). For example, high blood pressure results in a need for increased contractile strength, which is generally overcome through hypertrophy of the left ventricle. This disease, or cardiomyopathy, is referred to as hypertrophic cardiomyopathy (HCM). Being associated with thickening of the ventricle and increase in CM size, sarcomeric addition occurs in a parallel fashion. In contrast to HCM, the cells of the ventricle can also become longer and thinner while the ventricular space becomes dilated, called dilated cardiomyopathy (DCM). In order for cells to lengthen, sarcomere addition in DCM occurs in series. Although the underlying causes of cardiomyopathies are often largely unknown, the phenotypes can be recapitulated *in vitro* through manipulation of mechanical stimuli. In particular, cyclic mechanical stretch has been used as a hypertrophic stimulus, resulting in increased cell size as well as sarcomere assembly dynamics (Li et al., 2013).

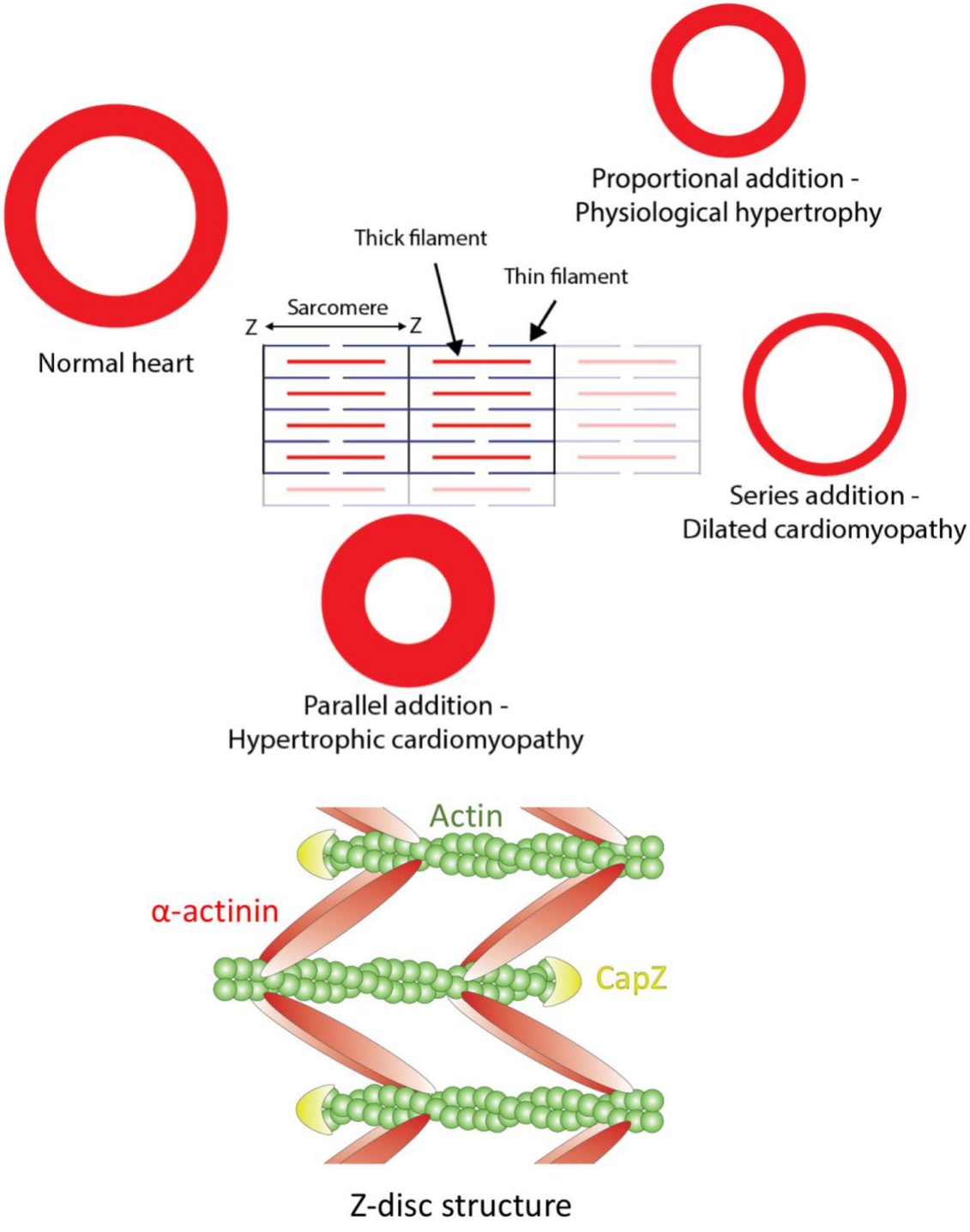

Figure 3. Models of sarcomere assembly in the heart

D. Adrenergic signaling in contractility and cytoskeletal assembly within the cardiomyocyte

A variety of pathways can be stimulated to elicit changes in contractility and cytoskeletal assembly. Signaling pathways are generally divided into ion-linked, enzyme-linked, or G-protein coupled receptors. A common chemical means of activating signaling in CMs is through the use of isoproterenol, which acts as a non-specific β-receptor agonist. Isoproterenol is particularly relevant due to its historical use in treating irregular heart rhythms. The β- and α_1-receptor pathways, with predicted signaling effects following isoproterenol treatment, are depicted in Figure 4.

In terms of cardiac contractility, isoproterenol results in increased inotropy as well as increased heart rate. This effect can be seen at both the cellular level and the organ level. Following treatment with isoproterenol, signal is internalized through the $G\alpha_s$ protein via a β-adrenergic G-protein coupled receptor (GPCR), activating the protein kinase A (PKA) signaling pathway. Cyclic adenosine monophosphate (cAMP) is produced following adenylyl cyclase activation, leading to PKA localization to the sarcomere and phosphorylation of various filament proteins. Typical sarcomeric targets for PKA include myosin binding protein C (cMyBC), titin, and troponin I (cTnI) (Kuster et al., 2012), phosphorylation of each having inotropic and relaxation effects. PKA signaling also alters calcium handling through phosphorylation of phospholamban and the ryanodine receptor (RyR), affecting chronotropy. Furthermore, increased cAMP production leads to [exchange factor directly activated by cAMP] (Epac) signaling and activation of the phospholipase C (PLC) pathway, which in turn results in activation of PKC signaling (Okumura, 2014; Li et al., 2015)—this particular signaling sequence likely

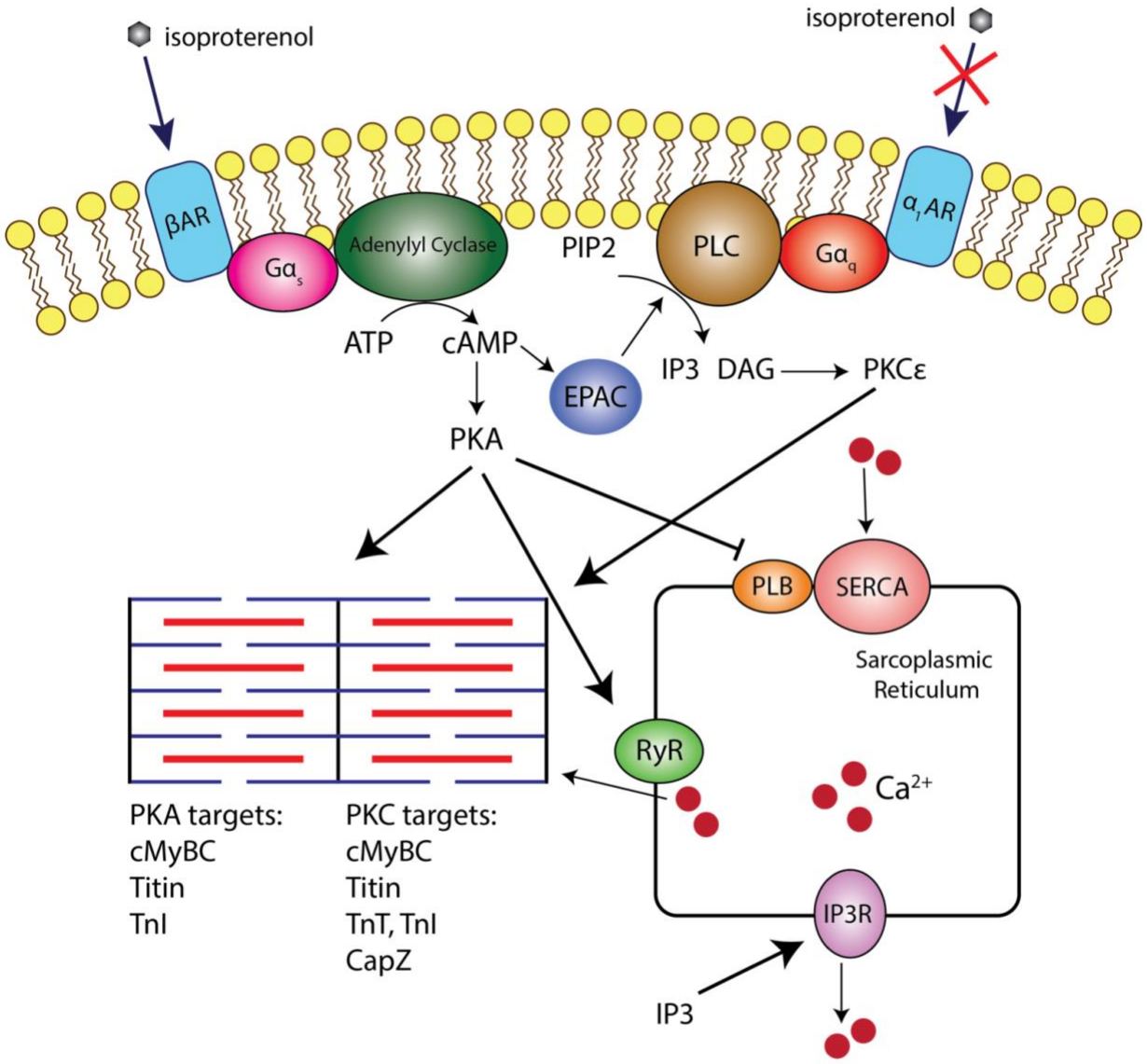

Figure 4. β-adrenergic signaling in cardiomyocytes

serves as the primary source of PKCε activation in chapter III of the thesis, PKCε being a common isoform found within the heart. Isoproterenol has been demonstrated to activate PKCε through this signaling cascade (Oesterich et al., 2009). α-adrenergic signaling within the cardiomyocyte can function through a $G\alpha_q$-coupled GPCR via the α_1-receptor, though isoproterenol has little to no affinity for these receptors. Nevertheless, this pathway leads to activation of the phospholipase C pathway, cleavage of PIP2 into diacylglycerol and inositol triphosphate, and subsequent activation of PKC for signaling at the sarcomere. Of note, the β1-receptor has been shown to have an attenuating effect on the adenosine A_1 receptor, leading to decreased PKCε translocation via a PKA-dependent mechanism (Komatsu et al., 2011).

Upon activation, PKCε undergoes rapid translocation to the membrane, anchoring preferentially via RACK2 (Csukai et al., 1997). Upon anchorage at the costamere, it has been shown to interact with the cytoskeleton to phosphorylate filament proteins such as troponin T, TnI, and cMyBC (Scruggs et al., 2006, 2016; Li et al., 2015). Our lab has demonstrated through mass spectrometry studies that actin capping protein, CapZ, is a potential target of PKCε (Lin et al., 2015). Functionally, CapZ phosphorylation leads to decreased binding affinity to the barbed end of actin, potentially due to a loosening of the β-tentacle, which serves to stabilize the protein on the filament (Lin et al., 2013). Decreased affinity of CapZ to the filament results in increased actin dynamics, which has implications for cell and tissue hypertrophy. IP3 also serves as a secondary messenger, functioning through the IP3 receptor on the sarcoplasmic reticulum to increase Ca^{2+} release to the cytoplasm (Kiviluoto et al., 2012).

Also pertinent is the direct effect of PIP2 in altering cell physiology through phospholipid-protein interactions. Although an intermediate in the PLC signaling pathway, PIP2 interacts with a variety of proteins at the focal adhesion complex. For example, PIP2 has been shown to activate auto-inhibitory activity of talin (Ye et al., 2016), clustering of FAK (Goñi et al., 2014), and also interact directly with vinculin (Goldmann, 2018). These changes can potentially lead to changes in focal adhesion stability, directly affecting mechanotransduction pathways. Our lab has also show how direct interaction of PIP2 with CapZ can lead to altered actin dynamics (Li et al., 2013).

E. Overview of studies

In the first study, I explore regulation of cell migration in cardiac fibroblasts. Cell migration is regulated by several mechanotransduction pathways, which consist of sensing and converting mechanical microenvironmental cues to internal biochemical cellular signals, such as protein phosphorylation and lipid signaling. While there has been significant progress in understanding protein changes in the context of mechanotransduction, lipid signaling is more difficult to investigate. Physical cues of stiffness (10 kPa, 100 kPa, 400 kPa, and glass), and microrod or micropost topography were manipulated in order to reprogram primary fibroblasts and assess the effects of lipid signaling on the actin cytoskeleton. In an *in vitro* wound closure assay, primary cardiac fibroblast migration velocity was significantly higher on soft polymeric substrata. Modulation of PIP2 availability through neomycin treatment nearly doubled migration velocity on 10 kPa substrata, with significant increases on all stiffnesses. The distance between focal adhesions and the lamellar membrane (using wortmannin treatment to

increase PIP2 via phosphoinositide 3 kinase (PI3K) inhibition) was significantly shorter compared to untreated fibroblasts grown on the same surface. PIP2 localized to the leading edge of migrating fibroblasts more prominently in neomycin-treated cells. The membrane-bound protein, lamellipodin, did not vary under any condition. Additionally, fifteen micron-high micropost topography, which blunts migration, concentrates PIP2 near to the post. Actin dynamics within stress fibers, measured by fluorescence recovery after photobleaching (FRAP), was not significantly different with stiffness, microtopography, nor with drug treatment. PIP2-modulating drugs delivered from microrod structures also affected migration velocity. Thus, manipulation of the microenvironment and lipid signaling regulatory drugs might be beneficial in improving therapeutics geared toward wound healing.

In the next study, I explore the effect of substrate stiffness on the response of CMs to isoproterenol treatment. The stiffness of the microenvironment surrounding a cell can result in cytoskeletal remodeling, leading to altered cell function and tissue macrostructure. For this study, I tuned the stiffness of the underlying substratum on which neonatal rat ventricular cardiomyocytes were grown in culture in order to mimic normal (10 kPa), pathological stiffness of fibrotic myocardium (100 kPa), and a non-physiological extreme (glass). CMs were then challenged by beta adrenergic receptor (βAR) stimulation through isoproterenol treatment to investigate the response to acute work demand for cells grown on surfaces of varying stiffness. In particular, the PKCε signaling pathway and its role in actin assembly dynamics were examined. Significant changes in contractile metrics were seen for CMs grown on different surfaces, but all cells responded to isoproterenol treatment, eventually reaching similar time to peak

tension (TPT). In contrast, the assembly rate of actin was significantly higher on stiff surfaces, so that only cells grown on soft surfaces were able to respond to acute isoproterenol treatment. Förster resonance energy transfer (FRET) of immunofluorescence on the cytoskeletal fraction of CMs confirmed that the molecular interaction of PKCε with the CapZ was very low on soft substrata, but significantly increased with isoproterenol treatment, or on stiff substrata. Therefore, the stiffness of the culture surface chosen for *in vitro* experiments might mask the normal signaling and affect the ability to translate basic science more effectively into human therapy. Interactions of fibroblasts and CMs with hyaluronic acid (HA) microrods are examined, as well as physiological metrics of CMs in response to rods. Additionally, localization of PKCε through flexing is studied, and a potential *in vitro* tool to study contractile behavior using magnetic microrods is assessed.

Through this work, I determine ways in which the mechanical environment elicits differential signaling responses. I combine engineering techniques with biochemical assays to elucidate the biology of cells in physiological and pathological conditions. Moreover, the mechanical properties of materials used in biological therapeutics can have potential implications on the response of cells. In order to better treat the heart undergoing various states of stiffness and disease, it is helpful to study these conditions *in vitro* to determine physiological and signaling responses.

II. LIPID SIGNALING AFFECTS PRIMARY FIBROBLAST COLLECTIVE MIGRATION AND ANCHORAGE IN RESPONSE TO STIFFNESS AND MICROTOPOGRAPHY

Text and figures adapted primarily from Mkrtschjan et al., (2017), Lipid signaling affects primary fibroblast collective migration and anchorage in response to stiffness and microtopography, Journal of Cellular Physiology; Le et al., (2018), Injectable hyaluronic acid based microrods provide local micromechanical and biochemical cues to attenuate cardiac fibrosis after myocardial infarction, Biomaterials. (See appendix)

A. Introduction

Fibroblast migration is regulated by remodeling of the actin cytoskeleton and anchorage under the plasma membrane of the advancing cell. There is good basic understanding of fibroblast behavior in response to critical chemotactic cues in the microenvironment of the wound bed (Theocharidis et al., 2015; Wells et al., 2016), but the equally powerful mechanical and topographical cues that guide fibroblasts remain unappreciated. Fibroblast proliferation, phenotype, migration, and gene expression are all affected by mechanisms that depend on mechanotransduction, whereby the cell converts a mechanical cue in its microenvironment into a chemical signaling pathway. Well-studied signals include phosphorylation of proteins, such as the integrin and focal adhesion complex (Samarel, 2014; Dupont, 2015).

Lipids are more difficult to study than proteins, but nonetheless have been shown to play a key role in mechanotransduction pathways leading to remodeling of the actin cytoskeleton. The initial mechanotransduction is almost instantaneous, whereas transcriptional regulation to control cell division and other essential properties is in the time scale of hours or days. Some transduction targets of signaling pathways are the proteins present in the actin cytoskeleton that rapidly regulate cell migration and a wide variety of physiological and pathological processes, such as those involved in wound

healing (Steinestel et al., 2015). The mechanisms underlying these rapid changes include lipid binding and post-translational modification by phosphorylation or acetylation of existing proteins that affect actin assembly or disassembly (Li and Russell, 2013; Li et al., 2014; Lin et al., 2013, 2015). Neomycin alters the level of an important phospholipid, phosphatidylinositol 4,5-bisphosphate (PIP2), in a cell, and PIP2 has been implicated in lamella formation (Safiejko-Mroczka and Bell, 1998 and 2001), subsequently affecting cell migration (Tsujita and Itoh, 2001; Wu et al., 2014). However, other evidence suggests it is not PIP2 but phosphatidylinositol 5-phosphate (PI5P) that affects cell migration (Haugsten et al., 2003).

A mechanism proposed for membrane adhesion and spreading requires continuously feeding PIP2 to the fibroblast cell periphery via actin filaments (Chierico et al., 2014). Moreover, PIP2 seems to play a role in the anchorage of the cell to the underlying flat substratum (Brückner et al., 2015). Here we report that PIP2 availability affects the velocity of the leading primary cardiac fibroblast from collective migration into a wound gap model *in vitro* (Haeger et al., 2015; Mayor and Etienne-Manneville, 2016). Furthermore, the lamellar architecture varies, suggesting that one role of PIP2 accumulation is to mediate the distance from the focal adhesions to the lamellar membrane.

Additionally, bioengineering approaches are applied to manipulate the physical cues of topography and stiffness that have been shown to reprogram stem cell and fibroblast behavior in many tissues (Doroudian et al., 2015). Here, primary rat cardiac fibroblasts are grown in culture on substrata in the physiological stiffness range (10-400 kPa) and with cell-sized microtopography in order to assess lipid signaling effects on the

actin cytoskeleton. Results show that PIP2 is regulated by these micromechanical cues to mediate changes in collective migration velocity and lamellar architecture of fibroblasts. Additionally, neomycin that affects the lipid signaling pathway was delivered by a rod-shaped polymeric microstructures and altered cell migration *in vitro*. This approach may provide a useful strategy in wound healing where fibroblast migration is an important factor.

B. Materials and Methods

a. Fabrication of substrata with varying stiffness and microtopography

Flat and microtopographical substrata of stiffness 100 kPa and 400 kPa were fabricated from PDMS (DowCorning, Midland, MI) by varying ratios of base to curing agent and spun onto cell culture glass-bottom dishes (In Vitro Scientific, Mountain View, CA), creating a surface approximately 50 μm thick, as previously described (Broughton and Russell, 2015). Softer substrata were made from PAA per protocols modified from other groups (Tse and Engler, 2010; Poellmann and Wagoner Johnson, 2013). For PAA substrata (10 kPa and 100 kPa), 40% unpolymerized acrylamide and 2% Bis solution (Bio-Rad, Hercules, CA) were diluted in water at final concentrations of 5% acrylamide, 0.3% Bis and 30% acrylamide, 0.3% Bis, respectively. Ammonium persulfate and tetraethylmethylenediamine (Bio-Rad, Hercules, CA) were added to initiate polymerization. 10 μl of the pre-polymer solution was then added to glass bottom dishes and covered with a circular coverslip. Substrata were allowed to polymerize for 10 minutes, then coverslips were gently pried up, leaving behind a flat, circular substrate. Dishes were washed 3 times in deionized water for 10 minutes at a time to remove

unpolymerized acrylamide. Indentation tests for elastic moduli using AFM were conducted to confirm stiffness, and a reference chart was created (Figure 5, Tables 1 and 2). 100 kPa PAA and 100 kPa PDMS yielded similar migration velocities, so these data were pooled for all analyses.

Microtopographical substrata were made by unmolding the PDMS (400 kPa) from a parylene template to yield 15 μm high, 25 μm wide, 75 μm spaced posts as done by us previously (Motlagh et al., 2003). Microposts unmolded with softer PDMS (100 kPa) deformed into a dome shape over time and could not be used. Additionally, PAA material did not retain three-dimensional structure with parylene templates.

b. Functionalization of substrata for cell culture

PDMS surfaces were functionalized with 3-aminopropyl triethoxysilane (Sigma Aldrich, St. Louis, MO) and coated with 10 μg/ml fibronectin. To functionalize the PAA for cell adhesion, substrata were treated twice by drying sulfosuccinimidyl 6-(4'-azido-2'-nitrophenylamino)hexanoate (sulfo-SANPAH) (ThermoFisher, Waltham, MA) in HEPES (50 mM, pH 8.5) on each surface for 60 minutes at 57°C. A UV exposure box (Spectronics Corporation, Westbury, NY) with a 365 nm bulb was used to link sulfo-SANPAH to substrata. Substrata were washed 3 times then covered in HEPES containing fibronectin (10 μg/ml) at 37 °C for at least 2 hours before UV-sterilizing in water for 20 minutes.

In order to rule out issues with the quantity of fibronectin covalently attached to the substrata in terms of distribution and uniformity of coating, coated and uncoated substrata were examined after fixation in 10% formalin and probed with 1:100 anti-

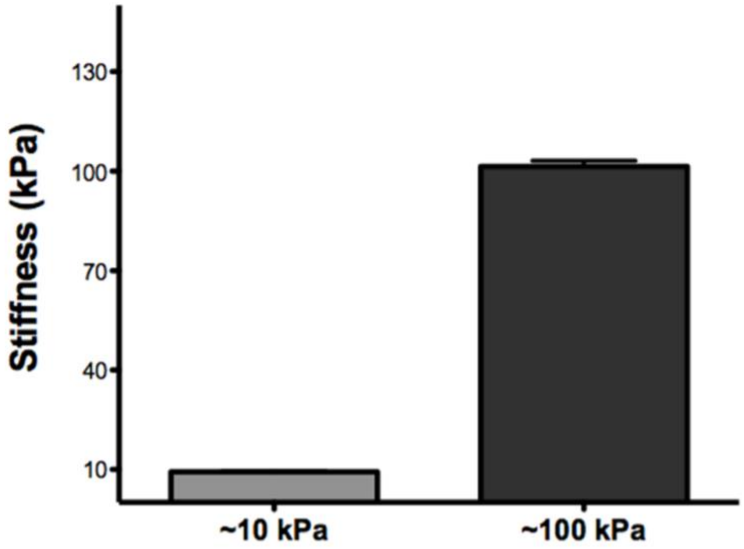

	~10 kPa	~100 kPa
	10.2219	112.2610
	9.4121	96.8087
	9.1350	101.9320
	8.7870	100.4640
	8.8704	101.7610
		99.5865
		98.1403
		100.6110
Average	9.2853±0.2585 kPa	101.4456±1.6629 kPa

Figure 5, Table 1. AFM measurements of 10 kPa and 100 kPa polyacrylamide substrata. Indentation measurements were performed on potential acrylamide mixtures to obtain approximately 10 kPa and 100 kPa polyacrylamide substrata.

%Acrylamide	Stiffness (kPa)	μL Acrylamide	μL Bis	μL Water
3	1.78	75	150	775
4	3.24	100	150	750
5	9.29	125	150	725
9	28.74	225	150	625
11	32.88	275	150	575
12	33.96	300	150	550
15.11	45.92	377.75	150	472.25
17	48.94	425	150	425
18	60.32	450	150	400
23	69.50	575	150	275
30	101.45	750	150	100

Table 2. Polyacrylamide gel stiffness reference chart. A reference chart for 3% Bis polyacrylamide hydrogels, based on AFM indentation measurements.

fibronectin antibody (Abcam, cat. ab-26245, Cambridge, MA) following standard substrate preparation. Surfaces were imaged using confocal microscopy, and no discernible differences to coating density and uniformity were seen, consistent with previous studies (Doroudian et al., 2013).

c. Microrod fabrication

50% v/v or 90% v/v solutions of poly(ethylene glycol) dimethacrylate (PEGDMA) MW 750 (Sigma Aldrich, St. Louis, MO) were prepared in phosphate-buffered saline (PBS). Photoinitiator 2,2-dimethoxy-2-phenylacetophenone was dissolved in 1-n-vinyl-pyrrolidone (100 mg/mL) and added to 50% PEGDMA (20 kPa) or 90% PEGDMA (60 kPa) precursor solutions to a final 1% concentration of photoinitiator. Photolithography was used to fabricate microrods that are 100 μm x 15 μm x 15 μm (Ayala et al., 2010).

d. Microrod degradation

To assess degradation, microrods were resuspended in sterile, warm saline and shaken in an incubator at 37° C. Phase microscopic images recorded over a period of 2 months were used to determine the rate of degradation by width measurement using ImageJ software. The mean width of 20 isolated microrods was measured at each time point.

e. Neomycin loading of microrods

Microrods (100 μm x 15 μm^2) have a volume of 22,500 μm^3 and the desired concentration of neomycin in the microrods needs to be equivalent to the drug delivered

from solution in the media. In order to achieve the maximum drug concentration, the microrods were resuspended for 24 hours at room temperature in 500 mg/mL neomycin trisulfate salt hydrate solution (Sigma-Aldrich, cat. no. 1405-10-3, St. Louis, MO). Microrods were centrifuged, supernatant removed, and resuspended in media for immediate use. Cells were then treated with neomycin-loaded microrods and compared with the drug added directly to media.

f. Neomycin delivery from microrods

50% or 90% PEGDMA microrods were loaded with neomycin as described above and washed 3 times by centrifugation immediately before starting the release study. The microrods were then incubated in 300 µl of PBS at 37°C. At each time point (1, 2, 3, 6, and 12 hours), the microrods were centrifuged and 200 µl of supernatant was removed and saved for analysis. 200 µl of fresh PBS was added and allowed to incubate until the next time point. 200 µl of each sample was placed into a UV-transparent plate and quantified by absorbance at 285 nm using a SpectraMax M5 by Molecular Devices, LLC (Sunnyvale, CA). The amount of neomycin released was normalized to total number of microrods and presented as neomycin per 50k microrods.

g. Fibroblast cell culture

All research animals were obtained and used in accordance with the guidelines of the NIH (Guide for the Care and Use of Laboratory Animals, 1996). Animal studies were approved by UIC institutional animal care and use committee and conducted according to the NIH Guide for the Care and Use of Laboratory Animals. Hearts were

removed and cells isolated from 1- to 2-day-old Sprague-Dawley rats using collagenase type II (Worthington, Lakewood, NJ) as previously described (Boateng et al., 2003). Cells were plated in 10 cm tissue culture dishes and neonatal rat ventricular fibroblasts (NRVFs) given one hour to attach before removing surrounding media along with unattached cells. Fibroblasts were incubated in DMEM (10% FBS, high glucose, pyruvate) (ThermoFisher, Waltham, MA) and plated at desired density on fibronectin-coated (10 μg/ml) dishes. Experiments were conducted on cells through no more than two passages.

h. Removable barrier wound closure migration assay and drug treatment

The traditional scratch assay gouged the soft surface, and therefore, that method was not used for migration studies. Following substrata functionalization and fibronectin coating, cloning cylinders were placed in the dish to form a removable barrier (Figure 6). Cells were added to the inner and outer compartments to obtain a density in each of approximately 35,000 cells/cm^2 and incubated for 48 hours. Cylinders were then removed gently creating a gap, approximately 500 μm wide devoid of cells into which cells could migrate. Phase images of fibroblast migration were taken using a Zeiss Axio Observer microscope with AxioVision software (Carl Zeiss, Oberkochen, Germany) following barrier removal at one hour (t1) and again after 7 hours (t7) to study the migration on different stiffness. Analysis was done using ImageJ software. Measurements from images at t1 and at t7 yielded the size of the gap in microns. Noting that cells are migrating from both sides, the gap distance was divided by two and the cell migration velocity was calculated in μm/hr. At barrier removal, fibroblasts were

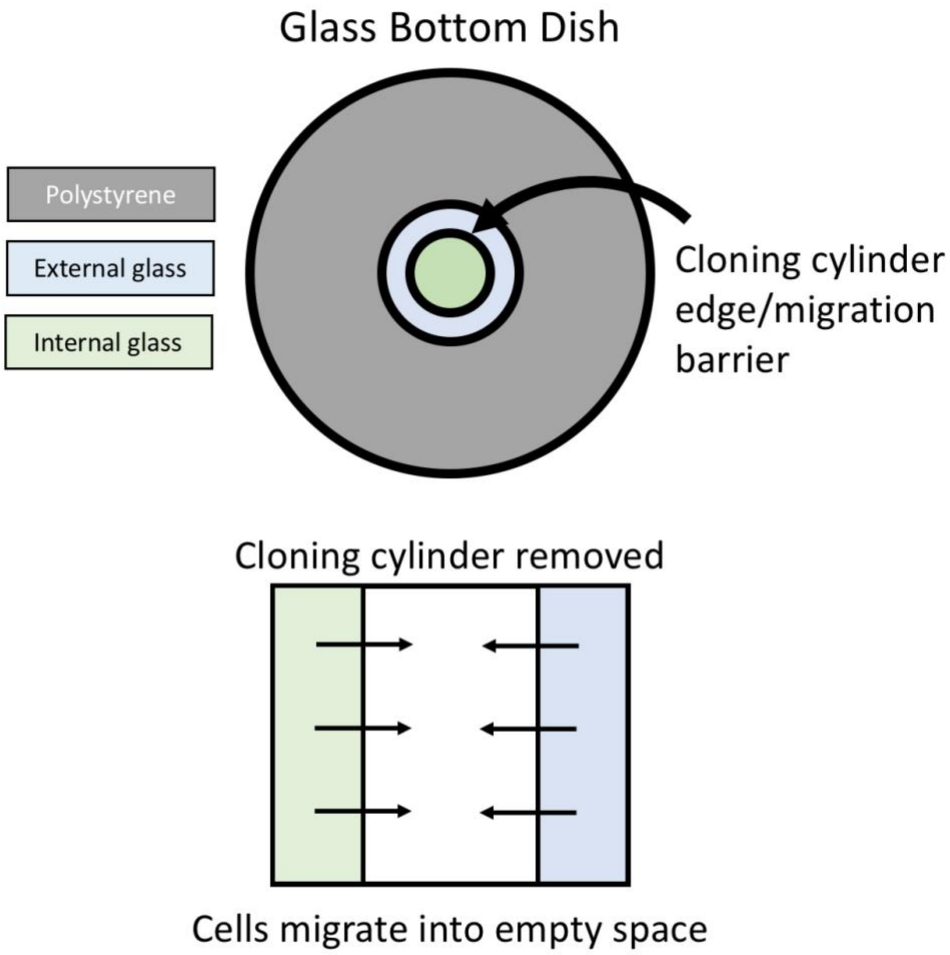

Figure 6. Schematic for cloning cylinder wound closure model. Cells are seeded at equal densities within and outside the cloning cylinder. Following 48-hour culture, the cylinder is gently removed to allow cells to migrate into the empty space that is created. If called for, cells are treated with drugs at time of barrier removal.

subjected to treatment with drugs that reduce PIP2 availability (neomycin, 500 μM) or increase PIP2 (wortmannin, 1 μM) (Sigma-Aldrich, cat. no. 19545-26-7). For migration assays, at least three separate cultures were analyzed per experimental condition, and at least two random regions were analyzed per culture.

i. Distance to lamellar membrane from end of actin fiber at focal adhesion

Fibroblasts grown on 10 kPa, 100 kPa, 400 kPa, or glass and treated with neomycin or wortmannin were fixed in 10% formalin at 7 hours after barrier removal, probed for focal adhesions with an antibody to phospho-paxillin [Y113] (Abcam, cat. ab32084, Cambridge, MA) in a 1% bovine serum albumin (BSA), 0.1% Tween-20 solution. Cells were then probed with 1:400 rhodamine phalloidin and secondary antibodies (ThermoFisher, Waltham, MA), mounted in a DAPI-containing solution (Vector laboratories, Burlingame, CA) to counterstain for nuclei, and imaged on a Zeiss Axio Observer microscope with AxioVision software. The actin fiber ending closest to the center of the lamella was determined and measurements were taken from it and the two to the right and left, resulting in five measurements per cell. The distances from the paxillin at the end of the 5 actin fibers to the lamellar periphery were measured using ImageJ software and averaged for each condition of stiffness and drug treatment. Cells at the leading edge of the wound closure were selected in an unbiased manner for each condition with about 5 cells in at least 3 cell cultures, yielding approximately 15 cells per condition.

j. Localization of lamellar proteins and lipids

Cells were treated as previously described to probe for actin and nuclei. Additionally, cells were probed at a 1:200 dilution with antibodies to lamellipodin (Santa Cruz, cat. sc-68380, Dallas, TX), PIP2 (Abcam, cat. ab2335, Cambridge, MA), or phosphatidylinositol 3,4,5-triphosphate (PIP3) (Echelon Biosciences, cat. Z-P345, Salt Lake City, UT). Secondary antibodies, Alexa Fluor 488 and Alexa Fluor 568, (ThermoFisher, Waltham, MA) were used at a 1:400 dilution. A Zeiss LSM 710 confocal microscope or Zeiss Axio Observer were used for imaging.

k. Gradient of PIP2 and PIP3 near the lamella membrane with drug treatment

The distribution of PIP2 and PIP3 detected by antibodies was quantified for fibroblasts grown on glass and selected in an unbiased manner, as described above. 5 line scans were taken through the leading edge of the cells in the direction of movement into the gap created by barrier removal. The average optical density for the five line scans was determined in arbitrary units for the 10 μm from the lamellar membrane and for five 10 μm line scans within the interior region surrounding the nucleus. Ratios of lamellar/interior were calculated to compile a histogram with at least 5 cells from at least 3 separate cultures.

Additionally, a PIP2 biosensor (PLCδ(C1-PH)-GFP) was used to detect distribution (Raucher et al., 2000). Cells were transfected with 0.05 μg of plasmid per 10,000 cells using a lipofectamine 3000 transfection system (ThermoFisher, Waltham, MA) and incubated for two days prior to viewing.

l. Actin dynamic exchange by fluorescence recovery after photobleaching

NRVFs were infected with actin-GFP virus (Invitrogen, cat. C10582, Carlsbad, CA) by incubation 24 hours prior to live-cell imaging, per previously used protocols (Lin et al., 2013). FRAP of actin-GFP was used to obtain the kinetic rate constant (kfrap, measured in s^{-1}). Fibroblasts were grown on either flat 10 kPa, 100 kPa, or 400 kPa substrata or anchored to 400 kPa microposts. Neomycin and wortmannin were applied to cells grown on glass. The region of interest (ROI) for FRAP was a uniform area along a stress fiber within the interior of the cell. The ROI was bleached to at least 40% initial intensity by a 488 nm laser. The recovery curve was fit to a nonlinear regression using OriginPro software to determine actin kfrap as an indication of the rate of actin assembly (Lin et al., 2013). For FRAP assays, the sample number was defined as individual cells, of which one to three cells were analyzed per culture and at least three separate cultures analyzed per experimental condition.

m. Time course of micropost attachment of cells

Cells were plated onto 400 kPa stiffness micropost substrata at a density of 100 cells/mm^2 and treated with neomycin (500 μM), wortmannin (1 μM), or left untreated. Images were collected every hour for the first four hours and again at 24 hours. Low magnification mages were analyzed for the total number of cells fully visible in the image, as well as the number of cells with at least one part of the cell terminating at a post. This anchorage at a post was used to score a cell as attached.

n. Statistics

Data were organized using Excel software (Microsoft, Redmond, CA) and statistical analysis was performed using GraphPad Prism (GraphPad Software, La Jolla, CA), all data are expressed as means ± SEM. Statistical significance was calculated using 1-way ANOVA with appropriate posttests.

C. Results

a. Fibroblast gap closure and substrate stiffness

After removal of the barrier, some fibroblasts leave the denser cell sheet and migrate into the gap devoid of cells over time (Figures 7A and B). Fibroblasts gap closure occurred at different velocities for fibroblasts grown on flat surfaces of PAA (10 kPa, 100 kPa), PDMS (100 kPa, 400 kPa) or glass. Untreated fibroblasts grown on 10 kPa PAA migrated the fastest at 5.14 μm/hr, while 100 kPa was 4.53 μm/hour, 400 kPa was 4.04 μm/hour and on glass surfaces was 4.54 μm/hour (Figure 7C). Untreated fibroblasts on 400 kPA were significantly slower at closing the gap compared to untreated cells on the 10 kPa surface ($p < 0.05$).

b. Migration gap closure rate is controlled by PIP2 signaling

When treated with neomycin, significant increases in migration velocity to close the gap were observed in 10 kPa, 100 kPa, 400 kPa and glass surfaces compared to untreated cells on the same stiffness ($p < 0.05$), Figure 7C. With neomycin, the fibroblast migration velocity was significant increased under all conditions and wortmannin treatment significantly retarded migration in 100 kPa, 400 kPa and glass surfaces compared to untreated groups. (Figure 7C).

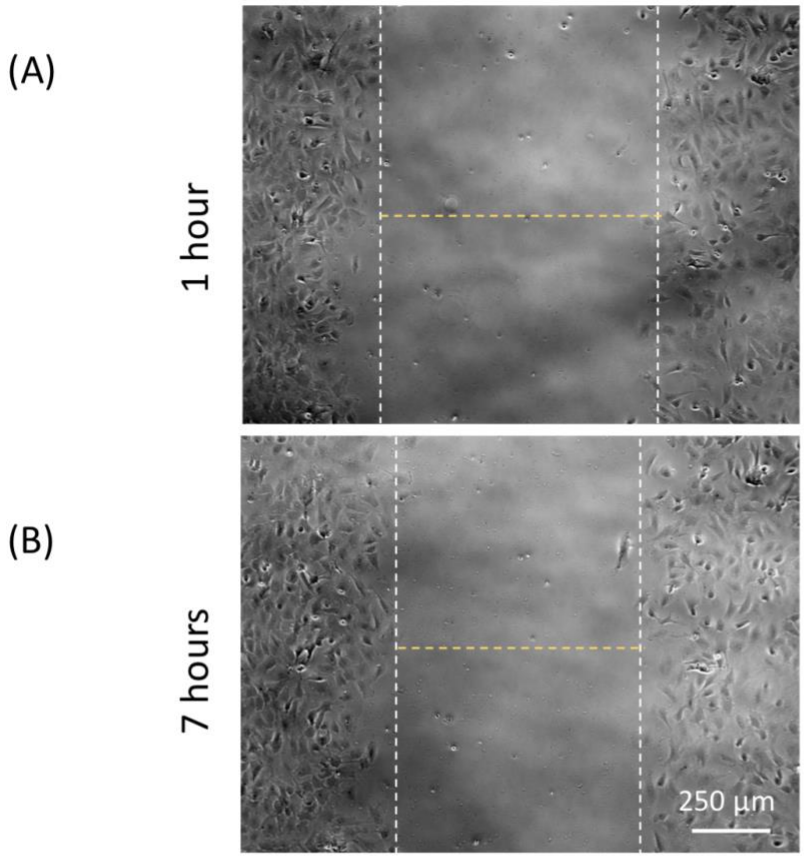
(A)
1 hour
(B)
7 hours
250 µm

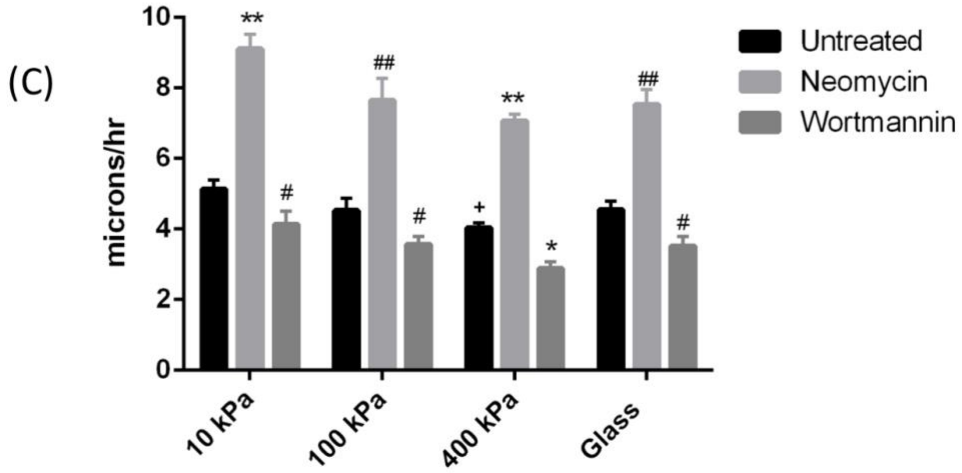
(C)
microns/hr
10
8
6
4
2
0
**
##
#
#
+
**
*
##
#
10 kPa
100 kPa
400 kPa
Glass
Untreated
Neomycin
Wortmannin

Figure 7. Fibroblast migration in a wound closure model is regulated by substrate stiffness and PIP2 availability. Fibroblasts were grown on flat surfaces with stiffness varying from 10 kPa to over 1 GPa (glass) and subjected to treatment with drugs that reduce PIP2 availability (neomycin, 500 μM) or increase PIP2 via PI3K inhibition (wortmannin, 1 μM). Phase images of cells grown on glass at (A) one hour after barrier removal (t1) and (B) at 7 hours after barrier removal (t7) to show distance migrated over time (scale bar = 250 μm). (C) Migration velocity was significantly highest on the softest surface (10 kPa) of untreated fibroblast compared to 400 kPa (+ in black bars, $p < 0.05$). Migration velocities on all stiffnesses showed significant increase in migration velocity with neomycin treatment with doubling on 10 kPa. Velocities were significantly retarded with wortmannin treatment on all surfaces. Means ± SE; * $p < 0.05$, ** $p < 0.01$, # $p < 0.001$, ## $p < 0.0001$ compared to untreated of equal stiffness, n = at least 7 cultures for each condition.

c. The actin cytoskeleton and lamellar architecture are modulated by PIP2 signaling

Images of fibroblasts grown on different stiffnesses with stains for actin, paxillin, and nuclei are shown with or without drug treatments that modify PIP2 signaling (Figure 8A). The terminal focal adhesions identified by paxillin were seen at the end of actin stress fibers in fibroblasts grown on all stiffnesses and with either neomycin or wortmannin drug treatment. There were no obvious differences in amount of paxillin or actin stress fibers with stiffness alone. However, the distance between the focal adhesion and the lamellar membrane appeared to vary with stiffness and drug treatment. Quantitative measurements of these distances are shown in histograms (Figure 8B). Untreated cells were similar at all stiffnesses (10 kPa, 100 kPa, or glass). On glass, the average distance between the terminal focal adhesion and the lamellar membrane was lowest at 3.53 μm, and significantly different (p = 0.03) from untreated fibroblasts with a distance of 6.39 μm. On glass, neomycin treatment also trends to a larger distance of 8.33 μm, but this was not significant compared to untreated cells. On 10 kPa (p = 8E0.06) and 100 KPa (p = 0.0002), there were also significant differences with wortmannin treatment of all corresponding stiffness, each having the shortest distance compared to its untreated control.

The distribution of lamellipodin, PIP2, and PIP3 are shown by immunostaining for fibroblasts grown on glass surfaces (Figure 9). Lamellipodin was widely distributed along the cell membrane of the lamellae under all conditions, regardless of stiffness or drug treatment (Figure 9A). Quantitative evaluation of PIP3 distribution shows a difference between the lamellar region and the cell interior, but there was no difference

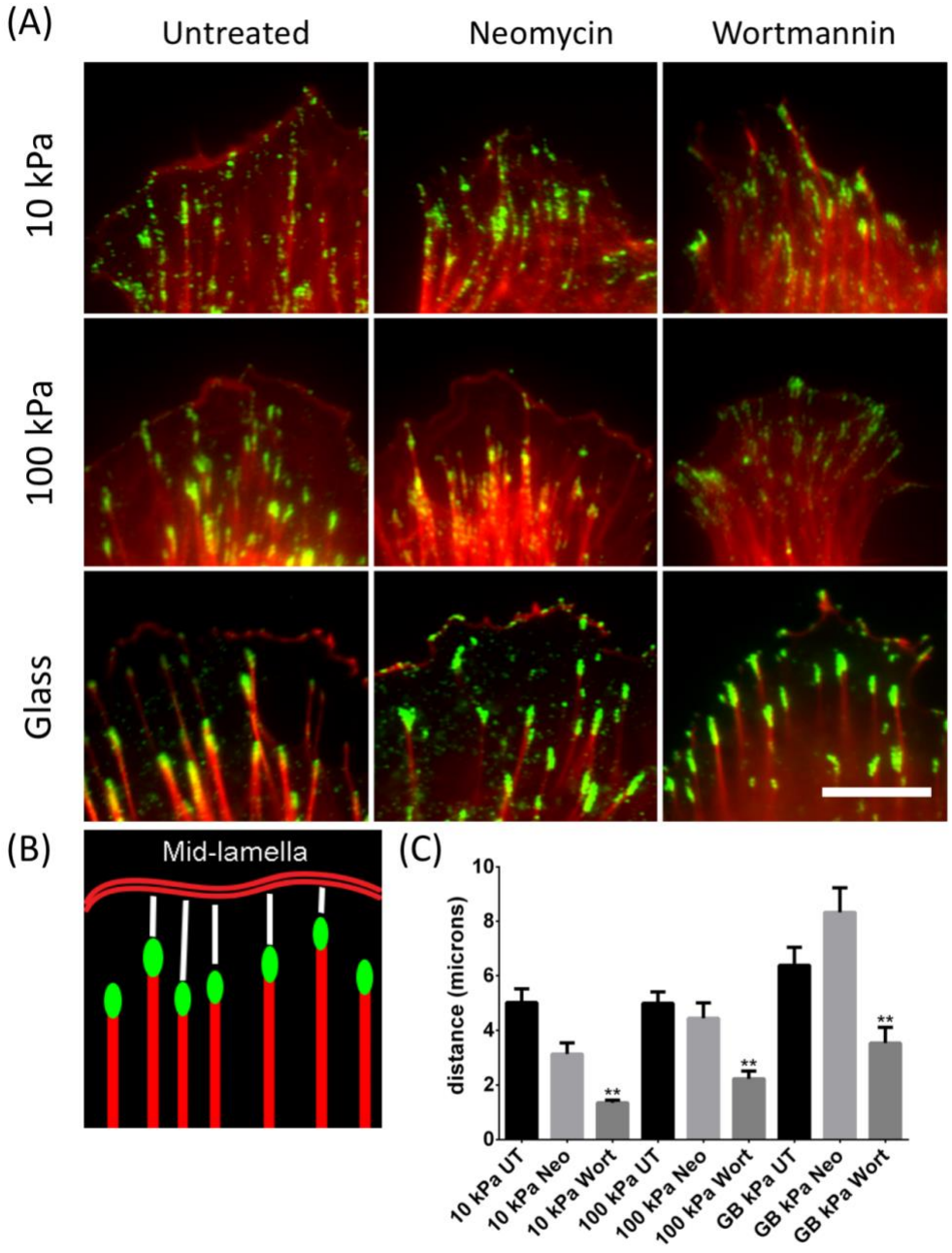
(A)
Untreated
Neomycin
Wortmannin
10 kPa
100 kPa
Glass
(B)
Mid-lamella
(C)
distance (microns)
10
8
6
4
2
0
**
**
**
10 kPa UT
10 kPa Neo
10 kPa Wort
100 kPa UT
100 kPa Neo
100 kPa Wort
GB kPa UT
GB kPa Neo
GB kPa Wort

Figure 8. Focal adhesion and actin stress fibers in leading lamella of migratory fibroblasts vary with stiffness and altered PIP2 level. Fibroblasts were grown on PAA substrate of 10 kPa or 100 kPa, or glass (> 1 GPa) stiffness and viewed with a fluorescent microscope. (A) Untreated fibroblasts (left panels), neomycin treatment (central panels), and wortmannin treatment (right panels) have similar cytoskeletal structure with actin stress fibers (red) ending in focal adhesions (green). Actin, red; nucleus, blue; focal adhesion, paxillin, green (scale bar = 10 μm). (B) Diagram to show sampling method for the distance between the focal adhesion and the lamella membrane by 5 white lines per cell. (C) Histogram with focal adhesion distance from leading edge membrane to show variation with stiffness and drug treatment. Means ± SE; ** $p < 0.01$ compared to untreated cells on same stiffness, n = at least 15 cells per condition from 3 separate cultures.

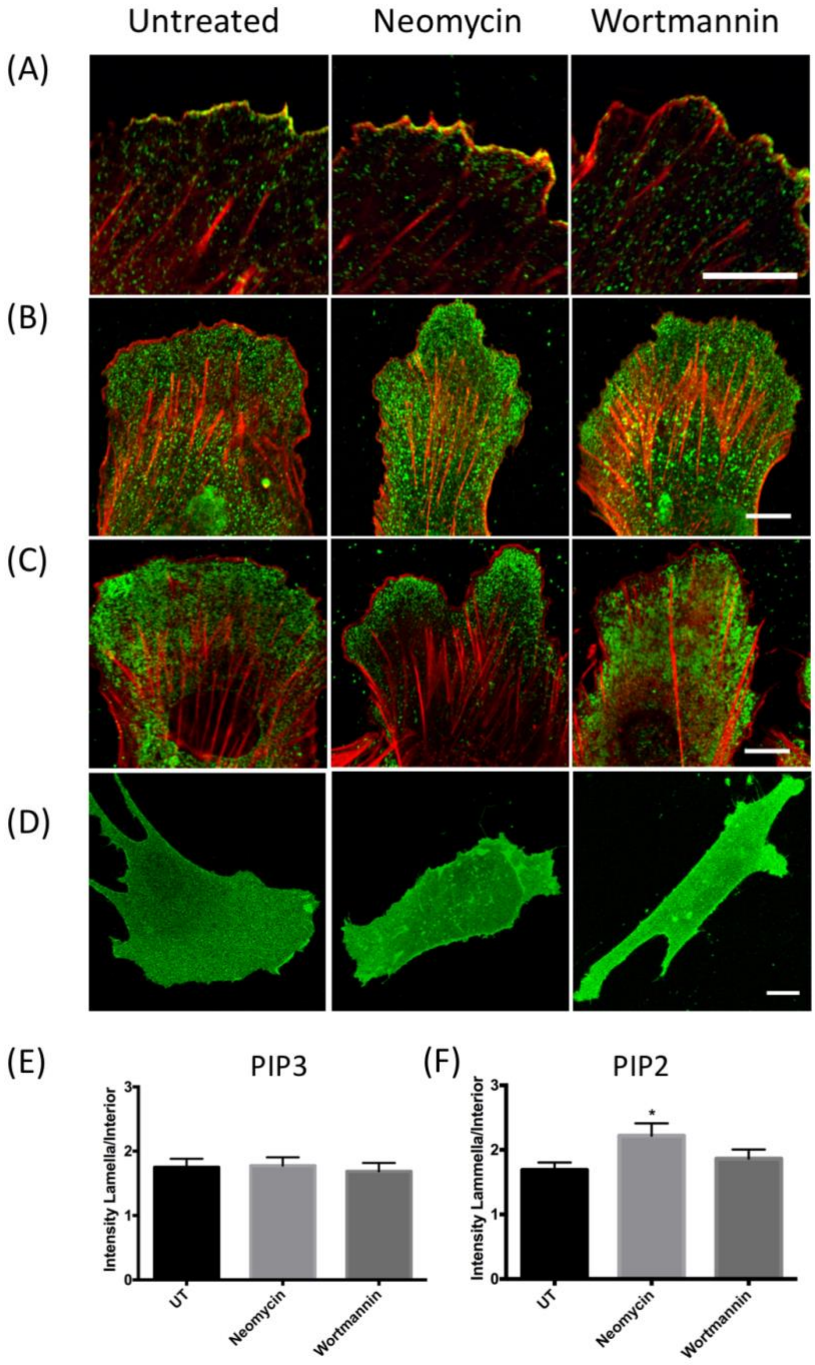
Untreated
Neomycin
Wortmannin
(A)
(B)
(C)
(D)
(E)
PIP3
Intensity Lamella/Interior
0
1
2
3
UT
Neomycin
Wortmannin
(F)
PIP2
*
Intensity Lammella/Interior
0
1
2
3
UT
Neomycin
Wortmannin

Figure 9. Localization of actin, lamellipodin, PIP2, and PIP3 with varying stiffness and altered PIP2 level. Fibroblasts grown on glass and viewed with a fluorescent microscope shown untreated (left panels), with neomycin treatment (central panels), and with wortmannin treatment (right panels). Actin, red; nucleus, blue; lamellipodin, PIP2, and PIP3 green with their respective antibodies (scale bar = 10 μm). (A) Lamellipodin is distributed on the leading edge membrane under all conditions. (B) PIP3 antibody shows diffuse pattern with elevation at lamella under all conditions. (C) PIP2 antibody shows localization near the leading edge of the fibroblast. Significantly, neomycin-treated cells show even greater localization at lamellar edge. (D) A PIP2 biosensor (green) transfected living fibroblasts grown on glass and shows a distribution similar to the PIP2 antibody detection. (E, F) Histogram to show the ratio of intensity of PIP3 or PIP2, respectively from ten microns near the leading edge to ten microns in the cell interior. PIP3 shows no difference between treatments. Ratio of lamellar to interior PIP2 is significantly higher in neomycin-treated cells compared to untreated. Means ± SE; * $p < 0.05$, n = 23 cells for PIP3, n = 32 cells for PIP2.

between treatments (Figure 9B and E).

PIP2 appears to concentrate at the leading edge of the migrating fibroblast (Figure 9C) in all conditions, but lamellar PIP2 is significantly higher in the neomycin-treated cells compared to untreated. The biosensor detection method for the PIP2 domain showed a similar appearance (Figure 9D). Quantitative assessment of the gradients of at least 5 cells in 3 separate cultures shows the lamellar/interior PIP2 with neomycin treatment is 2.22 times, which is a significant increase compared to untreated control (p = 0.02) (Figure 9F). No difference was seen with wortmannin treatment.

d. Microtopography: localization of cytoskeleton, PIP2, and PIP3

The three-dimensional micropost topography as seen by scanning electron microscopy was maintained with 400 kPa stiffness (Figures 10A and B). Microstructure shaped into microrods are seen with phase microscopy (Figures 10C and D).

Fibroblasts grown with microrods form strong focal adhesions and have many actin stress fibers, as shown through paxillin and actin fluorescence (Figure 11A). Cells grown on the microtopographical 400 kPa surface seen with three-dimensional confocal miscopy showed a diffuse PIP3 pattern through the entire cell away from the post viewed in confocal Z-stack (Figure 11B). In contrast, PIP2 aggregates around the micropost topography (Figure 11C).

Optimal actin-GFP viral infection concentration was determined (Figure 12). The kfrap kinetic rate constant of actin-GFP was measured in s^{-1} in fibroblasts on stress fibers of cells on flat or micropost topography (Figures 13A and B). There was no significant difference for stress fibers grown on varying stiffness, or with micropost

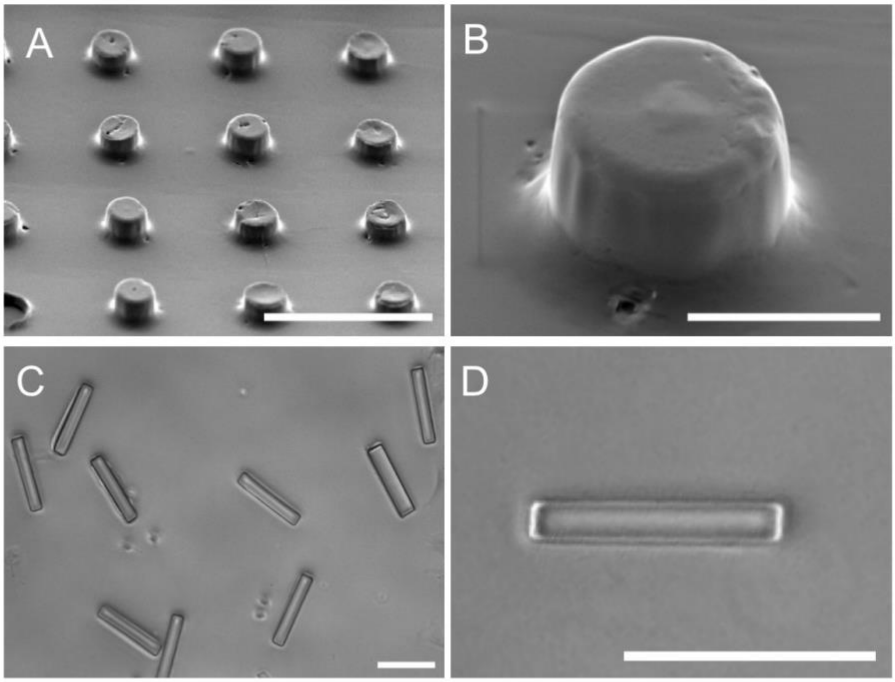

Figure 10. Micropost topography and microrods. Micropost topography fabricated by unmolding PDMS (400 kPa) from the template. Micropost surface is viewed by scanning electron microscopy from 45° angle (A) with low magnification showing tetragonal array (75 µm apart, 15 µm high and 25 µm diameter) (scale bar = 75 µm) and (B) at higher magnification (scale bar = 15 µm). Phase image of PEGDMA microrods showing shape (C) at low magnification (scale bar = 75 µm) and (D) at high magnification (scale bar = 100 µm).

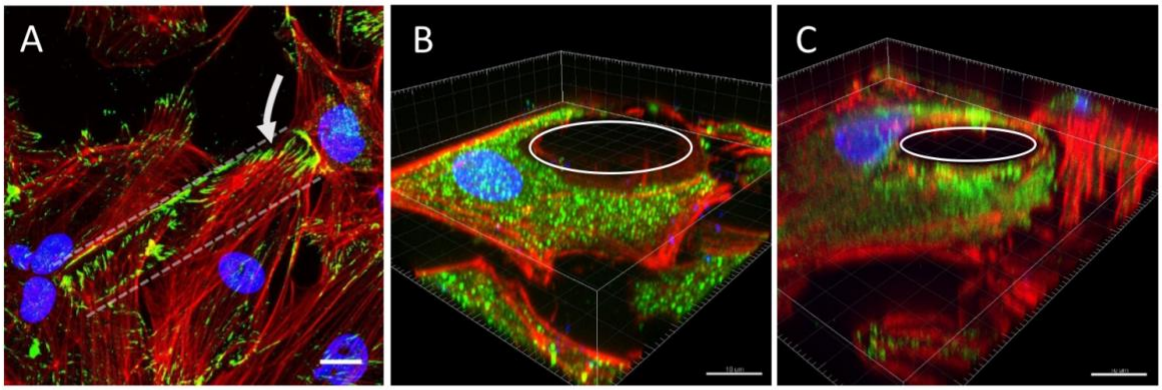

Figure 11. Microtopography and distribution of actin, PIP2, and PIP3. (A) Fibroblasts grown with microrod (between dashed lines) show strong focal adhesion formation (white arrow). (B, C) Fibroblasts on microtopography (PDMS, 400 kPa), show cells attached to micropost (top indicated by white line). Actin, red; nucleus, blue; PIP3, or PIP2 (B, C respectively), green (scale bar = 15 µm). PIP3 pattern is diffuse to cell periphery but PIP2 shows increased localization around microposts.

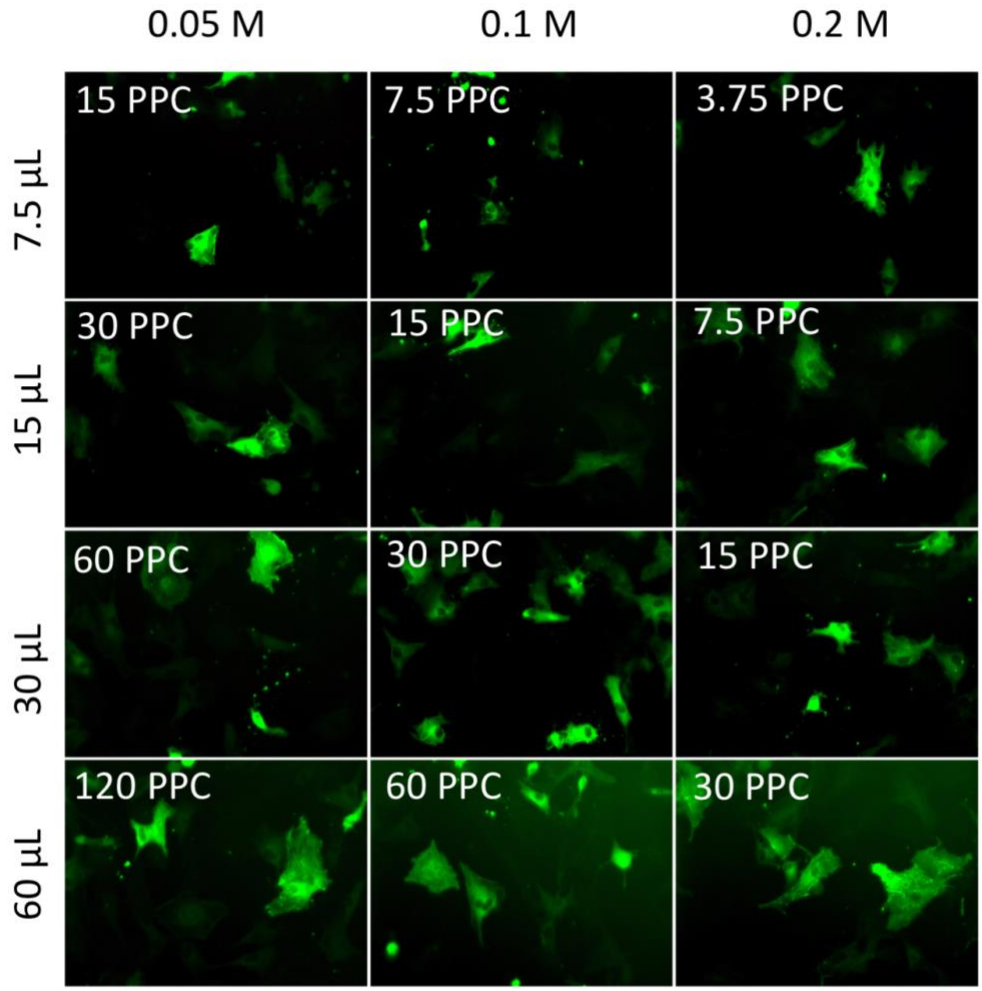

Figure 12. Actin-GFP concentration determination. Serial dilution of CellLight Actin-GFP, BacMam 2.0 was done to determine optimal concentration for use with primary cardiac fibroblasts. 15 PPC, 0.1M cells was chosen for subsequent experiments.

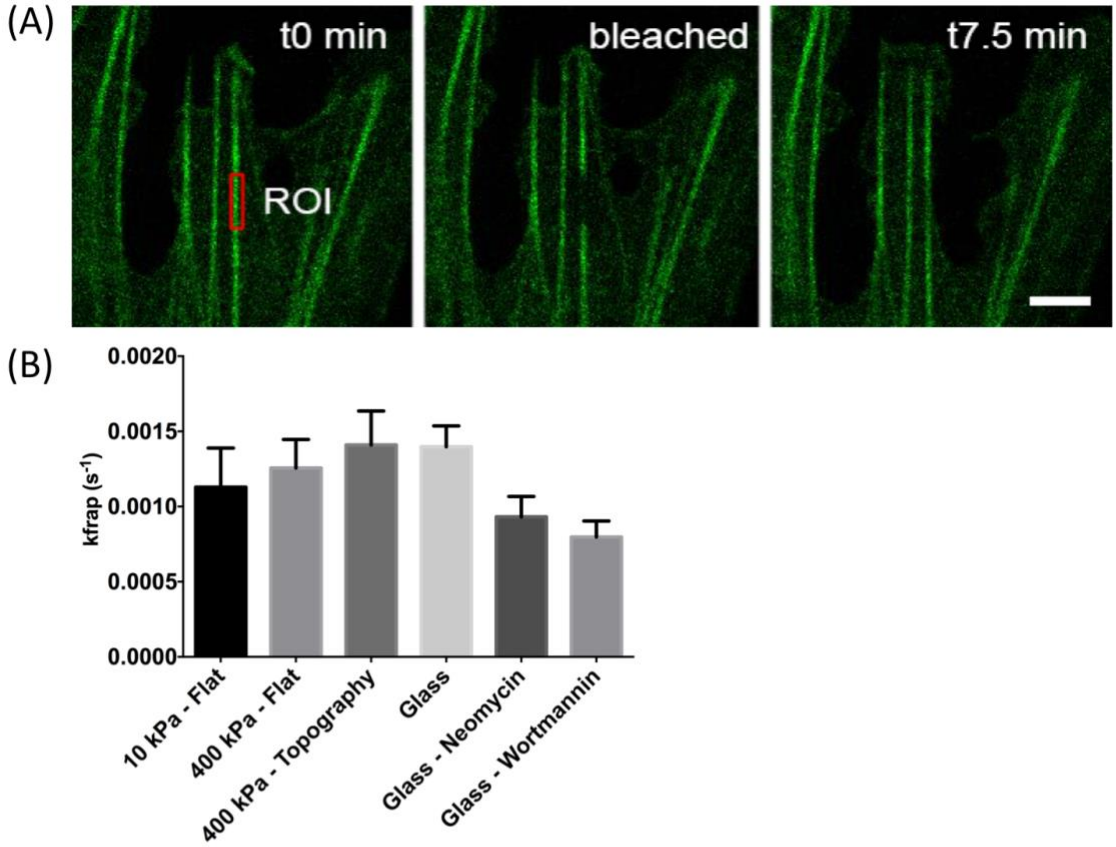

Figure 13. Stress fiber dynamics are not regulated by stiffness or altered PIP2. (A) To measure actin dynamics, a stress fiber region of interest (red box) was bleached to approximately 40% initial intensity by a 488 nm laser at high power and observed during recovery in cells grown on flat 10 kPa, 400 kPa, or glass surfaces, microtopography, or on glass with neomycin or wortmannin treatment (scale bar = 5 μm). (B) Time course of recovery of fluorescence intensity determined kfrap kinetic constant was not significantly difference on different stiffnesses, microtopography, or with drug treatment. Means ± SE. FRAP experiments in different conditions were conducted on cells from at least 3 separate cultures.

anchorage compared to an unattached cell (Figure 13E). Moreover, drug treatment with neomycin or wortmannin had no significant effect on kinetics.

e. Degradation of microrods

Continuous shaking in saline at 37 °C did not degrade microrods over 2 months. At day 1 and at 2 months, the width of microrods was approximately 15 μm. There was no significant difference in the mean width value of the microrods, implying no degradation under these conditions.

f. Neomycin delivery from PEGDMA microrods

The kinetics of neomycin release was assessed for both 50% or 90% PEGDMA microrods. As expected, 50% PEGDMA microrods released more neomycin compared to the 90% PEGDMA microrods, likely due to increased water and higher loading capacity (Figure 14A).

Neomycin released from PEGDMA microrods altered the fibroblast migration after removal of the barrier (Figure 14B). Blank microrods of different stiffness do not increase the migration velocity, which is similar to untreated at 4.54 μm/hour. The migration velocity increases with the neomycin release from the 50% PEGDMA microrods at 10.64 μm/hour, which is higher than the direct neomycin application (7.53 μm/hour, $p < 0.01$). However, the 90% PEGDMA microrods show a similar migration velocity (7.36 μm/hour, $p < 0.0001$) compared to the direct neomycin treatment.

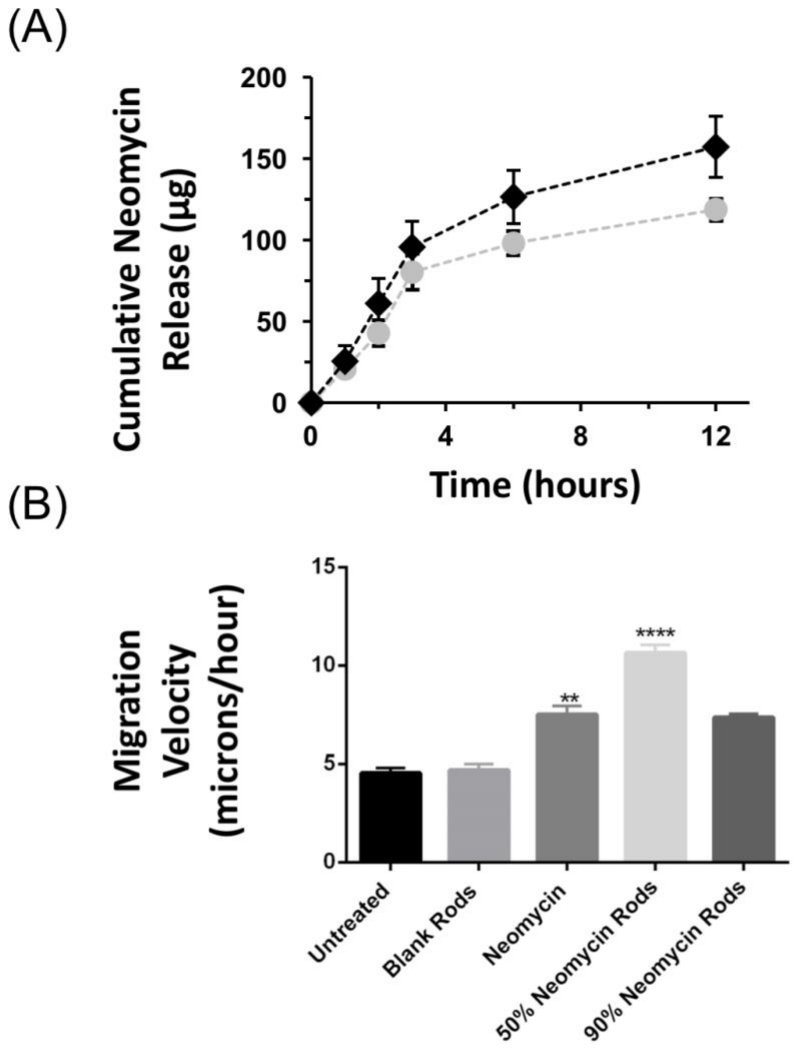

Figure 14. Release of neomycin from PEGDMA microrods. (A) Cumulative release of neomycin from 50,000 microrods in a 12-hour time period. Diamond from 50% PEGDMA, circle from 90% PEGDMA microrods. (B) Migration velocity of primary rat cardiac fibroblast grown on glass was significantly higher with neomycin delivered as a drug to the media or released from 50% PEGDMA microrods. Migration was not significantly different for blank microrods or from 90% PEGDMA microrods. Means ± SE; ** $p < 0.01$, **** $p < 0.0001$, n = at least 5.

g. Time course of fibroblast attachment to micropost topography with neomycin or wortmannin treatment

Fibroblast rate of attachment to micropost topography was assessed by low magnification brightfield imaging (Figure 15). A representative image from an untreated experiment is given, showing cells attached within the tetragonal micropost array (Figure 15A). Bar graph shows ratio of attached cells to total cells (Figure 15B) or through line graph (Figure 15C). Untreated and neomycin-treated cells did not show any difference in rate of attachment. Wortmannin-treated cells attached significantly slower than untreated control at each of the first four time points ($p < 0.05$, $p < 0.05$, $p < 0.0001$, $p < 0.0001$, respectively). At 24 hours, there was no difference in attachment of cells to microposts, as the vast majority of cells were now anchored. A linear regression of the first four hours of attachment was done for each condition to demonstrate the lower rate of attachment in wortmannin-treated cells (Figure 15D).

h. Interactions of fibroblasts and cardiomyocytes with hyaluronic acid rods

Additionally, interactions of NRVFs and CMs with HA rods were assessed. Fibroblasts cultured with HA rods and probed for paxillin and actin show prominent focal adhesions and direct interaction with rods (Figure 16). NRVFs and CMs were also probed for CD44 surface receptor (Abcam, ab157107, Cambridge, MA) (Figure 17). NRVFs show much greater expression of CD44 compared to myocytes, as well as direct association with HA rods. Contractile behavior of CMs was also studied in order to determine potential negative and positive effects on inotropy. No significant difference in beat rate or TPT were seen when cultured with HA rods or free HA (Figure 18).

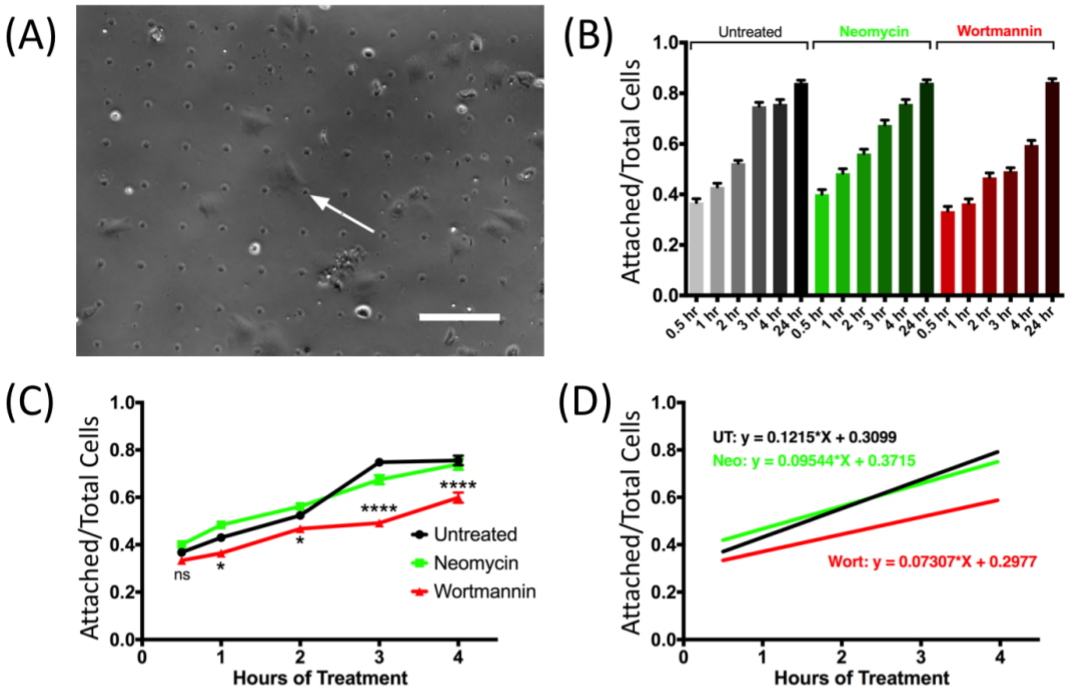

Figure 15. Fibroblasts attach more slowly to post microtopography when treated with wortmannin. (A) Representative brightfield image of fibroblasts on topographical substrata at four hours post plating. Scale bar = 100 µm. (B) % of cells attached in UT (grey), neomycin-treated (green), and wortmannin-treated (red) cells. Darkness of gradient increases with increasing attachment. (C) First four hours following treatment, showing lag of attachment in wortmannin-treated cells. (D) Linear fit of attachment curves. Mean ± SE. * $p < 0.05$, **** $p < 0.0001$. n = 5 frames per condition/time point over at least 3 separate experiments.

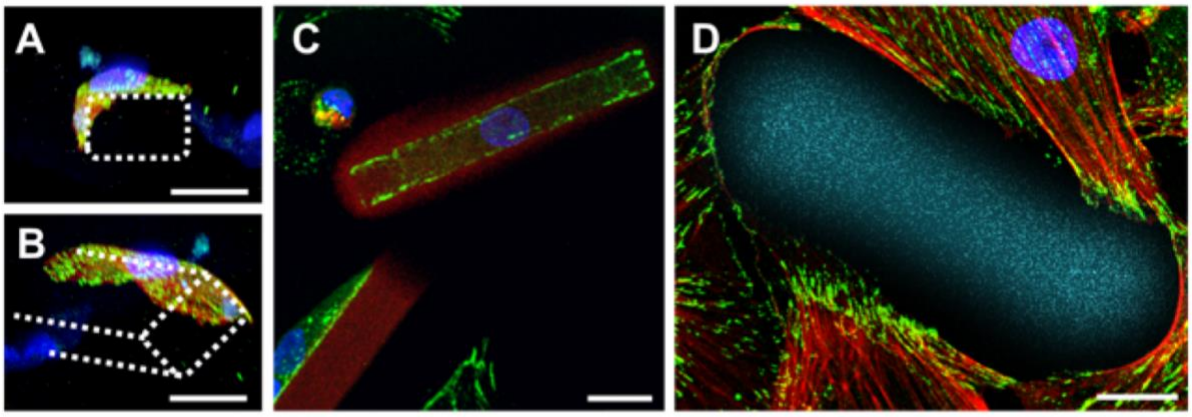

Figure 16. Fibroblasts interact with HA microrods *in vitro*. (A-D) Fluorescent immunofluorescent stain show that neonatal rat ventricular fibroblasts are highly interactive with HA microrods, actin (red), paxillin (green), nuclei (blue). Scale bars = 20 µm.

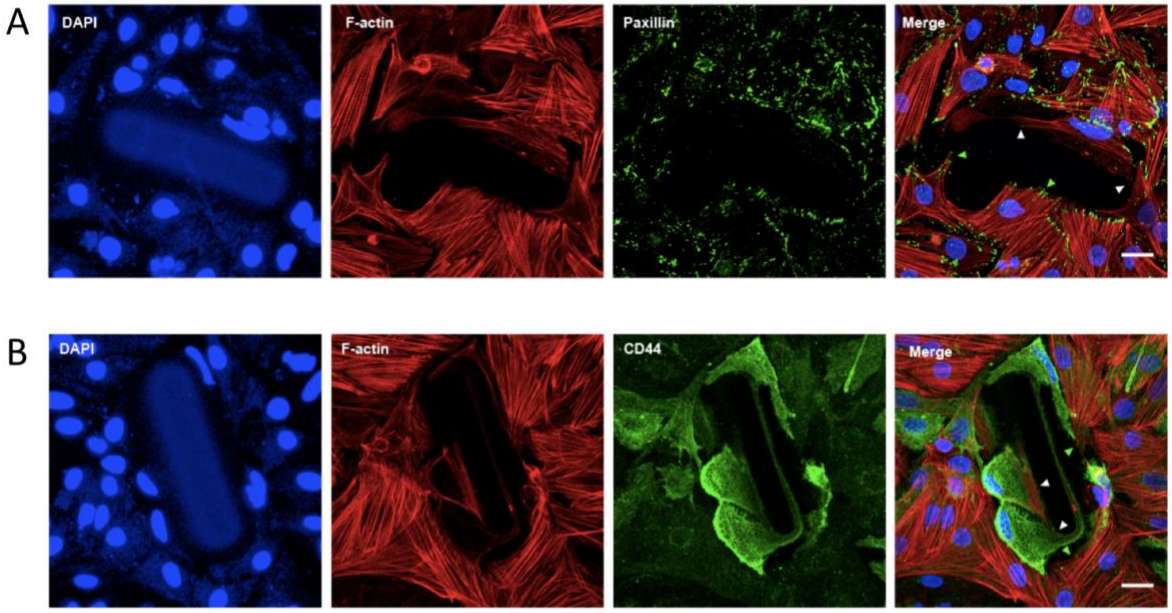

Figure 17. Interaction of HA microrods with primary neonatal ventricular cardiac myocytes and fibroblasts in co-culture. (A) Interaction between HA microrods with focal adhesions (paxillin) and myocytes (green arrows) and fibroblasts (white arrows). (B) CD44 receptor is more abundant in fibroblasts (white arrows) than in myocytes (green arrows). Staining of nucleus and HA microrods by DAPI (blue); F-actin by phalloidin (red); paxillin and CD44 with their respective antibodies (green). Scale bars = 20 µm

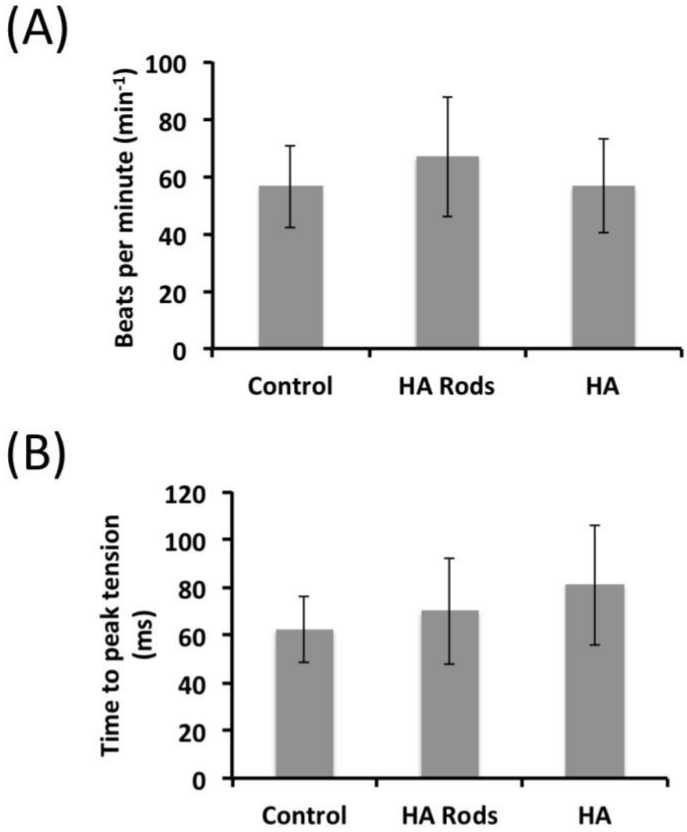

Figure 18. HA microrods and free HA do not interfere with the contractile properties of neonatal ventricular cardiomyocytes. Myocytes were platted on glass-bottom dishes (Control), in the presence of HA rods (HA Rods), or chronically incubated with 0.042 mg of HA per dish (HA). On the second day of incubation, kymographs derived from cross-sectional lines with DIC illumination were used to derive the beats per minute (A) and time to peak tension (B). For HA rods, line scans were developed on myocytes with high proximity to HA rods. No significance is found by multiple comparison of groups (mean ± SD; n=15, 15, and 14 for control, HA rods, and HA measurements, respectively, derived from three independent experiments).

D. Discussion

Fibroblast lamella formation is known to be regulated by substrate stiffness with remodeling of the actin cytoskeleton through many signaling pathways including PIP2 (Safiejko-Mroczka and Bell, 1998 and 2001). For the first time, a mechanism linking migration from the leading edge of a cell in a wound closure assay *in vitro* suggests dependence on the lamella architecture and actin cytoskeleton remodeling is related to the underlying lipid signaling pathway. Drug treatments to alter phospholipid availability show that cell migration depends on the level of production and distribution of PIP2. The distance between focal adhesions and the lamellar membrane was significantly shortest with wortmannin treatment (a PI3K inhibitor) compared to untreated fibroblasts grown on the same surface. The micromechanics imposed on the cell by increased substrate stiffness or by microtopography leads to strongly anchored fibroblasts, with PIP2 increasing near the micropost. The use of the PIP2 scavenger, the antibiotic neomycin, might affect its wound healing properties, since it doubles cell migration velocity on 10 kPa, a stiffness likely to occur in a wound.

Micromechanics, cell migration and the actin cytoskeleton

Mechanical feedback between mechanosensing and cytoskeleton of cells is important for collective migration in cell colonies (Lange and Fabry, 2013). Durotaxis is the term given to the net migration of cells on a flat surface with a stiffness gradient. Since cells decrease in velocity as the surface stiffens, the net result over time is an accumulation of cells at the stiff end (Harland et al., 2011). It is interesting to note that cells develop tension internally by myosin motor force generation against the actin

cytoskeleton. This net local tension explains the effect of crowds and sheets via collective migration versus individual cells in the migration of sheets (Ng et al., 2012; Haeger et al., 2015; Mayor and Etienne-Manneville, 2016).

This study focuses on the mechanisms underlying the mechanical cues to cell migration in addition to cell anchorage. Actin binding proteins control actin polymerization and formation of parallel bundles in stress fibers by formin or in branched networks of the spreading lamella by Arp2/3 (Hotulainen and Lappalainen, 2006; Koster and Mayor, 2016; Grikscheit and Grosse, 2016). Cells have a cortical layer with proteins binding the actin filaments to the membranes through PIP2 (Brückner et al., 2015). They also have dorsal stress cables for actin treadmilling to propel the cell forward. Immunofluorescent images of actin stress fibers show that distance of the actin cable anchored by a focal adhesion to the lamella membrane depended on PIP2 availability. Decreasing PIP2 availability could also lead to decreased WASP assembly activity, which is an Arp2/3 activator (Zhang et al., 2012).

The role of PIP2 signaling

The role of signaling pathways and cell migration in response to mechanical changes are most often reported for the TGF-β pathway after receptor binding, mediated by kinases and phosphatases (Samarel, 2014). Less is known about the lipid signaling pathways such as PIP2. Here, cell migration was retarded by wortmannin treatment, effectively increasing the presence of PIP2 by blocking the addition of a phosphate group to the 3' position of the phosphoinositide. Conversely, the PIP2 scavenger, neomycin, decreased the availability of PIP2, leading to near doubling of the

velocity of cellular migration on 10 kPa substrata. Interpretation of the role of PIP2 is complex because it is distributed on membranes throughout the cell and also binds to hydrophobic pockets of numerous actin binding proteins. For example, ezrin, focal adhesion kinase (FAK), talin, vinculin, and paxillin associate with each other and the cell membrane. Some of these partnering proteins control actin polymerization at sites far from the membrane, such as the muscle actin capping protein, CapZ (Li and Russell, 2013, Lin et al., 2015). Thus, lowering PIP2 may have a secondary effect on the actin stress fibers within the cell anchored for focal adhesions to a micropost or those involved in actin polymerization and treadmilling.

Cell migration depends on pushing the cell forward, so the effects of PIP2 on migration are likely to be at the actin binding complexes mediated by PIP2 located in the inner membrane bilayer by its hydrophobic fatty acid tails. PIP2 can be transported via actin stress cables (Chierico et al., 2014). Thus, neomycin reduction of PIP2 could prevent the linkage from the cortical actin via a protein like ezrin to the PIP2 in the membrane. Lack of ezrin bound in the membrane bilayer decreased the surface tension of the cell and allowed fluidity, which might enhance migration (Brückner, 2015). Furthermore, the Arp2/3 complex binds to PIP2 so that neomycin scavenging would be predicted to prevent the normal actin mesh from forming in the lamella (Koster and Mayor, 2016). Interestingly, the stress fiber binding partner is formin, and a lack of PIP2 would prevent the anchorage of the stress bundle to the membrane, disabling a filopodia from pulling a membrane sheath around it (Koster and Mayor, 2016). Moreover, phosphatidylinositol metabolism has been shown to induce membrane ruffling, and PIP2, which serves as a membrane dock for cytosolic phospholipase A,

would have increased presence in wortmannin-treated cells (Moes et al., 2010).

Lamellar protrusion initiates and defines the direction of cell movement in a PI3K dependent manner (Welf et al., 2012). Increased migration of breast cancer cells was observed due to the reduction of a pro-migratory molecule like Pfn1 through enhanced lamellar targeting of Ena/VASP proteins. Stable lamellar protrusion is a characteristic feature of gliding cell movement and involves lamellipodin (Bae et al., 2009). However, we did not find any difference in lamellipodin distribution under any condition.

Contact inhibition, anchorage and stress fiber formation

Contact inhibition and cell anchorage are generally viewed as the key mechanisms for the prevention of cell migration. This is usually thought to be mediated by a chemical process where the ligand and receptor interact to form focal adhesions. Surprisingly, a physical object without chemical cues is also effective. At the micron scale, anchored micropost projections blunted migration and blocked cell proliferation of fibroblasts in culture while similarly shaped unanchored objects did not (Boateng et al., 2003). The authors concluded cell properties are driven by the reactive forces first recognized in Newton's Third Law. Our lab has previously demonstrated an increased abundance of focal adhesion formation when cells bind to the microposts, leading to better anchorage of stem cells, fibroblasts, and cardiac myocytes in culture (Motlagh et al., 2003; Doroudian et al., 2013; Broughton and Russell, 2015). The mechanical and topographical cues act through mechanotransduction signaling pathways to form focal adhesions (Samarel, 2014). Initial attachment to microposts was slowed with

wortmannin treatment, perhaps indicating aberrations in focal adhesion formation in these cells.

PIP2 also localizes around the vertical projection on microtopographical surfaces. Strongly attached focal adhesions support actin assembly and stress fiber formation. A change in actin dynamics and thin filament assembly with mechanical loading was detected in cardiac myocytes by FRAP methods (Li and Russell, 2013), where increased PIP2 led to higher kfrap values. A similar loading mechanism might have been present in fibroblasts with substrate stiffness or topography. However, FRAP actin dynamics for stress fibers were the same on all substrata regardless of stiffness, topography, or drug treatment, suggesting that the rates are the same. The explanation for failure to detect any difference might be that the ROI was in the stable central part of the stress fiber and not analyzed at the growing tip near the periphery where actin polymerization is occurring. Measurements at the ends of the stress fibers or in the lamella were attempted, but they were unsuccessful due to rapid structural changes at the cell periphery.

Relevance for wound healing

Wound healing is a major clinical issue. It is worth noting, commercially available neomycin balms are used to prevent infection of cuts. In addition to its function as an antibiotic, here an added beneficial side effect is described, namely in its interaction with PIP2 to promote migration. Neomycin has a short half-life (2 hrs) and has undesirable systemic side effects like nephrotoxicity and neurotoxicity from percutaneous absorption (Gannu et al., 2014). Nevertheless, neomycin delivered locally from microporous

microrods might be advantageous in clinical use. In a similar manner, MGF eluted over several days from PEGDMA microrods (Doroudian et al., 2014) improved cardiac function after ischemic injury (Peña et al., 2015). PEGDMA microrods were loaded with high concentrations of neomycin and maintain release over 12 hours. Hence, development of these neomycin microrod devices for a single therapeutic application to a wound might enhance the migratory behavior of cells over a period of time, resulting in improved wound closure and better scar formation.

III. PKC EPSILON SIGNALING EFFECT ON ACTIN ASSEMBLY IS DIMINISHED IN CARDIOMYOCYTES WHEN CHALLENGED TO ADDITIONAL WORK IN A STIFF MICROENVIRONMENT

Text and figures adapted primarily from Mkrtschjan et al., (2018), PKC epsilon signaling effect on actin assembly is diminished in cardiomyocytes when challenged to additional work in a stiff microenvionment, Cytoskeleton; Lin et al., (2015), Cyclic mechanical strain of myocytes modifies CapZβ1 post translationally via PKCε, Journal of Muscle Research and Cell Motility. (See appendix)

A. Introduction

In response to functional demands, muscle remodels at the macroscopic level by changing the shape, cytoskeletal content, and performance of individual CMs. The mechanisms for CM shape and strength are not fully understood, but it is likely to involve multiple processes, such as gene transcription, protein translation, post-translational modification, and the assembly of the sarcomeres in cell hypertrophy (Russell et al., 2010; Sanger et al., 2010). Exercise or chronic disease increases cell hypertrophy, which has been modeled by static or dynamic strain of CMs in culture to reveal mechanisms by which sarcomeres are added (Li and Russell, 2013; Lin et al., 2013; Sharp et al., 1997; Torsoni et al., 2005; Yang et al., 2016; Yu and Russell, 2005). Most studies are done either with acute or chronic loading models, but little is done to determine how cells respond to acute work when they are already in a chronically loaded pathological state.

It is well accepted that increased load leads to muscle bulking. A cell senses external forces impinging on it, which are balanced against forces generated internally by the sarcomere. Increased cell tension triggers mechanotransduction pathways, leading to thin filament assembly. Multiple mechanosensors detect increased

mechanical loading to initiate actin filament assembly (Hoshijima, 2006; Skwarek-Maruszewska et al., 2009). Forces are transmitted to the Z-disc, where filament assembly increases length and widthwise throughout the CM (Samarel et al., 2013). At the Z-disc, the thin actin filaments insert and reverse their polarity, making it the pivotal sarcomere assembling site in CMs (Gautel and Djinovic-Carugo, 2016). Upon mechanical stimulation of CMs, assembly may be controlled in an hour by an acute bout of activity through modification of the actin capping protein, CapZ, where load increases actin dynamics, filament assembly, and cell size (Lin et al., 2013). Mechanotransduction arising from stress or strain modifies the function of CapZ by phosphorylation via protein kinase C (PKC) (Disatnik et al., 1994; Kim et al., 2010; Wear and Cooper, 2004), lipid binding with PIP2 (Hartman et al., 2009; Li et al., 2014; Li and Russell, 2013), and through acetylation (Lin et al., 2016). Here, we concentrate on phosphorylation, which has recently been thoroughly reviewed (Scruggs et al., 2016). In particular, the PKCε isoform translocates to the Z-disc when CMs are activated (Disatnik et al., 1994), where it is anchored to the myofilaments (Hartman et al., 2009; Pyle et al., 2006; Robia et al., 2001).

Mechanobiological cues are material-dependent and result in microscale, cell-specific instructions (Desai, 2013; Engler et al., 2008; Wozniak and Chen, 2009). Stiffness of a 3D matrix significantly affects maturation and differentiation into myocytes (Jacot et al., 2010), as well as force generation (Bhana et al., 2010; Broughton and Russell, 2015; Curtis et al., 2013; Hazeltine et al., 2012). The stiffness in the heart varies during development from embryonic/neonatal myocytes 5-10 kPa (Bhana et al., 2010) to the normal adult rat myocardium of 10-70 kPa (Yoshikawa et al., 1999). Infarct

stiffness and collagen content increase dramatically with time, so that by 6-weeks post-infarct it may rise to 400 kPa (Fomovsky et al., 2010; Fomovsky and Holmes, 2010). Traditionally, cell culture is done almost exclusively using flat, hard, plastic surfaces, which poorly mimic the external forces existing in normal living tissues. Thus, most studies in culture actually mimic pathological conditions, which may obscure the more normal physiological signal transduction.

In this study, we use 10-100 kPa PAA substrata along with glass surfaces to mimic the softness of the healthy and pathological heart in order to study mechanotransduction. We explore the effects of the combination of acute and/or chronic loading on mechanosignaling by applying acute challenges through βAR stimulation of CMs cultured on substrata of varying stiffness. βAR activation by epinephrine or isoproterenol causes positive inotropy and chronotropy (Kaumann and Molenaar, 2008). We assess contractility, actin assembly, PKCε signaling and distribution, as well as the molecular interactions between PKCε and CapZ. The effect of local tension and acute demand on CM contractility is assessed by line scan kymographs (Broughton and Russell, 2015). Additionally, FRAP of actin is used to study actin dynamics (Hartman et al., 2009; Lin et al., 2013). Proteomics, colocalization, and FRET are used to study the molecular interactions of Z-disc proteins and PKCε distribution in the sarcomere. By these approaches, we determine that the effect of PKCε signaling seen in a soft environment following βAR stimulation is diminished in CMs within a stiff environment, a phenomenon that could contribute to maladaptive responses in disease state.

B. Materials and Methods

a. Isolation of neonatal rat ventricular myocytes

Primary heart cultures were obtained from 1-2 day old neonatal rats according to the Institutional Animal Care and Use Committee at the University of Illinois at Chicago. Hearts were removed and CMs isolated from 1–2 day old Sprague-Dawley rats with collagenase type II (Worthington, Lakewood, NJ) as previously described (Li et al., 2016). Neonatal rat ventricular CMs were re-suspended, filtered through a 70 μm nylon sieve to remove large material, and plated in PC–1 medium (Lonza Group, Basel, Switzerland). Dishes were coated with fibronectin for at least 2 hours prior to plating. PAA (10 kPa and 100 kPa) substrata were functionalized according to previous studies prior to incubation with fibronectin (Li et al., 2016).

b. Line scans of live cardiomyocytes to measure contraction

Following 48-hour culture and drug treatment, CMs were placed into a temperature/CO_2 chamber connected to a Zeiss 710 or 880 (Zeiss, Oberkochen, Germany) confocal microscope system. Polarized, isolated individual CMs were selected in an unbiased manner, and a single line was scanned repeatedly at high speed along the contractile axis of the CM using transmitted light. Output kymographs were then analyzed using Zen software in order to measure TPT. At least 17 cells over three separate cultures were analyzed for each condition.

c. Actin fluorescence recovery after photobleaching

CMs were grown in culture 24 hours before infecting cells with actin-GFP virus (ThermoFisher Scientific, Waltham, MA). Cells were cultured an additional 24 hours

before FRAP studies were carried out on adequately expressing striated cells within a temperature/CO_2 chamber. A region of actin was photobleached to at least 50% of its original fluorescence intensity and re-imaged every five seconds for 450 seconds to monitor the rate of fluorescence recovery. The rate constant, k_{frap}, was determined using a single parameter, non-linear regression fit in OriginLab Pro (OriginLab Corp., Northampton, MA). Measurements were taken on cultures over several months, with at least 10 cells from each condition coming from 3 or more separate cultures. The actin-GFP construct used is specific for β-actin, which has been shown to localize to the Z-disc (Benz et al., 2013). It has previously been used effectively as a reporter of actin dynamics (Lin et al., 2015).

d. Immunofluorescence

CMs were fixed using a 10% formalin solution, incubated overnight at 4°C in a 1:200 primary antibody, 1% BSA, 0.1% Tween-20 solution. Primary antibodies used for IF were anti-phospho-PKCε (S729) (pPKCε) (ab88241, abcam, Cambridge, MA), and anti-α-actinin (ab9465, abcam). Dishes were then washed and incubated at room temperature for one hour in a secondary antibody (Goat Anti-Rabbit IgG H&L Alexa Fluor 488 or Goat anti-Mouse IgG H+L Alexa Fluor 568, Cat. # A-11034 and A-11004, ThermoFisher Scientific) in PBS. Secondary antibodies were diluted at 1:400 for α-actinin and 1:200 for pPKCε. Cells were counterstained using Vectashield Antifade mounting medium with DAPI (Vector Laboratories, Burlingame, CA). No changes were observed with antibodies to total-PKCε (ab124806, abcam) under any condition, so no data are reported.

e. Analysis of PKCε localization and phosphorylation using immunofluorescence

CMs grown in all conditions were fractionated to remove the membrane and cytosol but retain the cytoskeletal and nuclear fractions using the ProteoExtract Subcellular Proteome Extraction kit (MilliporeSigma, Billerica, MA) as described previously (Boateng et al., 2007; Lin et al., 2016; Ryba et al., 2017). CMs were then probed with anti-α-actinin and pPKCε. Phosphatase inhibitor (not standard with kit, #539131, MilliporeSigma) was included to preserve sites of phosphorylation. CMs were then probed with secondary antibodies and mounted. For each material, intensity levels were normalized on a week-by-week basis to account for small variations in antibody dilutions or probing efficiency. Due to differences in optical properties, analysis was only conducted between cells grown on the same material/stiffness with the same antibody combination. For normalization, a maximum laser intensity and gain was found in untreated dishes and scaled back to account for potential experimental changes in levels, thus preventing peaking of fluorophore signal in subsequent dishes where changes might occur. This process was done for α-actinin and pPKCε. Following the setting of levels, all dishes within that stiffness and antibody combination were imaged at the same settings. Polarized, isolated CMs were chosen in an unbiased manner. Following acquisition, ImageJ (NIH, Bethesda, MD) and a MATLAB (MathWorks, Natick, MA) script were used for analysis. Five line scans of at least 5 sarcomeres within a single cell were taken of α-actinin and pPKCε. Peak intensities of each Z-disc localization were determined, averaged, and the ratio of pPKCε/α-actinin was calculated and recorded. At least 5 cells were analyzed for each condition per culture, coming from at least 3 separate cultures.

f. Immunoblotting

The extraction kit was used per manufacturer protocol with the addition of phosphatase inhibitors as above. Samples were then prepared for western blot by adding 4X Laemmli sample buffer (BioRad, Inc., Hercules, CA). Protein extracts from sarcomeric subcellular fractions were resolved by SDS/PAGE, transferred to polyvinyl difluoride. Blots were blocked for one hour in 5% non-fat skim milk at room temperature and washed three times for 10 min each in tris-buffered saline, pH 7.5, containing 0.1% Tween-20. Blots were then probed in primary antibody overnight at 4°C. Antibodies were diluted in 2.5% bovine serum albumin and used at the following dilutions: 1:1000 anti-pPKCε (S729) (#06-821, MilliporeSigma) and anti-sarcomeric α-actinin.

g. Förster resonance energy transfer for molecular interactions of phosphorylated PKCε and CapZ

FRET interactions between CapZ-GFP and pPKCε by the acceptor photobleaching method (König et al., 2006) was used to determine nano-range interaction with higher resolution than can be determined with IF confocal microscopy of the Z-disc. CMs were infected with a mouse CapZβ1-GFP adeno-associated virus (MOI 20), incubated for 1 hour, washed with media, and left overnight as described (Hartman et al., 2009). CMs were incubated with 2.5 μM isoproterenol for 1 hour. Dishes were treated with a cytosolic and membrane extraction buffer as described above. After gentle washing, CMs were fixed, incubated with a 1:100 dilution of anti-pPKCε antibody, a secondary antibody chosen because of its smaller size ($F(ab')_2$ anti-rabbit Alexa Fluor

555, A21430, ThermoFisher Scientific), a second formalin treatment to stabilize the acceptor probe, and mounted.

FRET response was determined by the acceptor photobleaching method. Serial scans of donor CapZ-GFP (ex: 488, em: 509) and acceptor (pPKCε secondary antibody, ex: 568, em: 603) signals were captured with alternating acceptor photobleaching steps in designated regions of interest (ROIs). 20 scans taken over a two to three-minute time period were necessary to attain complete bleaching of the GFP donor necessary for the FRET analysis and curve flitting. Preliminary testing showing the optimal result was with an ROI of 100x500 μm^2. Average donor fluorescence intensities in the acceptor photobleached ROI (D), a reference ROI (D_r), and a background ROI (D_b) are used to compute the FRET efficiency $E(i)$ in step i:

$$E(i)=\left[1-\left(\frac{D(0)-D_b}{D(i)-D_b}\right)\left(\frac{D_r(0)}{D_r(i)}\right)\right]\cdot 100\%$$

where $D(0)$ and $D_r(0)$ are the fluorescence intensities before the photobleaching sequence begins. The recovered transfer efficiency is estimated by extrapolation of E as a function of the acceptor intensity to the origin, in order to determine the intercept with the y-axis that represents the recovered transfer efficiency.

h. Statistics

Statistical analysis of experiments involving substrata of varying stiffness was done using one-way ANOVA followed by Tukey's multiple comparisons test. For experiments testing the response of cells grown on a single stiffness following isoproterenol treatment (3 or more groups), the untreated group was considered the

control, and one-way ANOVA followed by Dunnett's multiple comparisons test was used. Student's t-test was used in experiments comparing two groups.

C. Results

a. Substrate stiffness and increased acute demand alter contractile time to peak tension

Following culture for 48 hours, contractile measurements of CMs were made on varying substrate stiffness with or without isoproterenol treatment. A representative image of a line scan readout on a 10 kPa substrate shows characteristic peaks from which TPT were obtained (Figure 19A). Untreated cells grown on 10 kPa, 100 kPa, and glass substrata had TPT values of 144 ms, 181 ms, and 206 ms, respectively (Figure 19B). Statistically significant differences were seen in untreated 100 kPa and glass groups when compared to untreated 10 kPa group ($p < 0.01$ and $p < 0.0001$, respectively), though there was no significance between 100 kPa and glass (Figure 19B). TPT in all CMs was significantly reduced by treatment with isoproterenol compared to untreated CMs grown on 10 kPa (Figure 19C), 100 kPa (Figure 19D), or glass (Figure 19E).

b. Actin cytoskeletal assembly rate increases with isoproterenol treatment on soft substrata

Actin-GFP infected cells cultured for 48 hours were photobleached to observe the rate of fluorescence recovery of actin over a 7.5 min time period (Figure 20A). Increased substrate stiffness led to significantly increased k_{frap} on 100 kPa and glass

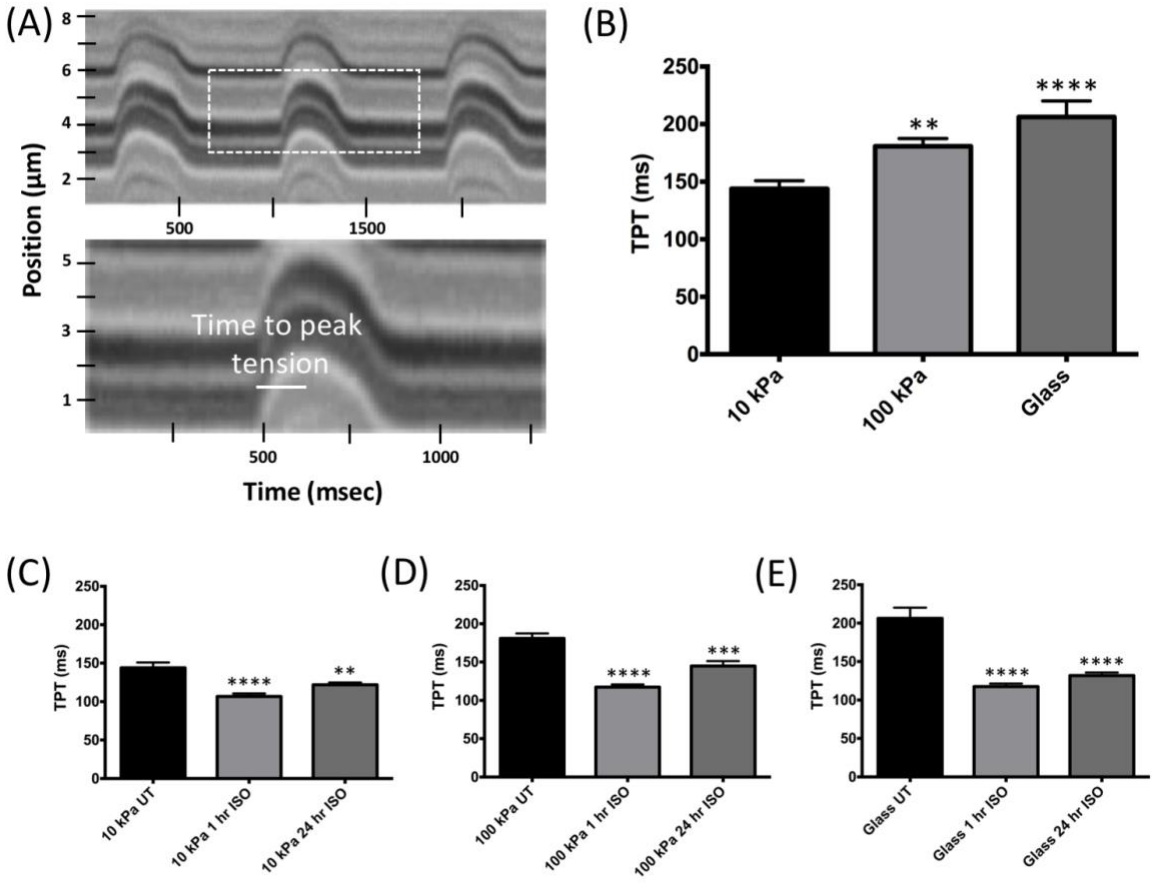

Figure 19. Contractile time to peak tension decreases with increased stiffness, and with isoproterenol treatment of CMs on soft substrata. (A) Representative line scan image acquisition showing how time to peak tension (TPT) was measured. y-axis is line scan position; x-axis is time. (B) Time to peak tension measurements for cells grown on 10 kPa (n = 28 cells), 100 kPa (n = 27 cells), and glass (n = 21 cells). CMs grown with 1- or 24-hour isoproterenol treatment on (C) 10 kPa (n = 24 and 22 for treated cells, respectively), (D) 100 kPa (n = 27 and 17 for treated cells, respectively), or (E) glass (n = 26 and 24 for treated cells, respectively). Values are mean ± SE. ** $p < 0.01$, *** $p < 0.001$, and **** $p < 0.0001$.

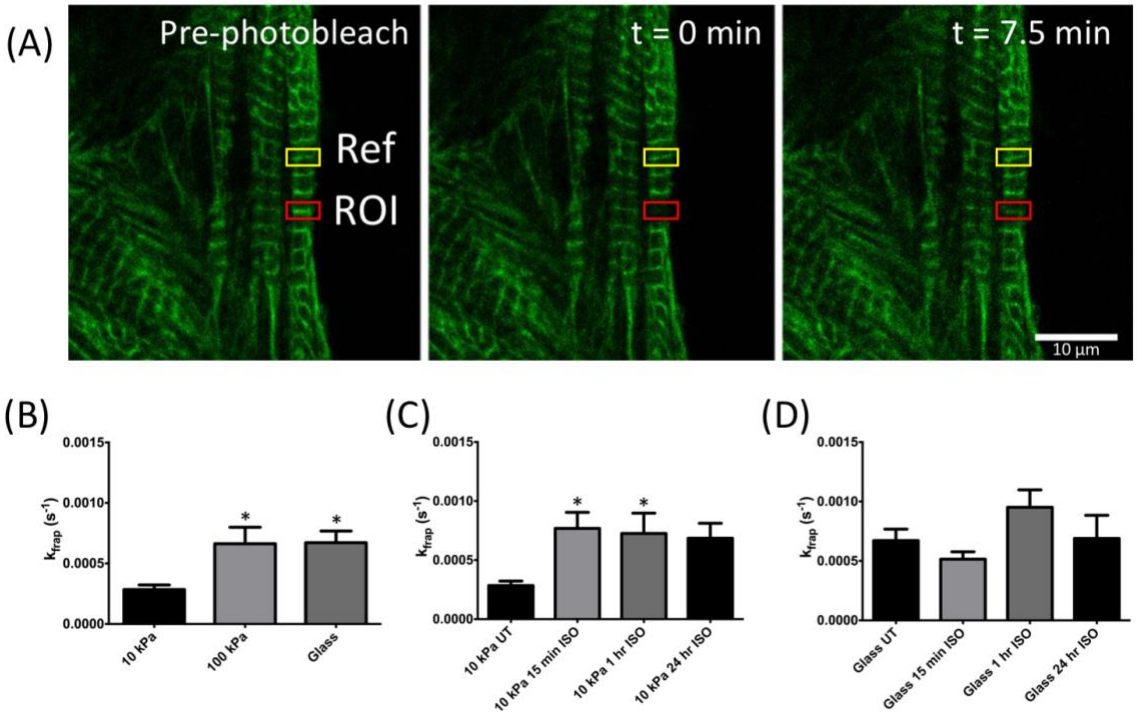

Figure 20. Actin dynamics increase with substrate stiffness, but only respond to isoproterenol treatment on 10 kPa substrata. (A) Representative images showing FRAP experiment within region of interest (red box, ROI), pre-bleached (left panel), immediately following bleaching (middle panel), and after 7.5 minutes of recovery time (right panel). Scale bar, 10 µm. (B) k_{frap} values for cells grown 10 kPa, 100 kPa, or glass substrata (n = 13, 17, and 15, respectively), and with 15-minute, 1-hour, or 24-hour isoproterenol treatment of CMs (C) on 10 kPa (n=12, 11, and 10 for treated cells, respectively), (D) or on glass (n = 12, 12, and 14 for treated cells, respectively). Values are mean ± SE. * $p < 0.05$.

substrata when compared to 10 kPa ($p < 0.05$), but no difference was observed between 100 kPa and glass groups (Figure 20B). k_{frap} values of untreated cells on 10 kPa, 100 kPa, and glass substrata were $2.8x10^{-4}$ s^{-1}, $6.6x10^{-4}$ s^{-1}, $6.7x10^{-4}$ s^{-1}, respectively. Notably, isoproterenol treatment led to significantly increased k_{frap} only on 10 kPa ($p < 0.05$ for 15-minutes and 1 hour) (Figure 20C), but there was no significant difference with isoproterenol treatment for CMs grown on glass (Figure 20D).

c. Time course of colocalization of phosphorylated PKCε and α-actinin with isoproterenol treatment of cardiomyocytes

CMs grown on 10 kPa, 100 kPa, or glass with membrane and cytosol extracted to retain the cytoskeleton were probed to study pPKCε distribution as a function of stiffness, and for the time course of increased muscle beating caused by βAR stimulation. Representative fluorescence images of pPKCε and α-actinin are shown in 10 kPa (Figure 21A) or glass (Figure 21B). Untreated CMs on 10 kPa had little yellow compared to treated groups, indicating lower colocalization at the Z-disc. A redistribution of pPKCε was seen with isoproterenol treatment as evidenced by increased yellow at the Z-disc, with peak levels reached between 15 minutes and 1 hour for cells grown on the soft substrate (Figure 21A), However, cells grown on glass remained strongly striated throughout isoproterenol treatment (Figure 21B). Line scans shown for 10 kPa and glass (left panels Figures 21A and 21B, respectively) were analyzed to acquire peak intensities and normalized to α-actinin. Histograms for ratios of pPKCε/α-actinin of fluorescence intensity (Figure 21C, D, and E for 10 kPa, 100 kPa, and glass, respectively) confirm the visual impressions. A significant difference due to

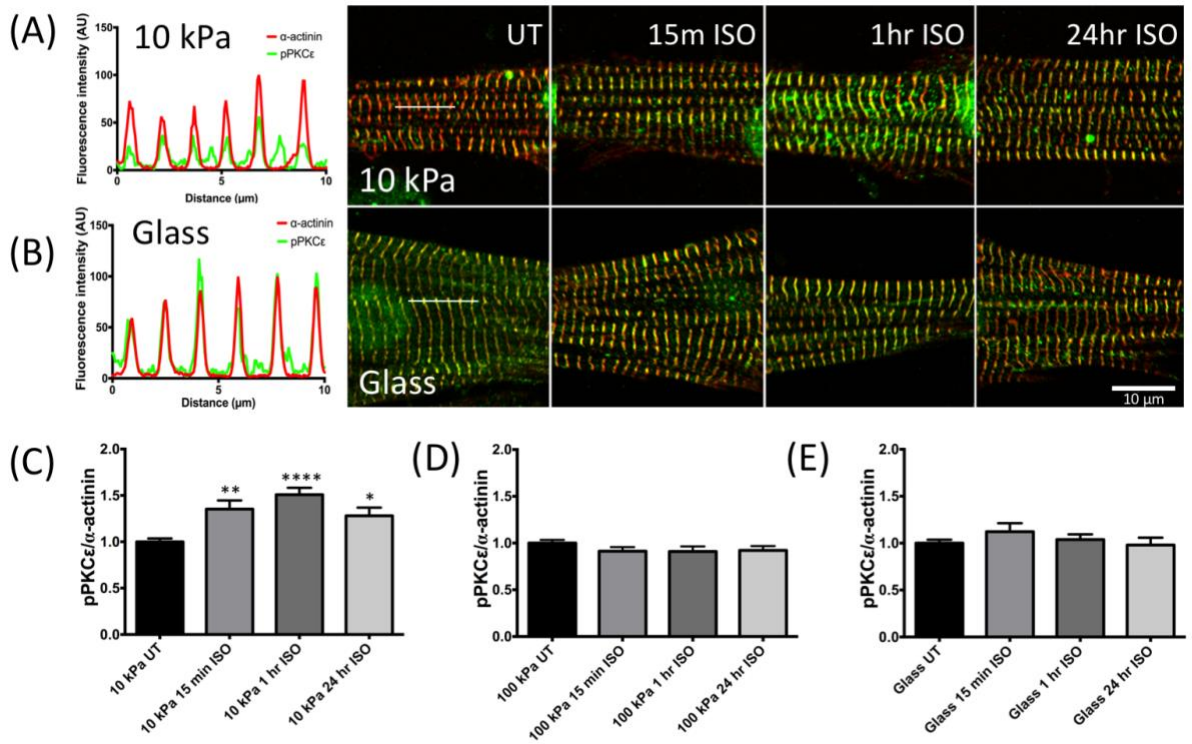

Figure 21. Immunofluorescence shows localization of phosphorylated PKCε at the Z-disc increases with isoproterenol treatment of CMs on 10 kPa substrata but not stiff substrata. Immunofluorescence images of CMs on 10 kPa or glass with phosphorylated PKCε (green), and α-actinin (red). (A) On 10 kPa substrata, pPKCε was low on untreated (UT) CMs but moved to the Z-disc with isoproterenol treatment, seen at 15 minutes, 1 hour, and 24 hours. (B) No change was seen over treatment time for cells grown on glass. (A) and (B) (left panels) show examples of line scans, drawn as white lines on UT panels, that were used to quantify colocalization of pPKCε and α-actinin with stiffness and time of isoproterenol treatment. Scale bar: 10 μm. (C), (D), (E): The ratio of pPKCε to α-actinin intensity at the Z-disc in untreated, 15-minute, 1-hour, and 24-hour isoproterenol treated cells was normalized within 10 kPa (n = 28, 18, 28, and 26 cells, respectively), 100 kPa (n = 42, 45, 34, and 42 cells, respectively), and glass (n=20 cells for all conditions) substrata, confirming increased localization only occurred on 10 kPa substrata. Values are mean ± SE. ** $p < 0.001$, **** $p < 0.0001$ compared to untreated 10 kPa group.

isoproterenol treatment was observed only on 10 kPa substrata (Figure 21C), with ratio changes at 15 min, 1 hr, and 24 hr of 1.35-, 1.51-, and 1.28-fold compared to untreated baseline ($p < 0.01$, $p < 0.0001$, $p < 0.05$, respectively). However, no changes in colocalization of pPKCε and α-actinin were observed on 100 kPa or glass. Additionally, no changes in tPKCε localization to the Z-disc were seen (Figure 22).

In order to confirm the findings of PKCε phosphorylation, an independent biochemical approach was used with Western blot analysis on the cytoskeletal fraction of CMs (Figures 23A and B). PKCε phosphorylation on 10 kPa substrata following isoproterenol treatment began to increase by 15 minutes (not significant) and reached a maximum at 1-hour ($p < 0.01$), which was sustained but not significant at 24 hours. From untreated group, changes of 1.19-, 1.63-, and 1.32-fold are seen at 15-minute, 1-hour, and 24-hour treatments, respectively. Changes were not observed with isoproterenol treatment for cells grown on stiff substrata (data not shown). Increased localization of tPKCε at the Z-disc was shown following cyclic mechanical strain for one hour, as assessed by fluorescence measurement against alpha-actinin or CapZ (Figures 24 and 25).

d. Molecular interactions of CapZ-GFP and pPKCε with stiffness and isoproterenol

Direct molecular interactions between CapZ-GFP and pPKCε were assessed by FRET (Figure 26A). Under glass and isoproterenol treatment for 1 hour, a typical ROI shown (Figure 26B left panel) was fully bleached after 20 scans (right panel), while the reference ROI was unchanged. Increasing donor fluorescence intensity (CapZ, green)

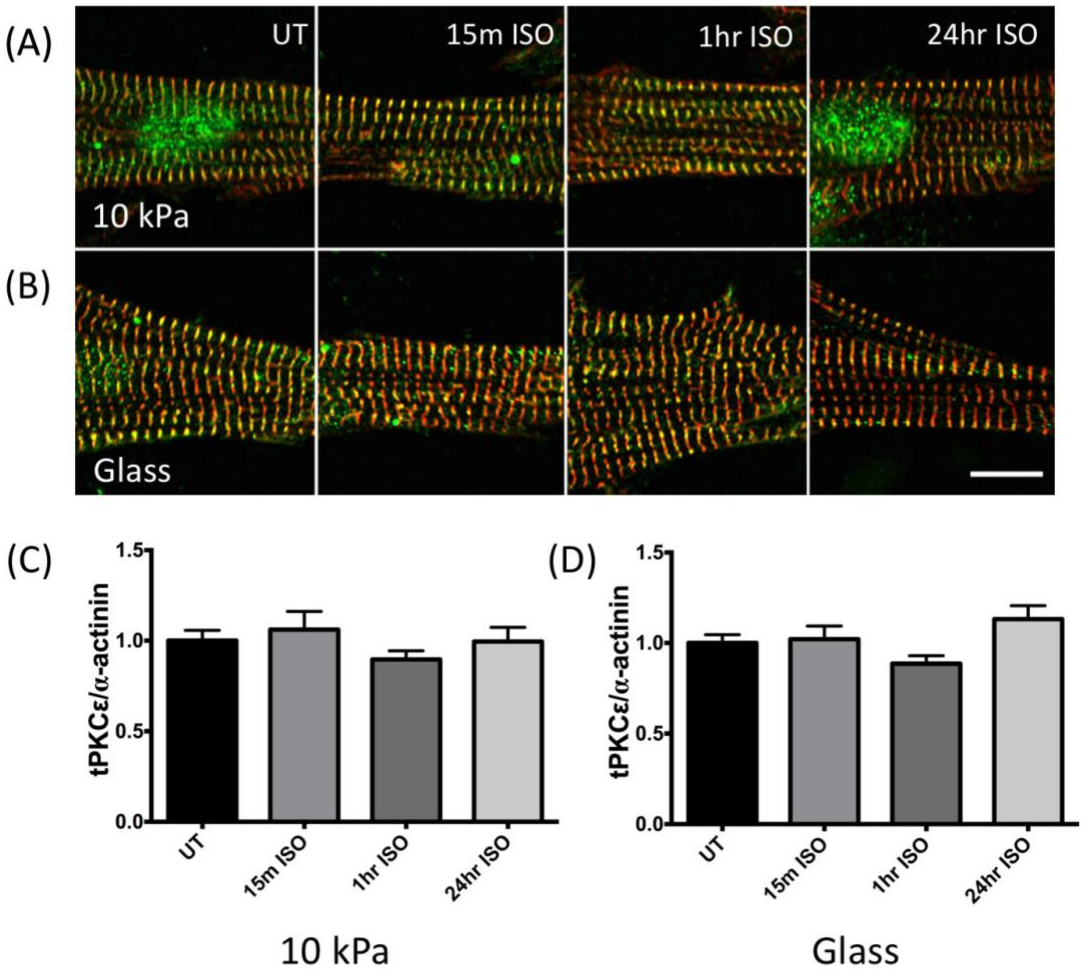

Figure 22. Immunofluorescence shows localization of total PKCε at the Z-disc does not change with isoproterenol treatment of CMs on either stiffness. Immunofluorescence images of CMs on 10 kPa or glass with total PKCε (green), and α-actinin (red). No change in co-localization on 10 kPa (A) and (C) or glass (B) and (D) surfaces following isoproterenol treatment. Scale bar: 10 μm. Values are mean ± SE.

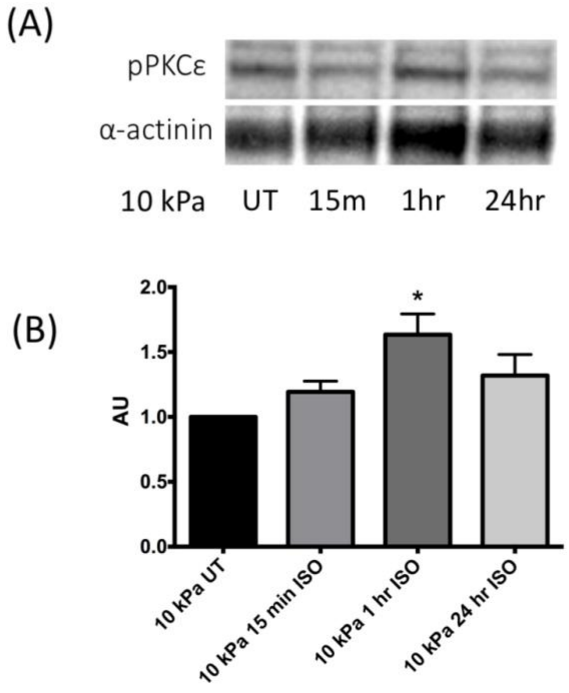

Figure 23. Cellular fractionation and western blot confirms increased pPKCε in the cytoskeleton. (A) Representative western blot performed on the cytoskeletal fraction of cells grown on 10 kPa substrata. (B) Histogram of phosphorylated PKCε over time of isoproterenol treatment normalized to α-actinin in the untreated group (n = 3). Values are mean ± SE. * $p < 0.05$.

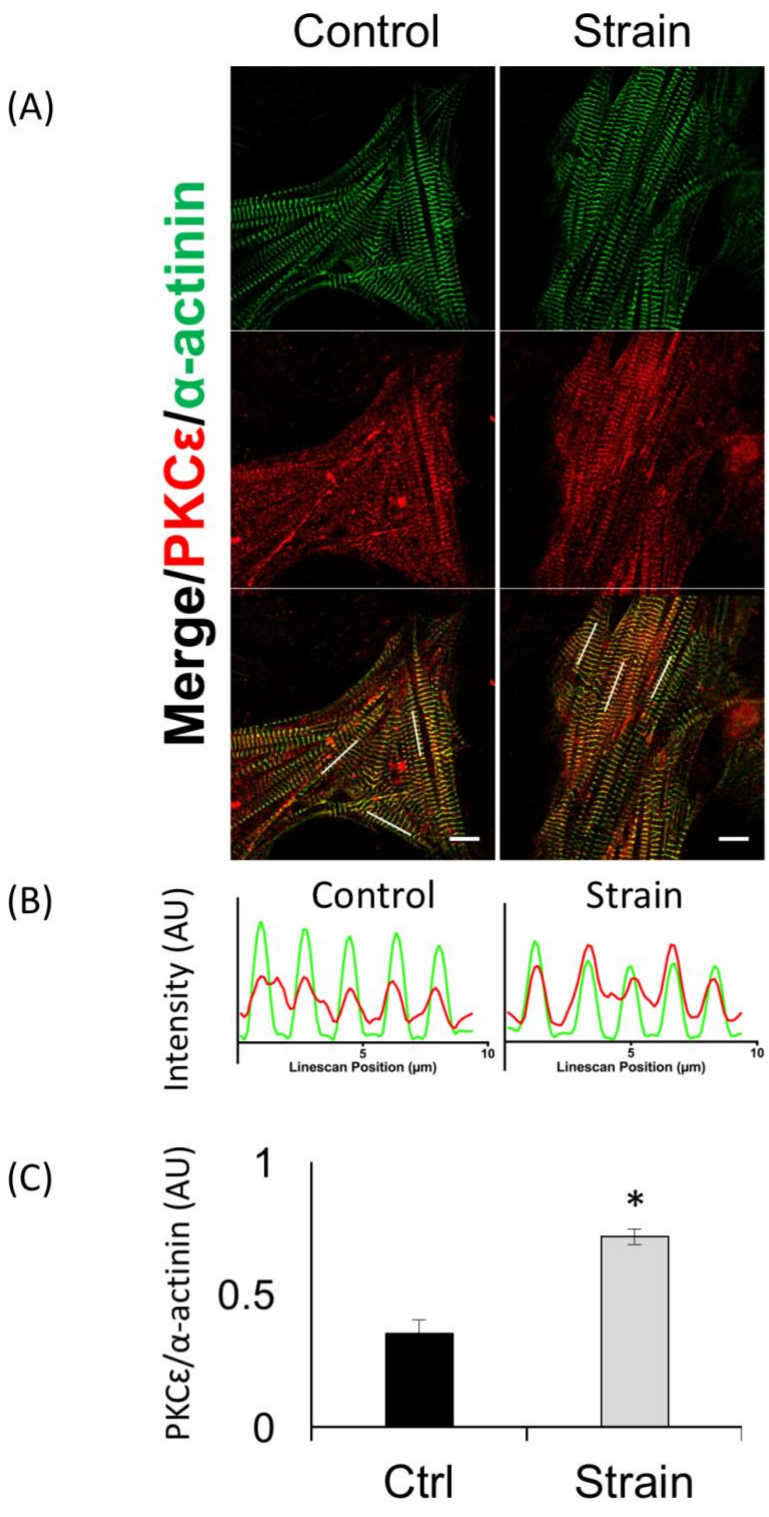
(A)
Control
Strain
Merge/PKCε/α-actinin
(B)
Control
Strain
Intensity (AU)
5
10
Linescan Position (μm)
5
10
Linescan Position (μm)
(C)
PKCε/α-actinin (AU)
1
0.5
0
*
Ctrl
Strain

Figure 24. Total PKCε colocalization with a-actinin increases at the Z-disc after cyclic strain of neonatal ventricular cardiac myocytes. (A) Myocytes were unstrained (control) or cyclically strained for 1 hour at 10% (strain) followed by confocal imaging for PKCε (red) with α-actinin (green). Note that only the cytoskeletal fraction remained after removal of the cytosol, membrane organelles and nuclei. Higher co-localization was seen in strained compared to non-strained myocytes. Scale bar: 10 μm. (B) Three line scans of at least 10 sarcomeres were taken per cell to measure relative intensities of PKCε to α-actinin. (C) Histogram for quantification under each condition showed increased colocalization of PKCε with α-actinin in the strained myocytes. Values are mean ± SE. n=10 cells, * $p < 0.00001$.

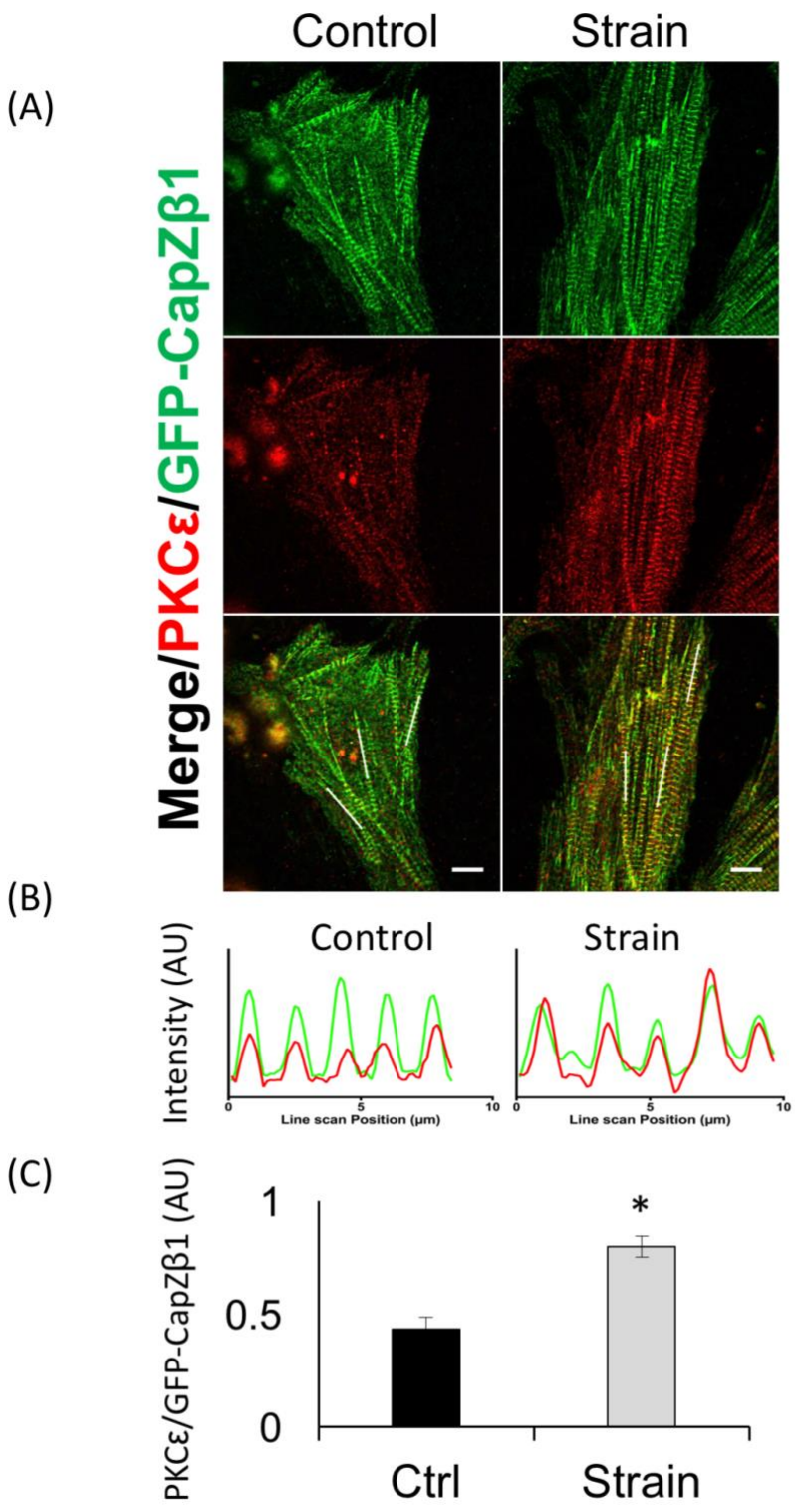
(A)
Control
Strain
Merge/PKCε/GFP-CapZβ1
(B)
Control
Strain
Intensity (AU)
0
5
10
Line scan Position (μm)
0
5
10
Line scan Position (μm)
(C)
PKCε/GFP-CapZβ1 (AU)
1
0.5
0
*
Ctrl
Strain

Figure 25. CapZβ1 colocalization with a-actinin increases at the Z-disc after cyclic strain of neonatal ventricular cardiac myocytes. (A) Myocytes were unstrained (control) or cyclically strained for 1 hour at 10% (strain) followed by confocal imaging for CapZβ1 (green) with α-actinin (red). Note that only the cytoskeletal fraction remained after removal of the cytosol, membrane organelles and nuclei. Higher co-localization was seen in strained compared to non-strained myocytes. Scale bar: 10 µm. (B) Three line scans of at least 10 sarcomeres were taken per cell to measure relative intensities of CapZβ1to α-actinin. (C) Histogram for quantification under each condition showed increased colocalization of CapZβ1with α-actinin in the strained myocytes. Values are mean ± SE. n=10 cells, * $p < 0.0001$.

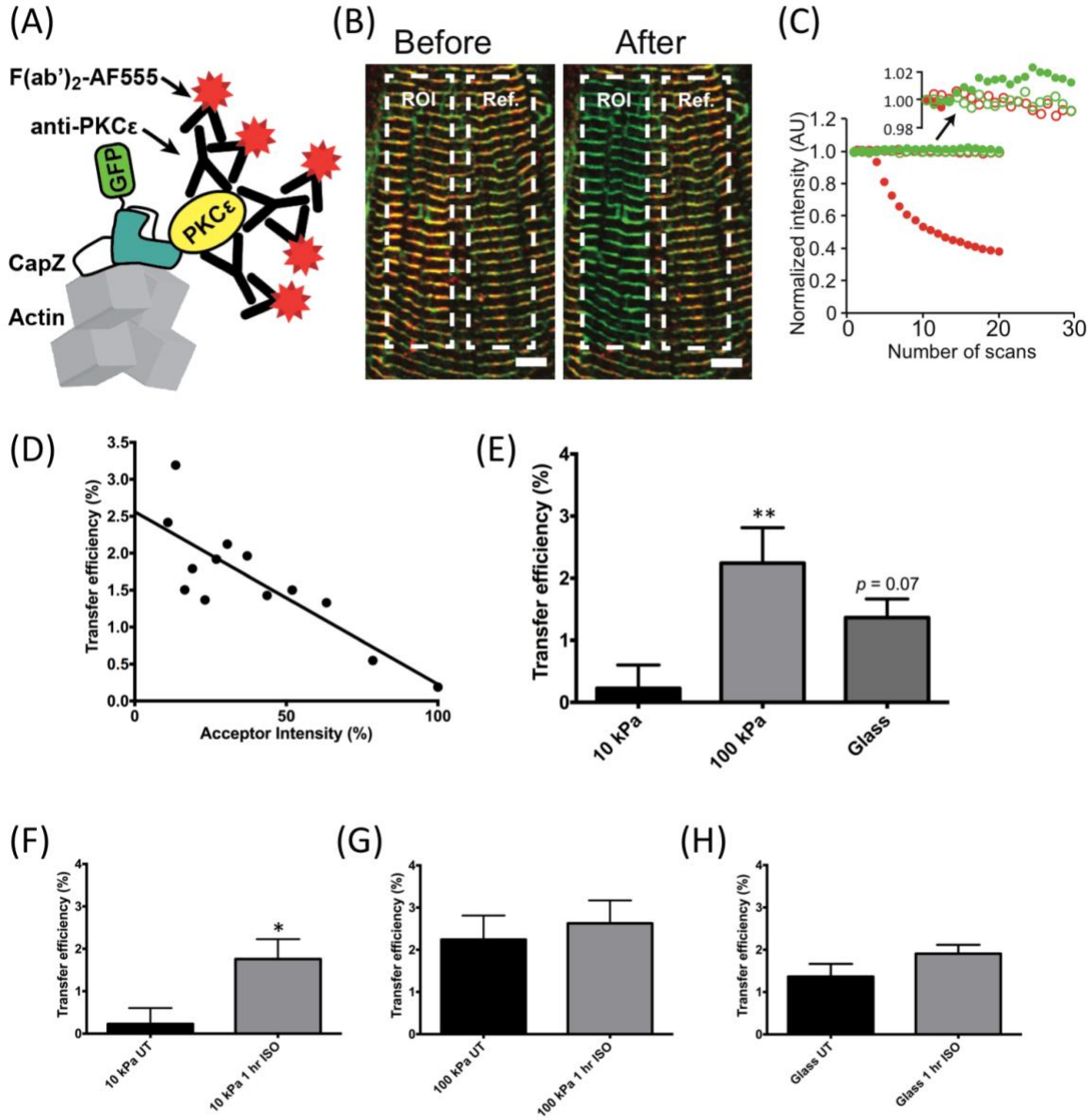
(A)
F(ab')2-AF555
anti-PKCε
GFP
PKCε
CapZ
Actin
(B)
Before
After
ROI
Ref.
(C)
Normalized intensity (AU)
Number of scans
(D)
Transfer efficiency (%)
Acceptor Intensity (%)
(E)
Transfer efficiency (%)
**
p = 0.07
10 kPa
100 kPa
Glass
(F)
Transfer efficiency (%)
*
10 kPa UT
10 kPa 1 hr ISO
(G)
Transfer efficiency (%)
100 kPa UT
100 kPa 1 hr ISO
(H)
Transfer efficiency (%)
Glass UT
Glass 1 hr ISO

Figure 26. FRET efficiency between PKCε and CapZ is low on soft substrata and increases with isoproterenol treatment, but does not change on stiff substrata. CMs grown on 10 kPa and 100 kPa substrata or glass were infected by CapZ-GFP. Untreated and 1-hour isoproterenol treated CMs were compared following component extraction, fixation, and immunolabeling with pPKCε antibody (S729) and red secondary antibody for confocal imaging and FRET analysis. (A) Diagram showing how molecular range interactions of CapZ with the GFP (green) as donor and a secondary antibody to pPKCε (red) as acceptor. (B) A typical scan for a striated CM on glass with 1-hour isoproterenol treatment before scanning a region of interest (ROI) and the unbleached reference panel (Ref). Right panel shows after 20 scans the red acceptor is bleached leaving only the green donor fluorescence. Scale bar: 5 µm. (C) Photobleaching trace of pPKCε acceptor (solid, red circles) over 20 scans showing steady bleaching over time while the acceptor in the reference region is unchanged (open, red circles). The GFP donor (solid, green circles) increased slightly in bleached ROI (expanded in upper area for clarity) relative to the donor in the reference region (open, green circles). (D) Linear fit of acceptor intensity and transfer efficiency, where the intercept represents the recovered transfer efficiency (intercept = 2.56 %, R^2 = 0.69). (E) Transfer efficiency significantly increased in 100 kPa compared to 10 kPa, but was not significantly different on glass (p=0.07). (F), (G), (H) Changes in transfer efficiency when treated with isoproterenol on different stiffness conditions. Only 10 kPa exhibited a significant change following treatment (n = 19 cells for 10 kPa and glass; n = 10 cells for 100 kPa). Values are mean ± SE. * $p < 0.05$ and ** $p < 0.01$.

was accompanied by concomitant acceptor intensity decay of pPKCε (red) (Figure 26C). The regression line between the acceptor intensity and transfer efficiency for this example (Figure 26D) showed a FRET response. Varying substrate stiffness resulted in a significant change in transfer efficiency in cells grown on 100 kPa substrata compared to 10 kPa ($p < 0.01$). Transfer efficiency was higher on glass substrata, but not significant ($p = 0.07$) (Figure 26E). Low transfer efficiency was seen for untreated cells on 10 kPa substrata, but this was significantly increased with 1-hour isoproterenol treatment ($p < 0.05$) (Figure 26F). Isoproterenol treatment did not lead to significant changes on stiff substrata (Figure 26G,H). These data suggest an increase in the molecular interactions between CapZ and pPKCε under stiff conditions, or when challenged to additional work under soft conditions. Based on these data, we propose a simple model for the interplay between substrate stiffness and isoproterenol treatment in PKCε-CapZ interactions and phosphorylation (Figure 27).

D. Discussion

The objective of this study was to investigate the response to acute work demand for cells grown on surfaces of varying stiffness. In particular, the PKCε signaling pathway and its role in actin assembly dynamics were examined. Interestingly, novel findings suggest that pathological stiffness diminishes the effect of PKCε signaling on actin assembly in neonatal rat heart cells. Immunofluorescence studies found that substrate stiffness similar to the normal neonatal heart leads to significantly increased PKCε activation in the CM cytoskeleton upon isoproterenol treatment, whereas this response is not seen on pathological and non-physiological substrate stiffness. The

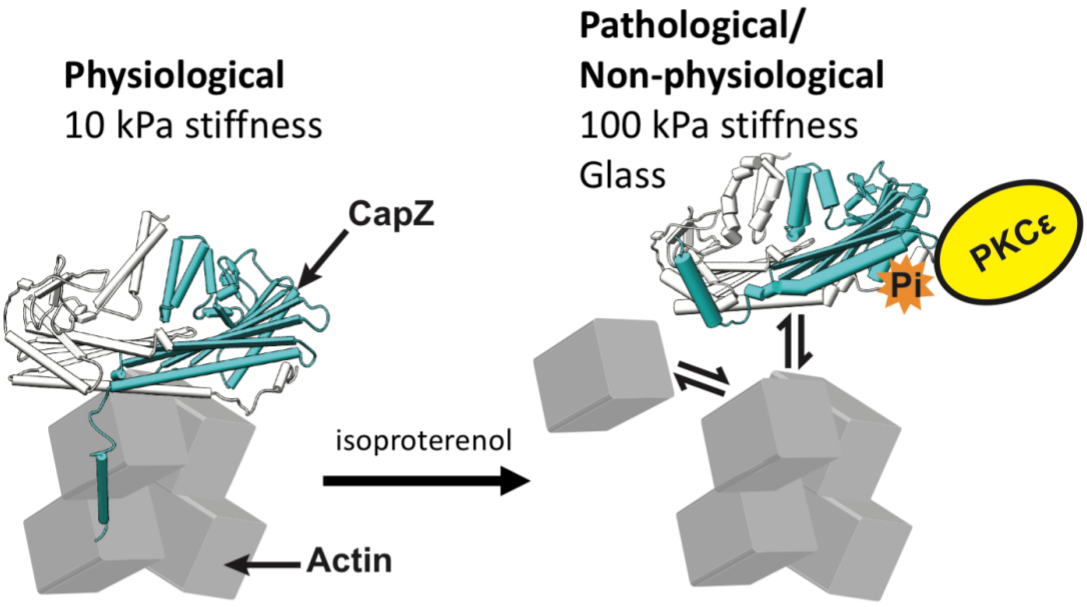

Figure 27. Model for altered isoproterenol response with increased substrate stiffness. Actin assembly rate is lower in CMs grown on surfaces mimicking physiological stiffness, and CMs are able to respond to isoproterenol treatment. CMs grown on surfaces mimicking chronic disease state are at a higher basal actin assembly rate and unable to respond to isoproterenol treatment. Conventional Petri dishes are stiffer than fibrotic tissue, so that many in vitro experiments might yield results that do not translate correctly for drug studies and human therapy.

FRAP and FRET data further support the notion that at the pathological stiffness, CapZ is already phosphorylated, loosening the capping conformation, which results in increased actin assembly rate. A proposed mechanism is depicted (Figure 27), where upon translocation of PKCε to the sarcomere, CapZ is phosphorylated, leading to a conformational change and decreased association with the actin barbed end. In that scenario, isoproterenol treatment could not lead to additional phosphorylation of CapZ, and the actin assembly rate would remain the same. Conversely, CMs grown on physiological stiffnesses are free to undergo CapZ phosphorylation by PKCε and increase assembly rate accordingly.

At the tissue level, translocation of PKCε to the sarcomere has been associated with cardiac hypertrophy (Mochly-Rosen et al., 2000), a phenomenon correlated with increased actin assembly rate. PKCε translocation has also been shown *in vitro* following CM stretch (Vincent et al., 2006). Our lab has demonstrated that mechanical stimulation through increased substrate stiffness or cyclic mechanical stretch leads to greater actin dynamics, which is mediated through a variety of signaling molecules, including PKCε, PIP2, and FAK (Li et al., 2016; Lin et al., 2015). It has been shown that isoproterenol treatment leads to rapid translocation of PKCε to the cell particulate fraction (Li et al., 2015), making it a strong candidate here for *implication* in increased actin assembly rate. Indeed, this is supported by the increased FRAP kinetics that were seen 15 minutes after isoproterenol treatment.

We demonstrate that although the physiological metric of TPT are altered by substrate stiffness, they each respond rapidly to βAR stimulation through isoproterenol stimulation, reaching common peak measurements. It is well known that changes in the

mechanical environment leads to aberrations in CM contractility. In particular, a substrate tuned in stiffness to the natural myocardium yields embryonic CMs that work optimally (Engler et al., 2008). Although the stiffness of the underlying substrata affected contractility, βAR stimulation still led to increases in contractile velocity, which is most easily explained by changes in calcium handling. PKCε-dependent phosphorylation of phospholamban (Okumura et al., 2014), as well as phospholamban and ryanodine receptor phosphorylation are triggered by various signaling molecules.

CMs here were grown on substrata of varying stiffness for two days before the acute isoproterenol treatment to provide time for the initial and subsequent response to occur. Lack of response under high stiffness could be part of a more persistent desensitization mechanism to β agonists. It is known that catecholamine response is depressed in the failing heart (El-Armouche and Eschenhagen, 2009). Results here suggest a desensitization mechanism in single myocytes with two days of chronic high stiffness that caused a blunted response of PKCε to isoproterenol. This time might be sufficient for activation of beta signaling desensitization mechanisms like upregulation of G-coupled receptor kinase 5 (Islam and Koch, 2012; Zelarayan et al., 2009). Findings suggest that the chronic pathological state can be replicated by manipulating substrate stiffness levels.

It seems likely that filaments are built to serve the functional work being demanded by the myocyte, and that local mechanical conditions ultimately regulate filament assembly and muscle mass. Findings demonstrate that the CM responds to acute changes in demand differentially based on the underlying matrix stiffness, a condition which would be altered with cardiac fibrosis. This could ultimately affect the

response an individual might have to particular drug therapies. Results also suggest that the matrix stiffness on which cells are cultured has implications for drug screening studies. Since cells become non-responsive to treatment when grown for several days on a pathologically stiff surface, investigators might fail to detect results that are necessary to translate *in vitro* studies more effectively to human therapy.

IV. CONCLUSIONS AND SIGNIFICANCE

A. Major Conclusions

PART I: LIPID SIGNALING AFFECTS PRIMARY FIBROBLAST COLLECTIVE MIGRATION AND ANCHORAGE IN RESPONSE TO STIFFNESS AND MICROTOPOGRAPHY

1. The cloning cylinder migration assay can be utilized to reproducibly recapitulate migration into a space devoid of cells, akin to a wound healing situation.
2. Migration velocity is regulated by substrate stiffness, with cells migrating faster on substrata of lower stiffness.
3. Migration velocity can be regulated by altering the availability and production of PIP2 by drugs (neomycin decrease; wortmannin increase), with migration velocities indirectly proportional to the availability of PIP2.
4. Focal adhesions at the termination of actin stress cables form closer to the lamellar edge when levels of PIP2 are increased. In contrast, decreasing PIP2 availability results in greater distance between lamellar edge and focal adhesion formation.
5. A prominent gradient of PIP2 is present when cells are treated with neomycin, with higher levels near the cell periphery.
6. PIP2 accumulates near areas of focal adhesions, as demonstrated through immunofluorescence studies of cells grown on micropost surfaces. PIP3 remains uniformly distributed along cell membrane.

7. Viral infection for actin-GFP expression can be used to study actin dynamics in cardiac fibroblast stress cables.
8. Neither substrate stiffness nor control of PIP2 availability regulate actin dynamics in well-formed actin stress cables.
9. Increasing PIP2 levels with wortmannin treatment results in a decreased rate of attachment to the micropost topography by cardiac fibroblasts, but long term attachment remains similar to untreated and neomycin-treated cells.
10. PEGDMA microrods loaded with neomycin can be used to increase migration rate of cells and potentially serve as a means of increasing wound healing.
11. Cardiac fibroblasts attach readily to HA microrods, which can be used in potential anti-fibrotic therapeutics.
12. Cardiac fibroblasts show greater affinity for HA microrods than myocytes. This might be regulated through the abundance of CD44 surface receptors on fibroblasts.
13. Free HA or culture with HA microrods does not interfere with contractile properties of CMs in terms of beat frequency and TPT.

PART II: SUBSTRATE STIFFNESS DIFFERENTIALLY AFFECTS SIGNALING RESPONSE TO ISOPROTERENOL TREATMENT IN CARDIOMYOCYTES

1. Contractile TPT increases with increasing substrate stiffness, and CMs do not respond differentially when treated with isoproterenol.

2. Sarcomeric actin dynamics increase with increasing substrate stiffness, but only CMs grown on soft substrata are able to respond to isoproterenol treatment with increased actin dynamics.
3. Activated PKCε increases in localization to the Z-disc on soft substrata following isoproterenol treatment but not on stiff substrata, as evaluated by both immunofluorescence and western blots.
4. Total PKCε does not increase in localization at the Z-disc on any stiffness following isoproterenol treatment, as determined by immunofluorescence.
5. FRET efficiency between CapZ and PKCε is greater on stiff substrata, suggesting molecule-level interactions. Only CMs grown on soft substrata respond to isoproterenol treatment with increased FRET efficiency.
6. Cyclic strain leads to increased localization of total PKCε at the Z-disc compared to unstrained control.

B. Significance

The goal of this dissertation was to understand how cell types within the heart adapt to various mechanical environments in terms of structure, physiological function, and response to drug treatment. I hypothesized that the mechanical properties of the underlying cell substrate regulate physiological outcomes and differential response to drug treatment. Indeed, the data suggest that cardiac fibroblast and myocyte physiology and structure are regulated by surface stiffness and topography, which together lead to differential responses to drug treatment. Furthermore, the mechanisms include regulation of membrane lipids in fibroblasts, and through βARs in CMs.

These mechanobiological mechanisms are significant for a number of reasons. Since many biological research labs do not culture cells within physiologically relevant systems, the context might lead to studies in which cells cannot respond in a normal manner. Although it would be helpful to use surfaces at a physiological stiffness or with topographical features, the most commonly utilized scheme is standard tissue culture plastic (TCP), which are hard and flat. Studies in this thesis provide evidence that culture in standard TCP can blunt signaling and function, even as far as masking the response that would normally be present. This highlights the need to properly tune the mechanical environment during *in vitro* experiments, especially when conducting research for medical purposes.

Furthermore, this work briefly explores interactions with microrods for potential anti-fibrosis and wound healing therapeutics, as well as the elicited physiological response. In particular, free HA and HA microrods do not negatively impact contractile behavior in CMs, making HA a viable material for cardiac therapies. Finally, incorporation of magnetic nanoparticles into PEGDMA microrods for manipulation with external magnets is a potential means of studying the effects of acute load on cells, though the system would have to be further controlled to be used.

C. Limitations

Over the course of experimental research, choices are made that might limit the scope and significance of the acquired data. These choices can include culture conditions, choice of assay, and drug choice or dose. Detailed here are some of the limitations within this dissertation.

One of the most significant decisions made in cell culture studies is the density at which the cells are seeded. In order to study a collective migration effect akin to wound healing, I chose to culture fibroblasts at a higher density. A higher density resulted in increased cell-to-cell interactions, potentially altering migratory behavior, as has been described by others (Ng et al., 2012; Haeger et al., 2015). A lower density and individual cell tracking might have indicated the behavior of a single cell, but it would not have achieved the wound healing relevance sought in the study. In order to focus purely on the effect of the physical microenvironment, I chose to culture the cardiomyocytes at a lower density. This particular decision negated the influence of mechano-electrical coupling of cells through desmosomes and gap junctions. However, there is anecdotal and experimental evidence that cardiomyocytes function with different mechanics when coupled.

Another cell culture choice is the ECM used to aid in cell attachment. For our experiments on fibroblasts and cardiomyocytes, fibronectin was used for its specificity to integrins present on both cell types. This allows for ample attachment, but it does not necessarily fully reflect an environment akin to the healthy or diseased myocardium. Recent work using decellularized porcine myocardium has been demonstrated as a stable means of culturing cells *in vitro* and has shown promise in novel therapeutic applications (Wang and Christman, 2016). Perhaps utilizing these kinds of matrices would better mimic the environment compared to synthetic hydrogels and provide more clinical relevance.

Choice and dose of drug are also crucial in studies. Since the scope of my research was concerned largely on the effect of the microenvironment in regulating cell

physiology, I did not seek data related to dose response. My goal was to elicit a response and study how the cells behave in various environments. A more comprehensive study might have utilized a dose response, but the time required for live cell assays makes this less feasible. Thus, single concentrations of neomycin, wortmannin, and isoproterenol were used.

Finally, there are some drawbacks to utilizing a fixed-cell FRET system, although it is probably the simplest and straight-forward means of studying FRET. In general, FRET efficiency is rather low, resulting in a low signal-to-noise ratio. This problem is compounded by fixing cells using formaldehyde, which can result in decreased E%. Additionally, FRET can be subject to artifacts due to bleed-through of the donor fluorescence to the acceptor, resulting in artificially high E%. This can be combatted by use of FLIM-FRET technique, which reduces the artifact by only monitoring the fluorescence of the donor. However, this technique requires additional instrumentation. Finally, fixed-cell FRET does not allow for monitoring of dynamic changes following drug challenge, which if desired, would require the use of customized fluorescent probes.

D. Future Directions

This research provides additional evidence for the importance of the microenvironmental effects on cell physiology and signaling response. It should provide a greater appreciation for tuning of the cell culture environment and lead researchers to utilize these engineering approaches to study their specific cells or tissues.

Great advances have been made with proteins and post-translational modification, but more is needed for lipids. A major drawback to the study of cellular

lipids is their limited capacity to undergo biochemical assays such as Western blotting. Therefore, available approaches for their study were limited. In future work, it would be helpful to utilize more live cell techniques to visualize the molecular movement in real time. This could be done using the PIP2 sensor like the one implemented here, but variable expression levels and transfection rate make it problematic. The cell membrane is highly dynamic, not only spatially, but in turnover of lipid components. Capturing the trafficking and phosphorylation of membrane lipids would provide greater detail to the regulation of physiological processes. Additionally, the use of drugs with greater specificity for regulating PIP2 would be beneficial to rule out the activation of alternative pathways in these types of studies.

In order to understand how the mechanical environment regulates PKCε signaling, additional approaches could be used. In particular, use of GFP-tagged PKCε to show live cell translocation could better elucidate the time course and destination of the signaling protein. This particular approach was attempted here using an AAV for expression of PKCε-GFP, but the cytosolic and membrane content of the protein had a tendency to obscure relevant cytoskeletal interactions as viewed with confocal microscopy, making the signal-to-noise ratio too low. This might be overcome by utilizing other microscopy techniques such as total internal reflection fluorescence to get a closer look at the costamere along the surface of the adhered cell. However, this would be limited greatly by working distance, as utilizing mechanically tuned substrata would require flipping the surface onto cover glass, and three-dimensional topography would be virtually impossible.

Utilizing three-dimensional topography with CMs, as opposed to flat substrata, to study how local mechanical forces affect PKCε signaling could provide greater detail as to the role of PKCε in mechanical regulation of actin assembly through CapZ phosphorylation. Using FRET methods to study myofibrils under particular high tension through micropost attachment might give further evidence of this role. Some work has been done already, but the study of directly involved components of the PLC signaling pathway, such as PIP2, provides a closer look at how PKCε signal is propagated in the cell.

Finally, the differences between acute and chronic activation of signaling pathways ultimately affects cytoskeletal remodeling. Additional studies with mechanical stretching or load-applying devices would show difference in acute and chronic signaling, and could potentially lead to a greater understanding of the signaling pathways that could be approached in developing therapeutics for heart failure or prophylactic therapy. More recently, labs have utilized substrata that can become softer or stiffer through photoactivation. Utilizing an approach like this could provide insight to how the heart might adapt in cases of long term fibrosis or acute remodeling of the heart. Our lab. Has completed preliminary studies on PEGDMA microrods containing ferromagnetic nanoparticles in order to apply load directly to cells using external magnetic. This approach would allow for single cell, realtime imaging assays to study acute change in load with the possibility of drug intervention.

CITED LITERATURE

1. Acharya, P.S., Majumdar, S., Jacob, M., Hayden, J., Mrass, P., Weninger, W., Assoian, R.K., & Pure, E. Fibroblast migration is mediated by CD44-dependent TGF activation. Journal of Cell Science, 121:1393–1402, 2008.

2. Ayala, P., Lopez, J.I., & Desai, T.A. Microtopographical Cues in 3D Attenuate Fibrotic Phenotype and Extracellular Matrix Deposition: Implications for Tissue Regeneration. Tissue Engineering Part A, 16:2519–2527, 2010.

3. Bae, Y., Ding, Z., Zou, L., Wells, A., Gertler, F., & Roy, P. Loss of profilin-1 expression enhances breast cancer cell motility by Ena/VASP proteins. Journal of Cellular Physiology, 219:354–364, 2009.

4. Benjamin, E.J., Virani, S.S., Callaway, C.W., Chang, A.R., Cheng, S., Chiuve, S.E., Cushman, M., Delling, F.N., Deo, R., de Ferranti, S.D., Ferguson, J.F., Fornage, M., Gillespie, C., Isasi, C.R., Jiménez, M.C., Jordan, L.C., Judd, S.E., Lackland, D., Lichtman, J.H., Lisabeth, L., Liu, S., Longenecker, C.T., Lutsey, P.L., Matchar, D.B., Matsushita, K., Mussolino, M.E., Nasir, K., O'Flaherty, M., Palaniappan, L.P., Pandey, D.K., Reeves, M.J., Ritchey, M.D., Rodriguez, C.J., Roth, G.A., Rosamond, W.D., Sampson, U.K.A., Satou, G.M., Shah, S.H., Spartano, N.L., Tirschwell, D.L., Tsao, C.W., Voeks, J.H., Willey, J.Z., Wilkins, J.T., Wu, J.H., Alger, H.M., Wong, S.S., & Muntner, P. Heart Disease and Stroke Statistics—2018 Update: A Report From the American Heart Association. Circulation, 2018.

5. Benz, P.M., Merkel, C.J., Offner, K., Abeßer, M., Ullrich, M., Fischer, T., Bayer, B., Wagner, H., Gambaryan, S., Ursitti, J.A., Adham, I.M., Linke, W.A., Feller, S.M., Fleming, I., Renné, T., Frantz, S., Unger, A., & Schuh, K. Mena/VASP and αII-Spectrin complexes regulate cytoplasmic actin networks in cardiomyocytes and protect from conduction abnormalities and dilated cardiomyopathy. Cell Communication and Signaling, 11:56:1–22, 2013.

6. Berry, M.F., Engler, A.J., Woo, Y.J., Pirolli, T.J., Bish, L.T., Jayasankar, V., Morine, K.J., Gardner, T.J., Discher, D.E., Sweeney, H.L., F, M., & J, T. Regulation and Function of Stem Cells in the Cardiovascular System Mesenchymal stem cell injection after myocardial infarction improves myocardial compliance. Therapy, 6085:2196–2203, 2006.

7. Bhana, B., Iyer, R.K., Chen, W.L.K., Zhao, R., Sider, K.L., Likhitpanichkul, M., Simmons, C.A., & Radisic, M. Influence of substrate stiffness on the phenotype of heart cells. Biotechnology and Bioengineering, 105:1148–1160, 2010.

8. Bidan, C.M., Fratzl, M., Coullomb, A., Moreau, P., Lombard, A.H., Wang, I., Balland, M., Boudou, T., Dempsey, N.M., Devillers, T., & Dupont, A. Magneto-

active substrates for local mechanical stimulation of living cells. Scientific Reports, 8(1464):1–13, 2018.

9. Biehl, J.K., Yamanaka, S., Desai, T.A., Boheler, K.R., & Russell, B. Proliferation of mouse embryonic stem cell progeny and the spontaneous contractile activity of cardiomyocytes are affected by microtopography. Developmental Dynamics, 238:1964–1973, 2008.

10. Boateng, S.Y., Hartman, T.J., Ahluwalia, N., Vidula, H., Desai, T.A., & Russell, B. Inhibition of fibroblast proliferation in cardiac myocyte cultures by surface microtopography. American Journal of Physiology - Cell Physiology, 285:C171–C182, 2003.

11. Boateng, S.Y., Belin, R.J., Geenen, D.L., Margulies, K.B., Martin, J.L., Hoshijima, M., de Tombe, P.P., & Russell, B. Cardiac dysfunction and heart failure are associated with abnormalities in the subcellular distribution and amounts of oligomeric muscle LIM protein. American Journal of Physiology - Heart and Circulatory Physiology, 292:H259–H269, 2007.

12. Bray, M.A., Sheehy, S.P., & Parker, K.K. Sarcomere alignment is regulated by myocyte shape. Cell Motility and the Cytoskeleton, 65:641–651, 2008.

13. Broughton, K.M., & Russell, B. Cardiomyocyte subdomain contractility arising from microenvironmental stiffness and topography. Biomechanics and Modeling in Mechanobiology, 14:589–602, 2015.

14. Brückner, B.R., Pietuch, A., Nehls, S., Rother, J., & Janshoff, A. Ezrin is a Major Regulator of Membrane Tension in Epithelial Cells. Scientific Reports, 5(14770):1–16, 2015.

15. Chierico, L., Joseph, A.S., Lewis, A.L., & Battaglia, G. Live cell imaging of membrane/cytoskeleton interactions and membrane topology. Scientific Reports, 3(6056):1–10, 2014.

16. Csukai, M., Chen, C.-H., DeMatteis, M.A., Mochly-Rosen, D. The coatomer protein b'COP: A selective binding protein (RACK) for epsilon protein kinase C. Journal of Biological Chemistry, 272:29200– 29206, 1997.

17. Curtis, M.W., Budyn, E., Desai, T.A., Samarel, A.M., & Russell, B. Microdomain heterogeneity in 3D affects the mechanics of neonatal cardiac myocyte contraction. Biomechanics and Modeling in Mechanobiology, 12:95–109, 2013.

18. Desai, T. In the spotlight: Tissue engineering. IEEE Reviews in Biomedical Engineering, 6:27-8, 2013.

19. de Tombe, P.P., Mateja, R.D., Tachampa, K., Ait Mou, Y., Farman, G.P., Irving,

T.C. Myofilament length dependent activation. Journal of Molecular and Cellular Cardiology. May;48(5):851-8, 2010.

20. Disatnik, M.H., Buraggi, G., & Mochly-Rosen, D. Localization of protein kinase C isozymes in cardiac myocytes. Experimental cell research, 210:287–297, 1994.

21. Discher, D.E. Tissue Cells Feel and Respond to the Stiffness of Their Substrate. Science, 310:1139–1143, 2005.

22. Doroudian, G., Curtis, M.W., Gang, A., & Russell, B. Cyclic strain dominates over microtopography in regulating cytoskeletal and focal adhesion remodeling of human mesenchymal stem cells. Biochemical and Biophysical Research Communications, 430:1040–1046, 2013.

23. Doroudian, G., Pinney, J., Ayala, P., Los, T., Desai, T.A., & Russell, B. Sustained delivery of MGF peptide from microrods attracts stem cells and reduces apoptosis of myocytes. Biomedical Microdevices, 16:705–715, 2014.

24. Dupont, S. Role of YAP/TAZ in cell-matrix adhesion-mediated signalling and mechanotransduction. Experimental Cell Research, 343:42–53, 2016.

25. El-Armouche, A., & Eschenhagen, T. β-Adrenergic stimulation and myocardial function in the failing heart. Heart Failure Reviews, 14:225–241, 2009.

26. Engler, A.J., Carag-Krieger, C., Johnson, C.P., Raab, M., Tang, H.Y., Speicher, D.W., Sanger, J.W., Sanger, J.M., & Discher, D.E. Embryonic cardiomyocytes beat best on a matrix with heart-like elasticity: scar-like rigidity inhibits beating. Journal of Cell Science, 121:3794–3802, 2008.

27. Fomovsky, G.M., & Holmes, J.W. Evolution of scar structure, mechanics, and ventricular function after myocardial infarction in the rat. American Journal of Physiology - Heart and Circulatory Physiology, 298:H221–H228, 2010.

28. Fomovsky, G.M., Thomopoulos, S., & Holmes, J.W. Contribution of extracellular matrix to the mechanical properties of the heart. Journal of Molecular and Cellular Cardiology, 48:490–496, 2010.

29. Fu, X., Blaxall, B.C., Molkentin, J.D., Fu, X., Khalil, H., Kanisicak, O., Boyer, J.G., Vagnozzi, R.J., Maliken, B.D., Sargent, M.A., Prasad, V., Valiente-alandi, I., Blaxall, B.C., & Molkentin, J.D. Specialized fibroblast differentiated states underlie scar formation in the infarcted mouse heart. The Journal of Clinical Investigation, 128:2127–2143, 2018.

30. Gautel, M., & Djinovic-Carugo, K. The sarcomeric cytoskeleton: from molecules to motion. Journal of Experimental Biology, 219:135–145, 2016.

31. Goldmann, W.H. Molecular interactions between vinculin and phospholipids. Cell Biology International, Aug;42(8):1076-1078, 2018.

32. Goñi, G.M., Epifano, C., Boskovic, J., Camacho-Artacho, M., Zhou, J., Bronowska, A., Martín, M.T., Eck, M.J., Kremer, L., Gräter, F., Gervasio, F.L., Perez-Moreno, M., Lietha, D. Phosphatidylinositol 4,5-bisphosphate triggers activation of focal adhesion kinase by inducing clustering and conformational changes. Proceedings of the National Academy of Sciences USA, Aug 5;111(31):E3177-86, 2014.

33. Grikscheit, K., & Grosse, R. Formins at the Junction. Trends in Biochemical Sciences, 41:148–159, 2016.

34. Haeger, A., Wolf, K., Zegers, M.M., & Friedl, P. Collective cell migration: Guidance principles and hierarchies. Trends in Cell Biology, 25:556–566, 2015.

35. Harland, B., Walcott, S., & Sun, S.X. Adhesion dynamics and durotaxis in migrating cells. Physical Biology, 8(015011):1–10, 2011.

36. Hartman, T.J., Martin, J.L., Solaro, R.J., Samarel, A.M., & Russell, B. CapZ dynamics are altered by endothelin-1 and phenylephrine via PIP2- and PKC-dependent mechanisms. American Journal of Physiology - Cell Physiology, 296:C1034–C1039, 2009.

37. Haugsten, E.M., Oppelt, A., & Wesche, J. Phosphatidylinositol 5-phosphate is a second messenger important for cell migration. Communicative and Integrative Biology, 6:1–4, 2013.

38. Hazeltine, L.B., Simmons, C.S., Salick, M.R., Lian, X., Badur, M.G., Han, W., Delgado, S.M., Wakatsuki, T., Crone, W.C., Pruitt, B.L., & Palecek, S.P. Effects of substrate mechanics on contractility of cardiomyocytes generated from human pluripotent stem cells. International Journal of Cell Biology, 508294:1-13, 2012.

39. Hoshijima, M. Mechanical stress-strain sensors embedded in cardiac cytoskeleton: Z disk, titin, and associated structures. American Journal of Physiology - Heart and Circulatory Physiology, 290:H1313–H1325, 2006.

40. Hotulainen, P., & Lappalainen, P. Stress fibers are generated by two distinct actin assembly mechanisms in motile cells. Journal of Cell Biology, 173:383–394, 2006.

41. Islam, K.N., & Koch, W.J. Involvement of nuclear factor κB (NF-κB) signaling

pathway in regulation of cardiac G protein-coupled receptor kinase 5 (GRK5) expression. Journal of Biological Chemistry, 287:12771–12778, 2012.

42. Jacot, J.G., Martin, J.C., & Hunt, D.L. Mechanobiology of cardiomyocyte development. Journal of Biomechanics, 43:93–98, 2010.

43. Kaumann, A.J., & Molenaar, P. The low-affinity site of the β1-adrenoceptor and its relevance to cardiovascular pharmacology. Pharmacology and Therapeutics, 118:303–336, 2008.

44. Kim, T., Cooper, J.A., & Sept, D. The interaction of capping protein with the barbed end of the actin filament. Journal of Molecular Biology, 404:794–802, 2010.

45. Kiviluoto, S., Vervliet, T., Ivanova, H., Decuypere, J.P., De Smedt, H., Missiaen, L., Bultynck, G., Parys, J.B. Regulation of inositol 1,4,5-trisphosphate receptors during endoplasmic reticulum stress. Biochimica et Biophysica Acta, Jul;1833(7):1612-24, 2013.

46. Komatsu, S., Dobson, J.G. Jr., Ikebe, M., Shea, L.G., Fenton, R.A. Crosstalk between adenosine A1 and β1-adrenergic receptors regulates translocation of PKCε in isolated rat cardiomyocytes. Journal of Cellular Physiology, Sep;227(9):3201-7, 2012.

47. König, P., Krasteva, G., Tag, C., König, I.R., Arens, C., & Kummer, W. FRET-CLSM and double-labeling indirect immunofluorescence to detect close association of proteins in tissue sections. Laboratory Investigation, 86:853–864, 2006.

48. Köster, D. V., & Mayor, S. Cortical actin and the plasma membrane: Inextricably intertwined. Current Opinion in Cell Biology, 38:81–89, 2016.

49. Kuo, P.L., Lee, H., Bray, M.A., Geisse, N.A., Huang, Y.T., Adams, W.J., Sheehy, S.P., & Parker, K.K. Myocyte shape regulates lateral registry of sarcomeres and contractility. American Journal of Pathology, 181:2030–2037, 2012.

50. Kuster, D.W.D., Bawazeer, A.C., Zaremba, R., Goebel, M., Boontje, N.M., & Van Der Velden, J. Cardiac myosin binding protein C phosphorylation in cardiac disease. Journal of Muscle Research and Cell Motility, 33:43–52, 2012.

51. Lange, J.R., & Fabry, B. Cell and tissue mechanics in cell migration. Experimental Cell Research, 319:2418–2423, 2013.

52. Leonard, A., Bertero, A., Powers, J.D., Beussman, K.M., Bhandari, S., Regnier, M., Murry, C.E., & Sniadecki, N.J. Afterload promotes maturation of human

induced pluripotent stem cell derived cardiomyocytes in engineered heart tissues. Journal of Molecular and Cellular Cardiology, 118:147–158, 2018.

53. Li, J., & Russell, B. Phosphatidylinositol 4,5-bisphosphate regulates CapZβ1 and actin dynamics in response to mechanical strain. American journal of physiology - Heart and circulatory physiology, 305:H1614-1623, 2013.

54. Li, J., Tanhehco, E.J., & Russell, B. Actin dynamics is rapidly regulated by the PTEN and PIP2 signaling pathways leading to myocyte hypertrophy. American Journal of Physiology - Heart and Circulatory Physiology, 307:H1618–H1625, 2014.

55. Li, J., Mkrtschjan, M.A., Lin, Y.H., & Russell, B. Variation in stiffness regulates cardiac myocyte hypertrophy via signaling pathways. Canadian Journal of Physiology and Pharmacology, 94:1–9, 2016.

56. Li, L., Cai, H., Liu, H., & Guo, T. β-adrenergic stimulation activates protein kinase Cε and induces extracellular signal-regulated kinase phosphorylation and cardiomyocyte hypertrophy. Molecular Medicine Reports, 11:4373–4380, 2015.

57. Lin, Y-.H., Li, J., Swanson, E.R., & Russell, B. CapZ and actin capping dynamics increase in myocytes after a bout of exercise and abates in hours after stimulation ends. Journal of Applied Physiology, 114:1603–1609, 2013.

58. Lin, Y-.H., Swanson, E.R., Li, J., Mkrtschjan, M.A., & Russell, B. Cyclic mechanical strain of myocytes modifies CapZβ1 post translationally via PKCε. Journal of Muscle Research and Cell Motility, 36:329–337, 2015.

59. Lin, Y-.H., Warren, C.M., Li, J., McKinsey, T.A., & Russell, B. Myofibril growth during cardiac hypertrophy is regulated through dual phosphorylation and acetylation of the actin capping protein CapZ. Cellular Signalling, 28:1015–1024, 2016.

60. Majkut, S.F., & Discher, D.E. Cardiomyocytes from late embryos and neonates do optimal work and striate best on substrates with tissue-level elasticity: Metrics and mathematics. Biomechanics and Modeling in Mechanobiology, 11:1219–1225, 2012.

61. Mayor, R., & Etienne-Manneville, S. The front and rear of collective cell migration. Nature Reviews Molecular Cell Biology, 17:97–109, 2016.

62. Mochly-Rosen, D., Wu, G.Y., Hahn, H., Osinska, H., Liron, T., Lorenz, J.N., Yatani, A., Robbins, J., & Dorn II, G.W. Cardiotrophic effects of protein kinase C e - Analysis by in vivo modulation of PKCe translocation. Circulation Research, 86:1173–1179, 2000.

63. Moes, M., Boonstra, J., & Regan-Klapisz, E. Novel role of cPLA2α in membrane and actin dynamics. Cellular and Molecular Life Sciences, 67:1547–1557, 2010.

64. Motlagh, D., Senyo, S.E., Desai, T.A., & Russell, B. Microtextured substrata alter gene expression, protein localization and the shape of cardiac myocytes. Biomaterials, 24:2463–2476, 2003.

65. Motlagh, D., Hartman, T.J., Desai, T.A., & Russell, B. Microfabricated grooves recapitulate neonatal myocyte connexin43 and N-cadherin expression and localization. Journal of Biomedical Materials Research, 67A:148–157, 2003.

66. Ng, M.R., Besser, A., Danuser, G., & Brugge, J.S. Substrate stiffness regulates cadherin-dependent collective migration through myosin-II contractility. Journal of Cell Biology, 199:545–563, 2012.

67. Nguyen, M.N., Kiriazis, H., Gao, X.M., & Du, X.J. Cardiac Fibrosis and Arrhythmogenesis. Comprehensive Physiology, 7(3):1009-1049, 2017.

68. Oakes, P.W., Banerjee, S., Marchetti, M.C., & Gardel, M.L. Geometry regulates traction stresses in adherent cells. Biophysical Journal, 107:825–833, 2014.

69. Oestreich, E.A., Malik, S., Goonasekera, S.A., Blaxall, B.C., Kelley, G.G., Dirksen, R.T., Smrcka, A.V. Epac and phospholipase Cepsilon regulate Ca2+ release in the heart by activation of protein kinase Cepsilon and calcium-calmodulin kinase II. Journal of Biological Chemistry, Jan 16;284(3):1514-22, 2009.

70. Okumura, S., Fujita, T., Cai, W., Jin, M., Namekata, I., Mototani, Y., Jin, H., Ohnuki, Y., Tsuneoka, Y., Kurotani, R., Suita, K., Kawakami, Y., Hamaguchi, S., Abe, T., Kiyonari, H., Tsunematsu, T., Bai, Y., Suzuki, S., Hidaka, Y., Umemura, M., Ichikawa, Y., Yokoyama, U., Sato, M., Ishikawa, F., Izumi-Nakaseko, H., Adachi-Akahane, S., Tanaka, H., & Ishikawa, Y. Epac1-dependent phospholamban phosphorylation mediates the cardiac response to stresses. Journal of Clinical Investigation, 124:2785–2801, 2014.

71. Pandey, P., Hawkes, W., Hu, J., Megone, W.V., Gautrot, J., Anilkumar, N., Zhang, M., Hirvonen, L., Cox, S., Ehler, E., Hone, J., Sheetz, M., & Iskratsch, T. Cardiomyocytes Sense Matrix Rigidity through a Combination of Muscle and Non-muscle Myosin Contractions. Developmental Cell, 44:326–336.e3, 2018.

72. Peña, J.R., Pinney, J.R., Ayala, P., Desai, T.A., & Goldspink, P.H. Localized delivery of mechano-growth factor E-domain peptide via polymeric microstructures improves cardiac function following myocardial infarction. Biomaterials, 46:26–34, 2015.

73. Pinney, J.R., Doroudian, G., Chew, P., Deasi, T.A., & Russell, B. Micromechanical Cues Converging on Fibroblasts, Cardiac Myocytes, and Stem Cells. Cells, Forces, and the Microenvironment, 1-34. Editors: Cuerrier, C.M., Pelling, A.E. Pan Stanford Publishing, 2015.

74. Poellmann, M.J., & Johnson, A.J.W. Characterizing and patterning polyacrylamide substrates functionalized with n-hydroxysuccinimide. Cellular and Molecular Bioengineering, 6:299–309, 2013.

75. Pyle, W.G., La Rotta, G., de Tombe, P.P., Sumandea, M.P., & Solaro, R.J. Control of cardiac myofilament activation and PKC-βII signaling through the actin capping protein, CapZ. Journal of Molecular and Cellular Cardiology, 41:537–543, 2006.

76. Raucher, D., Stauffer, T., Chen, W., Shen, K., Guo, S., York, J.D., Sheetz, M.P., & Meyer, T. Phosphatidylinositol 4,5-bisphosphate functions as a second messenger that regulates cytoskeleton-plasma membrane adhesion. Cell, 100:221–228, 2000.

77. Ribeiro, A.J.S., Ang, Y.-S., Fu, J.-D., Rivas, R.N., Mohamed, T.M.A., Higgs, G.C., Srivastava, D., & Pruitt, B.L. Contractility of single cardiomyocytes differentiated from pluripotent stem cells depends on physiological shape and substrate stiffness. Proceedings of the National Academy of Sciences, 112:12705–12710, 2015.

78. Robia, S.L., Ghanta, J., Robu, V.G., & Walker, J.W. Localization and kinetics of protein kinase C-epsilon anchoring in cardiac myocytes. Biophysical Journal, 80:2140–2151, 2001.

79. Russell, B., Curtis, M.W., Koshman, Y.E., & Samarel, A.M. Mechanical stress-induced sarcomere assembly for cardiac muscle growth in length and width. Journal of Molecular and Cellular Cardiology, 48:817–823, 2010.

80. Ryba, D.M., Li, J., Cowan, C.L., Russell, B., Wolska, B.M., & Solaro, R.J. Long-Term Biased β-Arrestin Signaling Improves Cardiac Structure and Function in Dilated Cardiomyopathy. Circulation, 135:1056–1070, 2017.

81. Safiejko-Mroczka, B., & Bell, P.B. Distribution of cytoskeletal proteins in neomycin-induced protrusions of human fibroblasts. Experimental cell research, 242:495–514, 1998.

82. Safiejko-Mroczka, B., & Bell, P.B. Reorganization of the actin cytoskeleton in the protruding lamellae of human fibroblasts. Cell Motility and the Cytoskeleton, 50:13–32, 2001.

83. Samarel, A.M., Koshman, Y., Swanson, E.R., Russell, B. Biophysical Forces Modulate the Costamere and Z-Disc for Sarcomere Remodeling in Heart Failure. In: Solaro R., Tardiff J. (eds) Biophysics of the Failing Heart. Biological and Medical Physics, Biomedical Engineering, Springer, New York, NY, 2013.

84. Samarel, A.M. Focal adhesion signaling in heart failure. Pflügers Archiv European Journal of Physiology, 466:1101–1111, 2014.

85. Sanger, J.W., Wang, J., Fan, Y., White, J., & Sanger, J.M. Assembly and dynamics of myofibrils. Journal of Biomedicine and Biotechnology, 2010:858606:1-8, 2010.

86. Schwan, J., Kwaczala, A.T., Ryan, T.J., Bartulos, O., Ren, Y., Sewanan, L.R., Morris, A.H., Jacoby, D.L., Qyang, Y., & Campbell, S.G. Anisotropic engineered heart tissue made from laser-cut decellularized myocardium. Scientific Reports, 6:1–12, 2016.

87. Scruggs, S.B., Walker, L.A., Lyu, T., Geenen, D.L., Solaro, R.J., Buttrick, P.M., Goldspink, P.H. Partial replacement of cardiac troponin I with a non-phosphorylatable mutant at serines 43/45 attenuates the contractile dysfunction associated with PKCepsilon phosphorylation. Journal of Molecular and Cellular Cardiology, Apr;40(4):465-73, 2006.

88. Scruggs, S.B., Wang, D., & Ping, P. PRKCE gene encoding protein kinase C-epsilon-Dual roles at sarcomeres and mitochondria in cardiomyocytes. Gene, 590:90–96, 2016.

89. Sharp, W.W., Simpson, D.G., Borg, T.K., Samarel, A.M., & Terracio, L. Mechanical forces regulate focal adhesion and costamere assembly in cardiac myocytes. American Journal of Physiology - Heart and Circulatory Physiology, 273:H546–H556, 1997.

90. Skwarek-Maruszewska, A., Hotulainen, P., Mattila, P.K., & Lappalainen, P. Contractility-dependent actin dynamics in cardiomyocyte sarcomeres. Journal of Cell Science, 122:2119–2126, 2009.

91. Sniadecki, N.J., & Chen, C.S. Microfabricated Silicone Elastomeric Post Arrays for Measuring Traction Forces of Adherent Cells. Methods in Cell Biology, 83:313–328, 2007.

92. Sniadecki, N.J., Lamb, C.M., Liu, Y., Chen, C.S., & Reich, D.H. Magnetic microposts for mechanical stimulation of biological cells: fabrication, characterization, and analysis. The Review of Scientific Instruments, 79 VN:44302, 2008.

93. Solaro, R.J. Mechanisms of the Frank-Starling law of the heart: the beat goes on. Biophysical Journal, Dec 15;93(12):4095-6, 2007.

94. Steinestel, K., Wardelmann, E., Hartmann, W., & Grünewald, I. Regulators of Actin Dynamics in Gastrointestinal Tract Tumors. Gastroenterology Research and Practice, 2015:2015.

95. Stempien-Otero, A., Kim, D.H., & Davis, J. Molecular networks underlying myofibroblast fate and fibrosis. Journal of Molecular and Cellular Cardiology, 97:153–161, 2016.

96. Theocharidis, G., Drymoussi, Z., Kao, A.P., Barber, A.H., Lee, D.A., Braun, K.M., & Connelly, J.T. Type VI collagen regulates dermal matrix assembly and fibroblast motility. Journal of Investigative Dermatology, 136:74–83, 2016.

97. Torsoni, A.S., Marin, T.M., Velloso, L. a, & Franchini, K.G. RhoA/ROCK signaling is critical to FAK activation by cyclic stretch in cardiac myocytes. American Journal of Physiology - Heart and Circulatory Physiology, 289:H1488–H1496, 2005.

98. Tse, J.R., & Engler, A.J. Preparation of hydrogel substrates with tunable mechanical properties. Current Protocols in Cell Biology, 10.16:1–16, 2010.

99. Tsujita, K., & Itoh, T. Phosphoinositides in the regulation of actin cortex and cell migration. Biochimica et Biophysica Acta - Molecular and Cell Biology of Lipids, 1851:824–831, 2015.

100. Vincent, F., Duquesnes, N., Christov, C., Damy, T., Samuel, J.L., & Crozatier, B. Dual level of interactions between calcineurin and PKC-ε in cardiomyocyte stretch. Cardiovascular Research, 71:97–107, 2006.

101. Wang, R.M., Christman, K.L. Decellularized myocardial matrix hydrogels: In basic research and preclinical studies. Advanced Drug Delivery Reviews, Jan 15;96:77-82, 2016.

102. Wear, M.A., & Cooper, J.A. Capping protein: new insights into mechanism and regulation. Trends in biochemical sciences, 29:418–428, 2004.

103. Welf, E.S., Ahmed, S., Johnson, H.E., Melvin, A.T., & Haugh, J.M. Migrating fibroblasts reorient directionality: By a metastable, PI3K-dependent mechanism. Journal of Cell Biology, 197:105–114, 2012.

104. Wells, A., Nuschke, A., & Yates, C.C. Skin tissue repair: Matrix microenvironmental influences. Matrix Biology, 49:25–36, 2016.

105. Wozniak, M.A., & Chen, C.S. Mechanotransduction in development: A growing

role for contractility. Nature Reviews Molecular Cell Biology, 10:34–43, 2009.

106. Wu, C.Y., Lin, M.W., Wu, D.C., Huang, Y.B., Huang, H.T., & Chen, C.L. The role of phosphoinositide-regulated actin reorganization in chemotaxis and cell migration. British Journal of Pharmacology, 171:5541–5554, 2014.

107. Yang, C., Tibbitt, M.W., Basta, L., & Anseth, K.S. Mechanical memory and dosing influence stem cell fate. Nature materials, 13:645–52, 2014.

108. Yang, H., Schmidt, L.P., Wang, Z., Yang, X., Shao, Y., Borg, T.K., Markwald, R., Runyan, R., & Gao, B.Z. Dynamic Myofibrillar Remodeling in Live Cardiomyocytes under Static Stretch. Scientific Reports, 6:20674:1-12, 2016.

109. Ye, X., McLean, M.A., Sligar, S.G. Phosphatidylinositol 4,5-Bisphosphate Modulates the Affinity of Talin-1 for Phospholipid Bilayers and Activates Its Autoinhibited Form. Biochemistry, Sep 13;55(36):5038-48, 2016.

110. Yoshikawa, Y., Yasuike, T., Yagi, A., & Yamada, T. Transverse elasticity of myofibrils of rabbit skeletal muscle studied by atomic force microscopy. Biochemical and biophysical research communications, 256:13–19, 1999.

111. Yu, J.G., & Russell, B. Cardiomyocyte Remodeling and Sarcomere Addition after Uniaxial Static Strain In Vitro. Journal of Histochemistry & Cytochemistry, 53:839–844, 2005.

112. Zelarayan, L., Renger, A., Noack, C., Zafiriou, M.-P., Gehrke, C., van der Nagel, R., Dietz, R., de Windt, L., & Bergmann, M.W. NF-κB activation is required for adaptive cardiac hypertrophy. Cardiovascular Research, 84:416–424, 2009.

113. Zhang, L., Mao, Y.S., Janmey, P.A., & Yin, H.L. Phosphatidylinositol 4, 5 Bisphosphate and the Actin Cytoskeleton. Phosphoinositides II: The Diverse Biological Functions, 177–215, 2012.

114. Zhou, P., & Pu, W.T. Recounting cardiac cellular composition. Circulation Research, 118:368–370, 2016.

APPENDIX

A. Animal approval forms

UIC UNIVERSITY OF ILLINOIS AT CHICAGO

Office of Animal Care and Institutional
Biosafety Committee (OACIB) (M/C 672)
Office of the Vice Chancellor for Research
206 Administrative Office Building
1737 West Polk Street
Chicago, Illinois 60612

6/21/2018

Brenda Russell
Physiology & Biophysics
M/C 901

Dear Dr. Russell:

The protocol indicated below was reviewed in accordance with the Animal Care Policies and Procedures of the University of Illinois at Chicago and **renewed on 6/21/2018.**

Title of Application: Isolation of Heart Cells From Neonatal Rats
ACC NO: 16-089
Original Protocol Approval: 7/8/2016 **(3 year approval with annual continuation required).**
Current Approval Period: 6/21/2018 **to** 6/21/2019

Funding: ***Portions of this protocol are supported by the funding sources indicated in the table below.***
Number of funding sources: 1

Funding Agency	**Funding Title**			**Portion of Funding Matched**
NIH	*Integrated Mechanisms of Cardiac Maladatation*			*Protocol is linked to form G G protocol 16-026*
Funding Number	**Current Status**	**UIC PAF NO.**	**Performance Site**	**Funding PI**
PO1 HL62426-16A1 (Yrs 16-20)	*Funded*	*2015-03159*	*UIC*	*John Solaro/ Brenda Russell (project 2)*

This institution has Animal Welfare Assurance Number A3460.01 on file with the Office of Laboratory Animal Welfare, NIH. **This letter may only be provided as proof of IACUC approval for those specific funding sources listed above in which all portions of the grant are matched to this ACC protocol.**

Thank you for complying with the Animal Care Policies and Procedures of the UIC.

Sincerely,

Timothy J. Koh, PhD
Chair, Animal Care Committee
TJK/*kg*
cc: BRL, ACC File

B. Publisher permissions

SPRINGER NATURE LICENSE TERMS AND CONDITIONS

Jul 16, 2018

This Agreement between Michael Mkrtschjan ("You") and Springer Nature ("Springer Nature") consists of your license details and the terms and conditions provided by Springer Nature and Copyright Clearance Center.

License Number	4390890111600
License date	Jul 16, 2018
Licensed Content Publisher	Springer Nature
Licensed Content Publication	Journal of Muscle Research and Cell Motility
Licensed Content Title	Cyclic mechanical strain of myocytes modifies CapZβ1 post translationally via PKCε
Licensed Content Author	Ying-Hsi Lin, Erik R. Swanson, Jieli Li et al
Licensed Content Date	Jan 1, 2015
Licensed Content Volume	36
Licensed Content Issue	4
Type of Use	Thesis/Dissertation
Requestor type	academic/university or research institute
Format	print and electronic
Portion	figures/tables/illustrations
Number of figures/tables/illustrations	2
Will you be translating?	no
Circulation/distribution	<501
Author of this Springer Nature content	yes
Title	Mechanical Inputs to Cardiac Fibroblasts and Myocytes Affect Structure, Function, and Signaling Response
Instructor name	n/a
Institution name	n/a
Expected presentation date	Jul 2018
Portions	Figure 3
Requestor Location	Michael Mkrtschjan 1045 Washington Blvd Apt 3S OAK PARK, IL 60302 United States Attn: Michael Mkrtschjan
Billing Type	Invoice
Billing Address	Michael Mkrtschjan 1045 Washington Blvd Apt 3S

JOHN WILEY AND SONS LICENSE TERMS AND CONDITIONS

Jul 16, 2018

This Agreement between Michael Mkrtschjan ("You") and John Wiley and Sons ("John Wiley and Sons") consists of your license details and the terms and conditions provided by John Wiley and Sons and Copyright Clearance Center.

License Number	4390881059110
License date	Jul 16, 2018
Licensed Content Publisher	John Wiley and Sons
Licensed Content Publication	Journal of Cellular Physiology
Licensed Content Title	Lipid signaling affects primary fibroblast collective migration and anchorage in response to stiffness and microtopography
Licensed Content Author	Michael A. Mkrtschjan, Snehal B. Gaikwad, Kevin J. Kappenman, et al
Licensed Content Date	Nov 24, 2017
Licensed Content Volume	233
Licensed Content Issue	4
Licensed Content Pages	12
Type of use	Dissertation/Thesis
Requestor type	Author of this Wiley article
Format	Print and electronic
Portion	Full article
Will you be translating?	No
Title of your thesis / dissertation	Mechanical Inputs to Cardiac Fibroblasts and Myocytes Affect Structure, Function, and Signaling Response
Expected completion date	Jul 2018
Expected size (number of pages)	125
Requestor Location	Michael Mkrtschjan 1045 Washington Blvd Apt 3S OAK PARK, IL 60302 United States Attn: Michael Mkrtschjan
Publisher Tax ID	EU826007151
Total	0.00 USD
Terms and Conditions	

TERMS AND CONDITIONS

This copyrighted material is owned by or exclusively licensed to John Wiley & Sons, Inc. or one of its group companies (each a"Wiley Company") or handled on behalf of a society with which a Wiley Company has exclusive publishing rights in relation to a particular work (collectively "WILEY"). By clicking "accept" in connection with completing this licensing transaction, you agree that the following terms and conditions apply to this transaction

Title: Injectable hyaluronic acid based microrods provide local micromechanical and biochemical cues to attenuate cardiac fibrosis after myocardial infarction

Author: Long V. Le,Priya Mohindra,Qizhi Fang,Richard E. Sievers,Michael A. Mkrtschjan,Christopher Solis,Conrad W. Safranek,Brenda Russell,Randall J. Lee,Tejal A. Desai

Publication: Biomaterials

Publisher: Elsevier

Date: July 2018

Cytoskeleton

Published by Wiley (the "Owner")

COPYRIGHT TRANSFER AGREEMENT

Date: July 16, 2018

Contributor name: BRENDA RUSSELL

Contributor address:

Manuscript number: CSK-18-034.R1

Re: Manuscript entitled PKC epsilon signaling effect on actin assembly is diminished in cardiomyocytes when challenged to additional work in a stiff microenvironment (the "Contribution")

for publication in Cytoskeleton (the "Journal")

published by Wiley Periodicals, Inc. ("Wiley")

Dear Contributor(s):

Thank you for submitting your Contribution for publication. In order to expedite the editing and publishing process and enable the Owner to disseminate your Contribution to the fullest extent, we need to have this Copyright Transfer Agreement executed. If the Contribution is not accepted for publication, or if the Contribution is subsequently rejected, this Agreement shall be null and void.
Publication cannot proceed without a signed copy of this Agreement.

A. COPYRIGHT

1. The Contributor assigns to the Owner, during the full term of copyright and any extensions or renewals, all copyright in and to the Contribution, and all rights therein, including but not limited to the right to publish, republish, transmit, sell, distribute and otherwise use the Contribution in whole or in part in electronic and print editions of the Journal and in derivative works throughout the world, in all languages and in all media of expression now known or later developed, and to license or permit others to do so. For the avoidance of doubt, "Contribution" is defined to only include the article submitted by the Contributor for publication in the Journal and does not extend to any supporting information submitted with or referred to in the Contribution ("Supporting Information"). To the extent that any Supporting Information is submitted to the Journal for online hosting, the Owner is granted a perpetual, non-exclusive license to host and disseminate this Supporting Information for this purpose.

2. Reproduction, posting, transmission or other distribution or use of the final Contribution in whole or in part in any medium by the Contributor as permitted by this Agreement requires a citation to the Journal suitable in form and content as follows: (Title of Article, Contributor, Journal Title and Volume/Issue, Copyright © [year], copyright owner as specified in the Journal, Publisher). Links to the final article on the publisher website are encouraged where appropriate.

B. RETAINED RIGHTS

Notwithstanding the above, the Contributor or, if applicable, the Contributor's employer, retains all proprietary rights other than copyright, such as patent rights, in any process, procedure or article of manufacture described in the Contribution.

C. PERMITTED USES BY CONTRIBUTOR

1. Submitted Version. The Owner licenses back the following rights to the Contributor in the version of the Contribution as originally submitted for publication (the "Submitted Version"):

a. The right to self-archive the Submitted Version on the Contributor's personal website, place in a not for profit subject-based preprint server or repository or in a Scholarly Collaboration Network (SCN) which has signed up to the STM article sharing principles [http://www.stm-assoc.org/stm-consultations/scn-consultation-2015/] ("Compliant SCNs"), or in the Contributor's company/ institutional repository or archive. This right extends to both intranets and the Internet. The Contributor may replace the Submitted Version with the Accepted Version, after any relevant embargo period as set out in paragraph C.2(a) below has elapsed. The Contributor may wish to add a note about acceptance by the Journal and upon publication it is recommended that Contributors add a Digital Object Identifier (DOI) link back to the Final Published Version.

b. The right to transmit, print and share copies of the Submitted Version with colleagues, including via Compliant SCNs, provided that there is no systematic distribution of the Submitted Version, e.g. posting on a listserve, network (including SCNs which have not signed up to the STM sharing principles) or automated delivery.

2. Accepted Version. The Owner licenses back the following rights to the Contributor in the version of the Contribution that has been peer-reviewed and accepted for publication, but not final (the "Accepted Version"):

a. The right to self-archive the Accepted Version on the Contributor's personal website, in the Contributor's company/institutional repository or archive, in Compliant SCNs, and in not for profit subject-based repositories such as PubMed Central, subject to an embargo period of 12 months for scientific, technical and medical (STM) journals and 24 months for social science and humanities (SSH) journals following publication of the Final Published Version. There are separate arrangements with certain funding agencies governing reuse of the Accepted Version as set forth at the following website: https://authorservices.wiley.com/author-resources/Journal-Authors/licensing-open-access/open-access/funder-ag . The Contributor may not update the Accepted Version or replace it with the Final Published Version. The Accepted Version posted must contain a legend as follows: This is the accepted version of the following article: FULL CITE, which has been published in final form at [Link to final article]. This article may be used for non-commercial purposes in accordance with the Wiley Self-Archiving Policy [https://authorservices.wiley.com/author-resources/Journal-Authors/licensing-open-access/open-access/self-archiv].

b. The right to transmit, print and share copies of the Accepted Version with colleagues, including via Compliant SCNs (in private research groups only before the embargo and publicly after), provided that there is no systematic distribution of the Accepted Version, e.g. posting on a listserve, network (including SCNs which have not signed up to the STM sharing principles) or automated delivery.

3. Final Published Version. The Owner hereby licenses back to the Contributor the following rights with respect to the final published version of the Contribution (the "Final Published Version"):

a. Copies for colleagues. The personal right of the Contributor only to send or transmit individual copies of the Final Published Version in any format to colleagues upon their specific request, and to share copies in private sharing groups in Compliant SCNs, provided no fee is charged, and further provided that there is no systematic external or public distribution of the Final Published Version, e.g. posting on a listserve, network or automated delivery.

C. Scripts used

Line scan analysis for peak intensities

```
%Input matrix “values’ must be matrix of equal rows and in the format of n*[line
%position, intensity 1, intensity 2]
values = [];
for i = 1:3:size(data,2)
  mat = data(:,i:i+2);
  [~,locations] = findpeaks(mat(:,2),'MinPeakHeight',mean(mat(:,2)));
  norm = mat(locations,3)./mat(locations,2);
  means = mean(norm);
  values = [values means];
end

finalvals = [];
for j = 1:5:size(values,2);
   y = mean(values(:,j:j+4));
   finalvals = [finalvals y];
end

finalvals
```

Vita

Michael A. Mkrtschjan

Education

Doctor of Philosophy in Bioengineering July 2018
University of Illinois at Chicago

Bachelor of Science in Molecular and Cellular Biology May 2011
University of Illinois at Urbana-Champaign

Graduate Research

Laboratory of Professor Brenda Russell Sept 2012 - Present
University of Illinois at Chicago

Professional Qualifications

- **Bench**: Culture of cardiac myocytes derived from human inducible pluripotent stem cells; isolation/culture of neonatal rat ventricular cardiac myocytes and fibroblasts; confocal microscopy, including fixed and live cell modes—FRAP, FRET, line scans for cardiomyocyte contractility, traction force microscopy, immunofluorescence; protein/DNA electrophoresis; western blot; polyacrylamide substrate preparation; photo and soft lithography; Flexcell culture system
- **Computer**: MATLAB, C, Adobe Photoshop/Illustrator, GraphPad Prism, OriginLab, ImageJ, Web design and maintenance w/ Wordpress
- **Language**: Conversational Spanish, 4 years study

Publications/Manuscripts

Mkrtschjan MA, Solís C, Wondmagegn AY, Majithia J, Russell B. PKC epsilon signaling effect on actin assembly is diminished in cardiomyocytes when challenged to additional work in a stiff microenvironment. Cytoskeleton (Hoboken). 2018 Jul 18. doi: 10.1002/cm.21472. PMID: 30019430.

Le LV, Mohindra P, Fang Q, Sievers RE, **Mkrtschjan MA**, Solis C, Safranek CW, Russell B, Lee RJ, Desai TA. Injectable hyaluronic acid based microrods provide local micromechanical and biochemical cues to attenuate cardiac fibrosis after myocardial infarction. Biomaterials. 2018 Jul;169:11-21. doi: 10.1016/j.biomaterials.2018.03.042. PMID: 29631164.

Mkrtschjan MA, Gaikwad SB, Kappenman KJ, Solís C, Dommaraju S, Le LV, Desai TA, Russell B. Lipid signaling affects primary fibroblast collective migration and anchorage in response to stiffness and microtopography. J Cell Physiol. 2018 Apr;233(4):3672-3683. doi: 10.1002/jcp.26236. PMID: 29034471.

Li J, **Mkrtschjan MA**, Lin YH, Russell B. Variation in stiffness regulates cardiac myocyte hypertrophy via signaling pathways. Can J Physiol Pharmacol. 2016 Jun 15:1-9. PMID: 27486838.

Lin YH, Swanson ER, Li J, **Mkrtschjan MA**, Russell B. Cyclic mechanical strain of myocytes modifies CapZβ1 post translationally via PKCε. J Muscle Res Cell Motil. 2015 Oct;36(4-5):329-37. doi: 10.1007/s10974-015-9420-6. PMID: 26429793.

Meetings and Abstracts

Mkrtschjan MA, Solís C, Wondmagegn AY, Russell B (2018). Substrate Stiffness Masks Cardiomyocyte PKCε Signaling Response to Beta Adrenergic Stimulation. UIC Bioengineering Research Symposium, Oral Presentation; Madison Myofilament Conference, Madison, WI.

McCann M, **Mkrtschjan MA**, Gil V, Russell B, Liew CW (2018). Firm that flab: Matrix stiffness promotes adipocyte thermogenesis. Combined Annual Meeting of CSCTR and MWAFMR, Chicago, IL.

Solís C, **Mkrtschjan MA**, Russell B (2018). Substrate stiffness and work affects myocyte hypertrophy and CapZ dynamics via PKCε and PIP2 signaling pathways. 62nd Annual Meeting of the Biophysical Society, San Francisco, CA.

Mkrtschjan MA, Wondmegegn A, Arena A, Li J, Russell B (2017). The superposition of work on a pathologic microenvironmental stiffness may regulate actin assembly via phosphorylation and sarcomeric redistribution of PKCε. Experimental Biology, Chicago, IL.

Mkrtschjan MA, Gaikwad S, Dommaraju S, Li J, Russell B (2017). Lipid signaling regulates fibroblast migration and the actin cytoskeleton in response to stiffness and microtopography. Experimental Biology, Chicago, IL.

Mkrtschjan MA, Le LV, Desai TA, Russell B (2016). A novel micromagnet system for loading living cardiac myocytes in vitro. Myofilament Meeting, Madison, WI.

Mkrtschjan MA, Li J, Russell B (2015). PIP2 levels in fibroblasts are altered in response to varying substrate stiffness and microtopography. Experimental Biology, Boston, MA; UIC CCVR Research Day, Chicago, IL; Chicago Cytoskeleton Meeting, Chicago, IL.

Mkrtschjan MA, Li J, Lin Y, Russell B (2014). Substrate stiffness differentially regulates PIP2 levels in neonatal rat ventricular myocytes and fibroblasts. Myofilament Meeting, Madison, WI.

Bionaz MA, **Mkrtschjan MA**, Kyrouac D, Hollister S, Wheeler MB (2011). In vitro migration of of adipose-derived stem cells from GFP pigs into polycaprolactone scaffolds treated with FGF or BMP2. 38th Annual Conference of the IETS, Phoenix, AZ.

Awards/Honors

- UIC Bioengineering Research Symposium, Invited oral presentation (2018)
- Contributed to successful NIH funded application for P01 grant—Integrated Mechanisms of Cardiac Maladaptation (PIs: R. John Solaro, Brenda Russell, Pieter de Tombe, 2016)
- Graduate College Image of Research Competition Honorable Mention, University of Illinois at Chicago (2016)
- Research Day Poster Prize, University of Illinois at Chicago, Center for Cardiovascular

Research (2015)
- Pre-doctoral Education for Clinical and Translational Scientists scholarship (2015-2016)
- Provost's Award for Graduate Research, University of Illinois at Chicago (2015)—used to learn microfabrication techniques from Dr. Tejal A. Desai, UC San Francisco, Department of Bioengineering and Therapeutic Science
- Training Grant—NIH T32 HL 07692. R. John Solaro (PI). Cellular signaling and the cardiovascular system (2014-2015)
- Board of Trustees Tuition and Service Fee Waiver, University of Illinois at Chicago (2013)
- Bioengineering Image of Research Competition Honorable Mention, University of Illinois at Chicago (2013)

Mentoring

- Kevin Kappenman, Undergraduate Biology student (2018), University of Illinois at Chicago, Honors College and Guaranteed Professional Program Admissions (Currently Senior at UIC, will attend UIC medical school in Fall 2018), co-authored one manuscript
- Snehal Gaikwad, Master's Bioengineering student (2017), University of Illinois at Chicago (Currently Process Engineer at Bristol-Myers Squibb), co-authored one manuscript
- Sagar Dommaraju, Undergraduate Math student (2016), University of Illinois at Chicago, Honors College and Guaranteed Professional Program Admissions (Currently Northwestern University M1), co-authored one manuscript

Community

- Sunday school teacher and worship leader, Hope Fellowship Church Lombard, IL — Sept 2013 - Present
- Song writer/arranger and touring musician, Restoration Project — 2011 – Present
- Middle school science fair judge - Pui Tak Christian School, Chicago, IL — 2017 and 2018
- Eagle Scout Rank — Aug 2006